Light-triggered release of bioactive compounds from HA/PLL multilayer films for stimulation of cells

Dissertation
zur Erlangung des akademischen Grades
”doctor rerum naturalium”
(Dr. rer. nat.)
in der Wissenschaftsdisziplin Biotechnologie

eingereicht an der
Mathematisch-Naturwissenschaftlichen Fakultät
der Universität Potsdam

von

Vladimir Z. Prokopović

Potsdam, August 2016

Online veröffentlicht auf dem
Publikationsserver der Universität Potsdam:
URN urn:nbn:de:kobv:517-opus4-97927
http://nbn-resolving.de/urn:nbn:de:kobv:517-opus4-97927

Dedicated to

my Mother

my Brother

and first and foremost

to my Father

for it is only with their love that I came ashore

Acknowledgements

The following work was done at the Fraunhofer Institute for Cell Therapy and Immunology in Potsdam. At this place I would like to express my gratitude to all those individuals without whom this would have been a futile endeavor.

First of all, my most sincere gratitude to my mentor, Dr. Dmitry Volodkin, for three and a half exciting years I spent in his research group. He taught me how to reason and act in order to get the best out of any situation, professional and personal alike. The knowledge I acquired during our conversations, ranging from physical chemistry to bioengineering, will be the main pillar of my future scientific career.

My second thanks goes to PD Dr. Claus Duschl, who despite his busy schedule always had patience and time to advise and assist me with problems of any sort I stumbled upon rather often during my work. The most important lesson I learned from him is that logical reasoning and well-founded arguments are the milestones of every meaningful discussion.

Thirdly, I sincerely thank Prof. Frank F. Bier who agreed to be my doctoral supervisor and whose kind approach and flexibility opened many doors which seemed to had been hopelessly sealed.

I am happy to have met Daniel Connor, Lena Danckert, and the brightest Iranian jewel, Andisheh Motealleh, my dear colleagues, office-mates, and friends who indeed made my life colorful. I even dare not recollect how many of my silly German-related questions Daniel and Lena have survived and answered without laughing at me. I am in eternal debt to all three of them.

I thank Dr. Narayanan Madaboosi Srinivasan and Thomas Paulraj for their experimental and scientific experience which saved me a lot of trouble and time. Not to forget their friendship, through which they brought the rich and exotic Indian culture to my senses.

It was only with the help from David Šustr, Alena Sergeeva, Ana Vikulina, and Guy Guday that I was able to conduct a number of experiments. I thank Natalia Feoktistova, Dr. Johannes Tanne, Dr. Nieves Godino-Amado, Carena Taufelhart, and Natalia Velk for being wonderful coworkers and friends.

I thank Beate Morgenstern, Dr. Stephan Schmidt, and Alexander Christmann for their skills they shared with me. I specially thank Christian Marschner, who always had an answer before I even had a question. I also own my gratitude to Dr. Nenad Gajović, Dr. Thomas Leya, and Dr. Katja Uhlig.

My lovely thanks to Nevena Petrović, my flat-mate in Berlin, friend, and countryman, who never let me forget who I am and where I come from, and who sometimes knew me better than I knew myself. To Batke, Jeka, Kula, Bo, Radojević, Miloš, Aleksandar, Vasko, Boki, Nata, and all other dear people for their friendship and understanding.

In the end, the most important ones. My family. The words of my gratitude have been multiplying as the time went by. Alas, today I stand in silence, muted by the love and sincerity they have devoted to me so that I can become the man I am. From you I learned the most valuable thing in life – what it means to love and be loved unconditionally. Thank you.

Selbständigkeitserklärung

Hiermit erkläre ich, dass ich die vorliegende Dissertation selbständig verfasst und keine anderen als die angegebenen Quellen und Hilfsmittel benutzt habe.

Ferner versichere ich, dass ich diese Dissertation noch an keiner anderen Universität eingereicht habe, um ein Promotionsverfahren zu eröffnen. Ich habe mich auch früher um keine Promotion bemüht.

Abstract

Light-triggered release of bioactive compounds from HA/PLL multilayer films for stimulation of cells

The concept of targeting cells and tissues by controlled delivery of molecules is essential in the field of biomedicine. The layer-by-layer (LbL) technology for the fabrication of polymer multilayer films is widely implemented as a powerful tool to assemble tailor-made materials for controlled drug delivery. The LbL films can as well be engineered to act as mimics of the natural cellular microenvironment. Thus, due to the myriad possibilities such as controlled cellular adhesion and drug delivery offered by LbL films, it becomes easily achievable to direct the fate of cells by growing them on the films.

The aim of this work was to develop an approach for non-invasive and precise control of the presentation of bioactive molecules to cells. The strategy is based on employment of the LbL films, which function as support for cells and at the same time as reservoirs for bioactive molecules to be released in a controlled manner. UV light is used to trigger the release of the stored ATP with high spatio-temporal resolution. Both physico-chemical (competitive intermolecular interactions in the film) and biological aspects (cellular response and viability) are addressed in this study.

Biopolymers hyaluronic acid (HA) and poly-L-lysine (PLL) were chosen as the building blocks for the LbL film assembly. Poor cellular adhesion to native HA/PLL films as well as significant degradation by cells within a few days were shown. However, coating the films with gold nanoparticles not only improved cellular adhesion and protected the films from degradation, but also formed a size-exclusion barrier with adjustable cut-off in the size range of a few tens of kDa.

The films were shown to have high reservoir capacity for small charged molecules (reaching mM levels in the film). Furthermore, they were able to release the stored molecules in a sustained manner. The loading and release are explained by a mechanism based on interactions between charges of the stored molecules and uncompensated charges of the biopolymers in the film. Charge balance and polymer dynamics in the film play the pivotal role.

Finally, the concept of light-triggered release from the films has been proven using caged ATP loaded into the films from which ATP was released on demand. ATP induces a fast cellular response, i.e. increase in intracellular [Ca^{2+}], which was monitored in real-time. Limitations of the cellular stimulation by the proposed approach are highlighted by studying the stimulation as a function of irradiation parameters (time, distance, light power). Moreover, caging molecules bind to the film stronger than ATP does, which opens new perspectives for the use of the most diverse chemical compounds as caging molecules.

Employment of HA/PLL films as a nouvelle support for cellular growth and hosting of bioactive molecules, along with the possibility to stimulate individual cells using focused light renders this approach highly efficient and unique in terms of precision and spatio-temporal resolution among those previously described. With its high potential, the concept presented herein provides the foundation for the design of new intelligent materials for single cell studies, with the focus on tissue engineering, diagnostics, and other cell-based applications.

Zusammenfassung

Licht-induzierte Freisetzung von Biomolekülen aus Hyaluronsäure-Poly-L-Lysin-Schichten zur Stimulierung von Zellen

Das Konzept des Targetings von Zellen und Geweben mittels kontrollierter Wirkstoffverabreichung ist im Bereich der Biomedizin unerlässlich. Die layer-by-layer (LbL) Technologie ist eine etablierte Methode für die Herstellung von Polyelektrolyt-Multischichten, um intelligente, maßgeschneiderte Materialien für eine kontrollierte Wirkstoffabgabe aufzubauen. Die LbL Filme können das Verhalten einer natürlichen zellulären Mikroumgebung nachahmen. Wegen der unzähligen Möglichkeiten dieser Filme sind nicht nur das Wachstum und die Beeinflussung der Zellen, sondern auch die kontrollierte Wirkstoffabgabe leicht umzusetzen.

Das Ziel der vorliegenden Arbeit war die Entwicklung eines nicht-invasiven Systems für die präzise Verabreichung von Biomolekülen an einzelne Zellen. Die Strategie beruht auf LbL Filmen, die einerseits als geeignete Oberfläche für das Zellwachstum dienen, andererseits aber auch die kontrollierte Abgabe von Biomolekülen ermöglichen. Die zeitlich und räumlich präzise Freisetzung von ATP wurde durch UV Bestrahlung eingeleitet/ausgelöst. Sowohl die physiko-chemischen als auch die biologischen Eigenschaften des Verfahrens wurden analysiert.

Die LbL Filme wurden auf Basis der biokompatiblen Polymere Hyaluronsäure (HA) und Poly-L-Lysin (PLL) assembliert. Nach der Assemblierung waren die Filme zunächst zellabweisend und wurden von den Zellen innerhalb von ein paar Tagen abgebaut. Die Beschichtigung der Filme mit Gold-Nanopartikeln verbesserte nicht nur die Adhäsion der Zellen, sondern auch den Schutz gegen Abbau. Zudem wurde gezeigt, dass die Beschichtigung eine Molekulargewichtsausschlussgrenze mit verstellbarem cut-off in einem Bereich von nur einigen 10 kDa darstellt.

Weiterhin wurde gezeigt, dass die Filme eine enorme Beladungskapazität aufweisen (bis hin zu einer Beladung im mM Bereich). Darüber hinaus konnten die Biomoleküle, die in diese Filme eingebettet wurden, langfristig und nachhaltig freigesetzt werden. Die Beladung und Freisetzung der Moleküle erfolgt durch die Interaktion zwischen eingebetteten Molekülen und freien Ladungen innerhalb des Polymerfilms. Das Ladungsverhältnis und die Polymerdynamik spielen dabei eine zentrale Rolle.

Schließlich wurde gezeigt, dass die in Filmen eingebetteten caged-ATP Moleküle gezielt durch einen Laser freigesetzt werden können. ATP verursacht die schnelle zelluläre Antwort durch den Anstieg von intrazellulären Ca^{2+}-Ionen, der in Echtzeit beobachtet werden kann. Um die Limitierungen dieses Ansatzes bei der zellulären Stimulation hervorzuheben, wurden verschiedene Bestrahlungsparameter (Zeit, Abstand, Laserleistung) analysiert. Außerdem binden viele caging-Moleküle stärker an die Polymerfilme als ATP, wodurch eine Vielzahl von chemischen Verbindungen als geeignete Moleküle für die Caging zur Verfügung stehen.

Der Einsatz von HA/PLL Filmen als neue Oberfläche für Zellwachstum und als Reservoire für die Einbettung bioaktiver Moleküle samt der Möglichkeit einzelne Zellen mittels fokussierter Laserbestrahlung anzuregen, machen die Methode hoch effizient und einzigartig. Die Vorteile dieser Methode kommen durch die zeitliche und räumliche Präzision zustande. In Zukunft kann das in dieser Arbeit beschriebene Konzept für den Entwurf neuer Materialien für Untersuchungen mit einzelnen Zellen eingesetzt werden; mit dem Fokus auf Tissue Engineering, Diagnostik und anderen Zell- und biomedizinisch-basierten Applikationen.

Contents

1 INTRODUCTION

The road to the advanced medications is not always smoothly paved as experiments often demanded test subjects, which in some cases exceeded the ethical norms or the possibilities of the logistics to provide them. Therefore, the researchers had to procure a manner to conduct their investigations on the entities which were obtained by ease and were made readily available in copious amount. Since the final destination of the drugs is to specifically affect defined structures and functions at the molecular level, cells and tissues emerged as the perfect candidates.

The behavior of cells *in vivo* is governed by a multitude of intra- and extracellular molecular interactions in the exact spatiotemporal arrangement and with defined concentration profile. In order to employ cells for *in vitro* studies, these interactions have to be integrated into the architecture of biomedical mimetic systems. Thus, the contemporary research in the fields of biomedicine and bioengineering prioritizes the development of biomaterials which are the basis of these systems. Engineering them is a challenging task, since profound interdisciplinary knowledge has to be applied in order to design such biomaterials which could offer broad possibilities for the control of cells.

In this context, mimics of the extracellular matrix (ECM) have emerged as supports for cell culturing *in vitro* at conditions which emulate the natural *in vivo* milieu as authentically as possible. ECM mimics allow precise control over cellular growth and tissue behavior, as well as understanding of the main questions in the cell biology. Their cardinal feature is their ability to present bioactive molecules (drugs) which are crucial in defining cell fate and function. Thus, the layer-by-layer (LbL) deposited polyelectrolytes film have become increasingly important in the field of biomaterial science since their chemical, mechanical and topological features can be altered to influence the cell behavior. Furthermore, equally important is the feature of LbL films to act as effective drug reservoirs from which stored drugs can be released on demand.

Drug delivery systems are mostly based on the bulk release of the drugs which leads to the stimulation of the whole population of cells, whereas single cell stimulation by localized drug release is still a fairly undeveloped concept. For the release, unspecific and non-localized triggers such as changes in pH, ionic strength, temperature or some other property of the whole system are used, and these changes might as well affect the normal functions of cells.

Addressing the problems of localization of the release, stimulation of the individual cells, and the non-invasive drug release triggering would pave a way for the development of a new generation of (single) cell assays. The major challenge here is to develop a bioactive system that can stimulate individual cells by providing highly localized delivery of drugs. In addition, the trigger for the delivery should not affect the cells. A solution to the problems could lie in the application of laser light for drug release from the predetermined parts of the

system, as it would ensure high spatio-temporal precision of cell stimulation. Furthermore, it would be applied in a way to affect neither cells nor the whole system, as the laser can be setup to affect subcellular-sized areas.

Considering all the aspects mentioned above, the main goal of this research is to establish a bioactive system for controlling the presentation of drugs to cells. The current study deals with the design of a cell assay for external and non-invasive stimulation of cells with high precision in space and time. The strategy is based on employing the LbL films as the support for cells and at the same time as reservoirs for drugs, while UV light is used to trigger the release of stored molecules. Therefore, the following objectives described below were set and Fig. 1.1 gives an overview of different aspects of the study:

1) To design stable, cell-compatible, and cell adhesive LbL-assembled films;

2) To understand loading and release mechanism of drugs that are stored in and presented from the film;

3) To establish an approach with high spatio-temporal precision for the externally-triggered release of drugs from the LbL films in order to locally affect cells. Light is chosen as the stimulus;

4) To understand limitations and perspectives and to apply the developed approach for stimulation of cells.

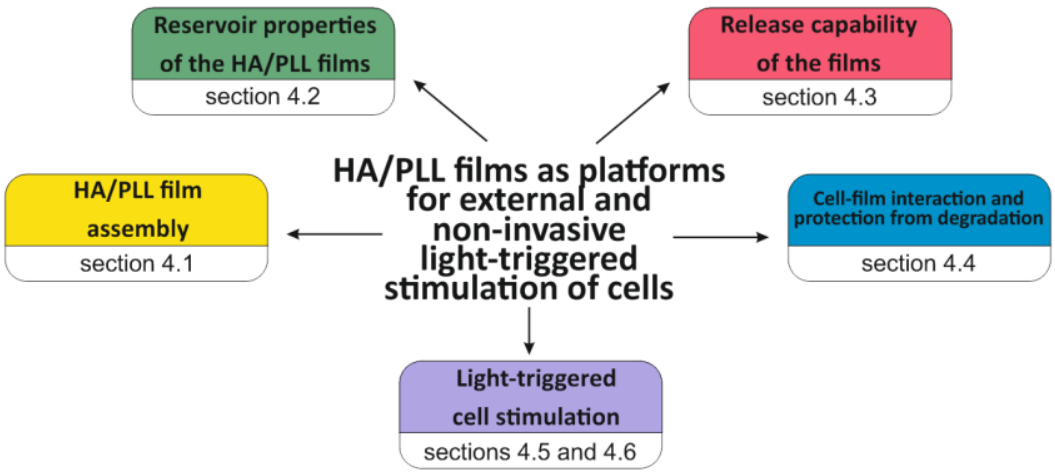

Figure 1.1. Outline of the major aspects of the present study. As the main topic was to develop a cell assay, various features of the system had to be addressed: the design of the support, drug storage and release, and controlled stimulation of cells. The challenge was subdivided into different aspects that were worked on separately. For each aspect the respective section that deals with it in detail is highlighted.

2 FUNDAMENTAL PRINCIPLES AND CURRENT STATE OF THE RESEARCH

2.1 Layer-by-layer films

The design of advanced functional materials with properties that can be controlled is immensely interesting for fundamental research as well for application in many fields of biomedicine such as directed cellular growth, tissue engineering, regenerative medicine, etc.[1] The last few years have witnessed intense research efforts to shape such materials, from submicrometer capsules and liposomes to mimics of the extracellular matrix that were all modifiable in terms of morphology, composition, and mechanical properties. Special place among them belongs to polymer films, or polyelectrolyte multilayers (PEMs) which were successfully engaged in many areas of basic and applies science. Hence, this entire introductory section is dedicated to PEMs with special regard to their design, properties, and application possibilities.

2.1.1 The layer-by-layer principle

The method of layer-by-layer (LbL) deposition of oppositely charged materials on a substrate was first described 50 years ago.[2] However, only after the introduction of LbL technique for production of PEMs in the early nineties by Decher, Möhwald, and Lvov was this field revolutionized.[3–5] The LbL principle for production of films is based on the alternating deposition of oppositely charged polyelectrolytes (polymers with repeating charged groups) onto a solid surface, with intermittent rinsing steps (Fig. 2.1A). The method was recognized and accepted almost instantaneously and the original paper[6] by Decher published in Science remains one of the most cited in the field of fabrication of thin films. The ingenuity of the method is reflected in its simplicity, versatility of materials, tunable deposition conditions, potential full automation of the process, and, at the end, inexpensive equipment required.

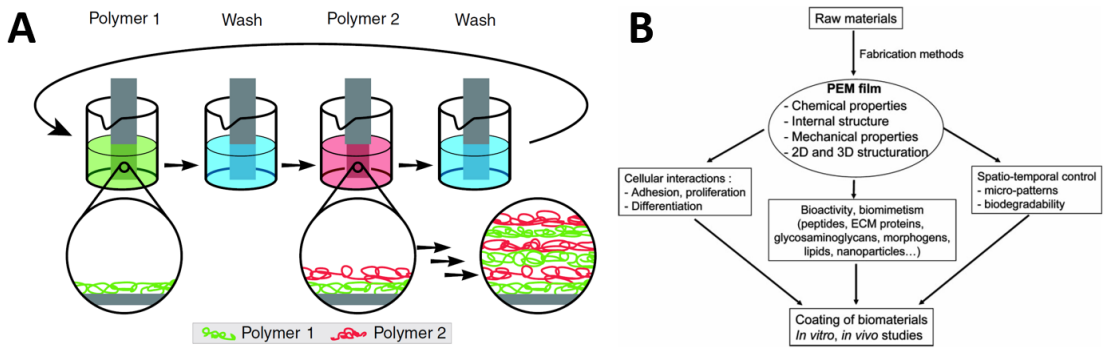

Figure 2.1. Principle of the layer-by-layer deposition of PEM. (**A**) Schematics of the film deposition process. The four steps are the basic buildup sequence and can be varied to meet the requirements of the system. Adapted from [7]. (**B**) Schematic view of the different aspects of LbL deposition that can lead to PEMs with defined functionalities. Adapted from [8].

The variety of the LbL films that can be assembled using this technique is primarily based on easiness to alter their properties which have been extensively studied since the breakthrough of the LbL method. Functionalization of these films opens countless possibilities to control cells by way of tuning chemical, mechanical, biological, structural, and organizational features, as shown in Fig. 2.1B. The efficiency of film functionalization and practical approach turned LbL films into a necessity in disparate fields including coating of biomedical devices, drug delivery, mimicking extracellular matrix, enzyme mobilization, cell and tissue engineering and many others.

2.1.2 Aspects of fabrication

The driving forces for deposition of polyelectrolytes are numerous and include both electrostatic and non-electrostatic interactions including hydrogen bonding,[9] hydrophobicity,[10] even covalent bonding,[11] van der Waals forces, and host-guest interactions.[8] Although, at the first glance, the method may seem rather simple, it requires careful planning at each step starting from the choice of ionic strength, polymers, pH, deposition time and speed, up to post-deposition treatment and storage. Despite all the efforts and detailed studies, the underlying mechanism of LbL assembly is still not well understood.[12,13] However, unclear fundamental principles of LbL film formation were not an obstacle for the development of a few techniques which have been successively used for deposition: spraying, spin coating, dip coating, among them technologically advanced ones based on microfluidics and electromagnetism. The contemporary methods are summarized in a recent review[14] on recent technological advances in the assembly of LbL films. Any surface could be used as a substrate, provided that proper polymers or other layer materials are chosen – this opens up inconceivable possibilities for the design and application (Fig 2.2).

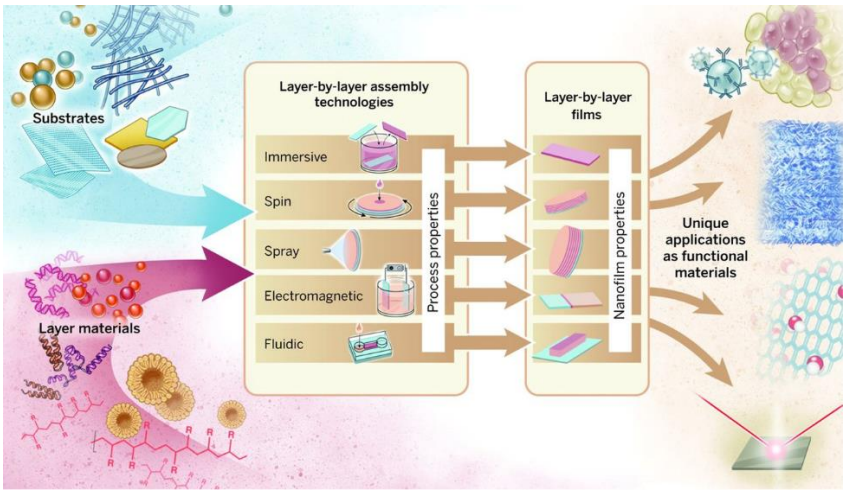

Figure 2.2. The applications of the resulting films depend on the substrate and layer material choices, as well as the assembly technology. Adapted from [14].

For the purpose of this study, only the dip coating (or dipping) method of LbL film assembly has been used (Fig. 2.1A) as it is the most commonly used technique, due to its simplicity, low-cost technology, efficiency, and ease-of-use.[8]

A variety of polymers is used for the assembly of films, both synthetic polystyrene sulphonate (PSS), poly(allylaminehydrochloride) (PAH), poly(diallyldimethylammonium chloride) (PDADMAC), polyacrylic acid (PAA) and natural biopolymers hyaluronan (HA) and chitosan,[15,16] alginate,[17] different polypeptides (poly-L-lysine (PLL), poly-glutamic acid),[18,19] proteins,[20] nucleic acids,[21,22] etc. Aside with constituents, various prerequisites (choice of polymers, concentration, ionic strength, temperature) need to be controlled in order to have effective LbL deposition.[23] Proper selection of constituents determines biomedical compatibility and applicability. Furthermore, properties of film such as elasticity and permeability depend heavily on water content (hydration)[24] and it was shown that the properties of polysaccharide-based PEMs depend on hydration and internal composition.[25] pH[26–30] and ionic strength[31,32] have as well been shown to be essential parameters for film assembly, tuning of properties, and stability. A study by Crouzier and coworkers shows tight relationship between ion pairing, pH, salt content, polymer diffusion, and hydration in the film, indicating an interplay between these parameters.[33] Moreover, the variation of polymer size affects the behavior and stability of films as speed of polymer diffusion and integration into the film depends on its size.[34] Finally, the mass of a film during deposition might increase linearly all the time, or might grow exponentially during the first few deposition steps but increases linearly during later steps. This phenomenon of growth depends on all parameters of film deposition condition described above.[35–37] For example the mass of the HA/PLL films grow exponentially and at one point of deposition starts growing linearly,[38] while the mass of PSS/PAH films grow linearly[39] during the whole deposition process. Thus, the advantages of LbL technique are obvious, as it allows assembly of films with the widest span of variations in thickness, stiffness, roughness, and biocompatibility.[23,40–48] In order to keep such a complexity under control, all deposition parameters for LbL films for this study were kept constant to ensure reproducibility.

2.1.3 Reservoir properties: loading and release of molecules

Increasing development of biotechnology and biomedicine puts high attention on systems that can store and release bioactive compounds on-demand. The attractiveness of controlled release from such systems can offer high delivery efficacy. Owing it to the versatility of structural, chemical, and physical properties which equip them with most versatile ways to store molecules, LbL films have been attracting significant attention since they have been shown to act as reservoirs for numerous biologically active molecule species such as nucleic acids, proteins, and peptides[42,49–53], and for small bioactive molecules[54–56] as well. These reservoirs are used for delivery of stored molecules in a variety of different *in vitro* and *in vivo* systems.

To call an LbL film a reservoir, molecules (drug) of interest have to be stored inside. This is achieved either by using the molecule as a component of the film or by post-loading by diffusion. In the first case biomolecules like peptides/proteins[57–59] and DNA[60–62] replace one of the polyelectrolytes, and are combined with an oppositely charged polyelectrolyte.[63] The second case includes more commonly used methods of post-loading, e.g. loading by

incubation in the drug solution. It is often a case that a simple fluorescent dye or fluorescently labeled molecules are used as model molecules due to the variety of physicochemical features they can provide, such as hydrophobicity, charge balance, steric hindrance etc., and especially due to the fact that they can be monitored directly by means of fluorescence methods. Hydrated films are especially suited for drug loading as they offer a milieu which is rather well suited for diffusion of a drug. For example, fluorescently labeled paclitaxel was homogenously distributed throughout highly hydrated LbL films composed from hyaluronic acid and poly-L-lysine.[56] Likewise, it is possible to load the anti-inflammatory drug diclofenac into crosslinked LbL film, and the amount of the stored drug is higher in thicker films, indicating homogenous distribution.[64]

To fully exploit these films for bioapplications for manipulation of cells and tissue engineering, it is essential that these systems allow release of stored molecules as well. The trigger for the release could be any change in physico-chemical properties of the film or of the surrounding medium: temperature, pH, composition, ionic strength, hydrolysis, and light.[65–67] This process can be employed for both short term[54] and long term[68] release. However, although it has been shown that paclitaxel loaded into films was released and successful in killing cells with an efficiency of about 90 %,[55] and that few more small drugs[55,69] as well as some oligopeptides[70] were released from LbL films, it is still not clear in detail how the mechanisms of release work. So far assumptions have been made that variation of the number of layers in the film affects both loading and release rate of large molecules such as oligo- and polypeptides.[71]

Though the possibilities for application are countless, the exact mechanism by which molecules are stored and released from the film is unknown since there are just a few publication dealing with this topic.[55,56,71–74] However, it can be speculated that the transport of charged molecules into/from films composed of charged polyelectrolytes is due to a concentration gradient and different affinities in different media. These affinities are a function of the interplay between intrinsic, polyelectrolyte-polyelectrolyte, and extrinsic, polyelectrolyte-counterion, interactions where loaded molecules represent counterions. The understanding of the mechanisms by which a drug can be stored and released would open a completely new field that would provide tools to precisely tune the reservoir properties and to design films with features of controlled release of drugs.

2.1.4 Application

The versatility of LbL films produced in the last few years led to increased efforts to exploit and practically apply them in most different fields ranging from photonics and nanoreactors to manipulation of cells and tissue engineering.[8,63,75] For example, Kotov and coworkers fabricated LbL films sensitive to light exposure which can act as optical gates,[70] whereas the group of Kurth designed films with optical memory effect.[76,77] One research demonstrates the application of the LbL technology for the production of dye-sensitized solar cells based on TiO_2.[78] Furthermore, the films were utilized for fabrication of semiconductor transistors,[79] nanoreactors,[80] and super hydrophobic surfaces[81].

However, the biological applications were always more pursued (Fig 2.3),[63,82] as biofunctionalization, biomimetism, biocompatibility, and biodegradability offer incredible options for biomedical purposes.[8,48,66,75,83–86] Following the trend, important advances are constantly being reported since 2000s, all of them achieved by adjustment of physicochemical properties of LbL films.[15] Almost all of the studies show that film properties (mechanical and physicochemical) are decisive for different aspects of cellular interaction with the film: adhesion, cellular behavior, viability, and even those complex ones, such as cell differentiation and apoptosis. The complexity, application and challenges of utilization of LbL films in biomedicine are given in a recently published book[87] edited by Picart, Caruso, and Voegel.

For example, adhesion of endothelial cells,[88] fibroblasts,[89,90] osteoblastic cells,[91] and hepatocytes[92] was shown to be rather good on LbL film composed of PSS and PAH. Another study suggests that adhesivity of films can be controlled by the pH of assembly.[93] Additional stiffening of the film surface by nanoparticles increases adhesion of fibroblasts,[46] while crosslinking increases spreading of skeletal muscle cells.[18,66] Simple addition of heparin into LbL made these film a perfect coating for implants;[94] while the addition of chondroitin sulfate shows potential in turning LbL films into suitable coatings for bone implants.[95]

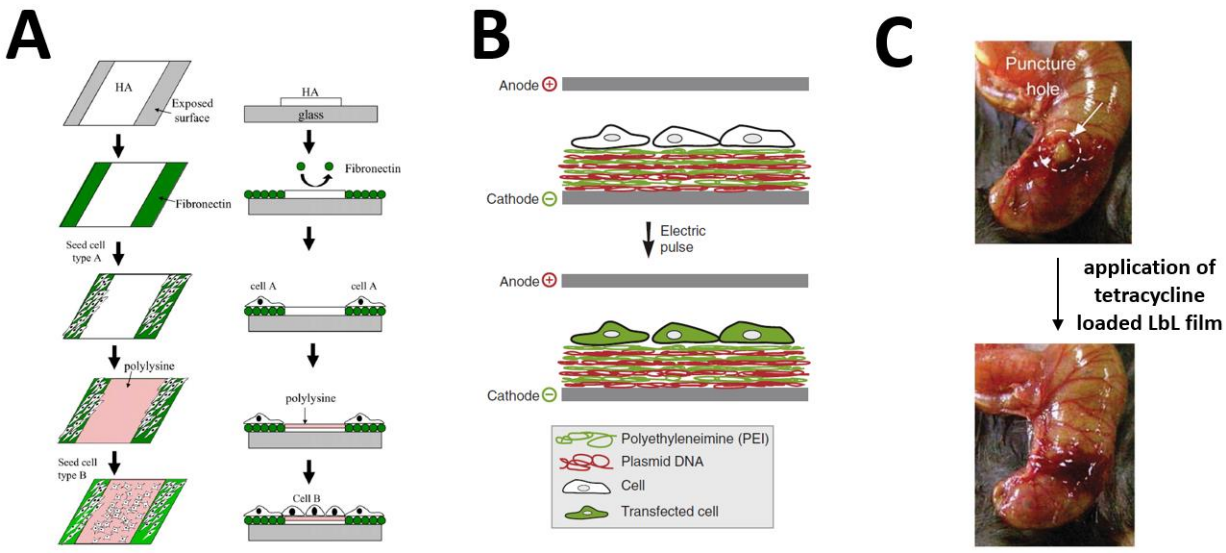

Figure 2.3. Biomedical applications of LbL films. (**A**) Schematic diagram of the HA-PLL layering approach to pattern co-cultures. Reproduced from [96]; (**B**) Spatially controlled release of plasmid DNA for transfection of cells growing on LbL films by an electric pulse that induces film disassembly. Adapted from [7]; (**C**) Macroscopic images after treating a murine cecal puncture hole with a chitosan/alginate based tetracycline carrier. Reproduced from [1].

Furthermore, a rapid differentiation of endothelial progenitor cells was observed on LbL films, in higher extent than on conventional surfaces.[97] They were as well used for *in vivo* repair of blood vessels.[98] Healing of cornea by differentiation of corneal progenitor cells mediated by LbL films was also reported,[99] and LbL deposited film were even successfully used as healing patches for the mammalian appendix (Fig 2.3C).[1] Moreover,

patterning of cellular co-cultures was achieved using LbL assembled films (Fig. 2.3A).[96,100,101] The combination of electrochemical methods and LbL films composed of polyethyleneimine (PEI) and plasmid DNA enabled design of the system that aid transfection of cells (Fig. 2.3B).[7]

It is expected that LbL technique will contribute greatly to the development of new functional devices with high perspectives for the administration of active agents, supports for cells in regenerative medicine and tissue engineering, biosensing and construction of microtissues and disease models in the laboratory.[1] In conclusion, the properties of LbL films as well as the relation between cells and LbL films have to be understood in detail if the fields of their application are to be further developed.

2.2 HA/PLL films

The characteristics of LbL films are to a high extent determined by the polymers they are composed of. Therefore, the choice of film constituents represents one of the most important steps in engineering the film with thoughtfully intended features. One of the best studied LbL-assembled systems are polymer films assembled from hyaluronic acid (HA) and poly-L-lysine (PLL).[102] The biocompatibility of these polymers plays a pivotal role, since it allows HA/PLL films to be applied without fear of toxicity or other detrimental effects. The versatility of features HA/PLL films can deliver, their physicochemical properties, aspects of biocompatibility, and application are the main subjects of the following section.

2.2.1 Physico-chemical properties

HA is a natural linear polysaccharide consisting of alternating disaccharide units of d-glucuronic acid and *N*-acetyl-d-glucosamine with β(1→4) interglycosidic linkage.[103] The pKa of the carboxyl group of HA is 2.9[104], which makes HA negatively charged at physiological pH 7.4. The negative charge allows electrostatic interaction with a polycationic polymer that is positively charged at physiological conditions. PLL, a natural homopolymer of L-lysine produced by *Streptomyces* strain,[105] emerges as a perfect candidate, both due to its biocompatibility and pKa value of ε-NH_2 of 10.5[106]. Structures of both HA and PLL are given in Fig. 2.4.

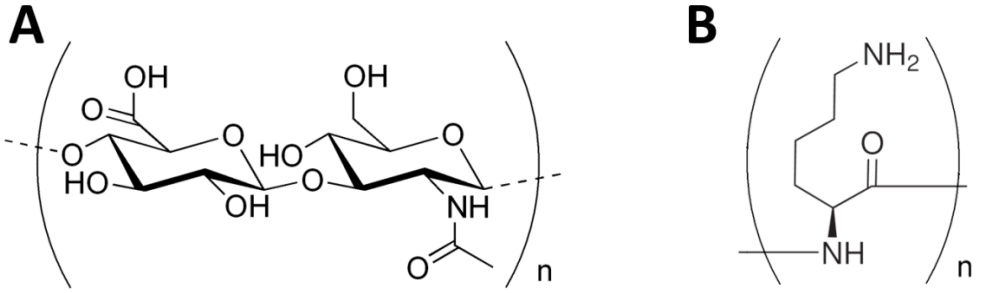

Figure 2.4. Chemical structures of (**A**) hyaluronic acid (HA) and (**B**) α-poly-L-lysine (PLL).

The fabrication of HA/PLL films by dipping (the method exclusively used in this study) is the example of the LbL deposition in which the polyelectrolytes are alternately deposited onto a solid support by dipping the support into HA and PLL solutions, with intermittent washing steps. The cycle is repeated until the desired number of bilayers (bL) or thickness of the film is achieved. The deposition is based on electrostatic interaction and charge compensation and it was shown that the charge ratio between lysine residues in PLL and negative charges of HA stabilizes around 2 after 6 bL are deposited.[33] The thickness of the film and the number of deposited layers do not correlate linearly – at the beginning of the deposition, the mass of the film increases exponentially up to a certain point after which the mass starts increasing linearly with the number of deposition steps.[36] The details of the growth mechanism and behavior of HA/PLL films were the subject of numerous studies that all suggest complex dependence on the assembly conditions such as polymer concentration,[28] salt concentration and type,[107] polymer size and concentration,[28,34,107] temperature,[108,109] etc. Although there is a detailed study by Porcel[34] which shows that the thickness increment after every deposition step decreases when molecular weight of HA increases and is independent from the molecular weight of PLL, there is rather scarce data on the effect of the polymer chain length on the properties of the film which is also a topic dealt with in this study.

From the morphological point of view, up to deposited 12 bL films do not have continuous surface but are rather composed of small islets of deposited polymers; above 12 bL film become smooth with minimum variations in Young's modulus.[110] The threshold of 12 bL correlates with the above mentioned transition point from exponential to linear growth, and it could be speculated that it is the consequence of the formation of initially inhomogeneous film surface during the buildup.[111] Anyhow, these films can be assembled so as to reach up to few micrometer thickness[36,109] and due to high hydration of HA,[112,113] HA/PLL films have high water content of about 80 % (w/w).[33] High water content renders these films very soft with a Young's modulus of the order of few tens of kPa.[46,110] This softness presents the main challenge for adhesion and growth of the majority of cell lines, as they prefer solid supports with the Young's modulus of at least few hundreds of kPa.[18,46,114]

2.2.2 Adjustment of mechanical properties

Tuning of mechanical and physicochemical properties of HA/PLL films, stiffness in the first place, is one of the prerequisites to implement these films for cellular studies. Strategies to overcome this problem include chemical crosslinking[19,115,116] or additional layers of stiffer polyelectrolyte[69]. Although carbodiimide (EDC) crosslinking increases the stiffness over two orders of magnitude,[117] chemical crosslinking alters structure and composition of polymers, which might decrease the ability of the film to act as a reservoir for biomolecules. However, if the biodegradability is not a desired feature of the film, it can be prevented by crosslinking.[118]

In order to avoid potential hazards of crosslinking, Schmidt and his coworkers proposed an inventive approach for stiffening of the surface.[46] It is based on the

incorporation of nanoparticles onto HA/PLL films as a mean to alter the material properties for optimized cell adhesion. The idea was inspired by earlier works[119,120] which have shown that the addition of diverse nano-sized assemblies into gels and polymers improves mechanical stability and robustness. The authors used 5 nm gold nanoparticles (AuNPs) which are embedded in HA/PLL films in form of aggregates and not uniformly, as confirmed by AFM studies.

The authors suggest that the main contribution of AuNPs was the increase of the film stiffness. Along with the increase of the relative concentration of AuNPs (γ), both Young's modulus and roughness of the HA/PLL films increased (Fig. 2.5A). Young's modulus ranges from few tens of kPa for native films, up to 1.2 MPa for the films with the AuNPs coatings. It is obvious that the introduction of AuNPs coatings on the surface of HA/PLL films is a powerful tool to increase film stiffness. However, the study does not deal with numerous questions concerning the effect on storage capabilities and biodegradability of the films.

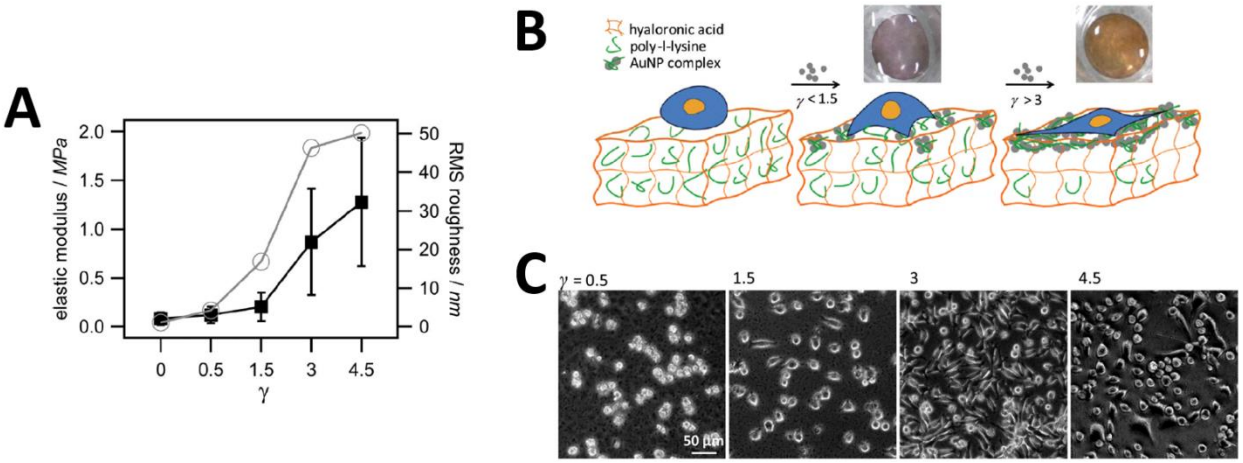

Figure 2.5. Application of AuNPs for stiffening of the surface of HA/PLL films. (**A**) General scheme of the HA/PLL film structure; AuNPs (gray spheres) bind with PLL (in green) by complexation to the film. By addition of different amounts of AuNPs their surface concentration γ is increased. As a result, changes of the cellular adhesion can be expected, as depicted. (**B**) Optical microscopy (phase contrast) images of the cell adhesion after incubation for five days; the cell adhesion is most pronounced for $\gamma = 3$. (**C**) Elastic modulus (solid squares) and root-mean-square (RMS, open circles) surface roughness increase monotonically with γ; the elastic modulus changes 15 fold from 80 kPa ($\gamma = 0$) to 1.3 MPa ($\gamma = 4.5$); drastic changes occurred for $\gamma > 1.5$. Adapted from [46].

2.2.3 Cellular adhesion

The ability to adhere onto the surfaces with different stiffnesses is one of the major features that differs cell types one from another. Thus, the manipulation of cells in terms of adhesion is not an easy task since each cell line demands specific condition to thrive, both physicochemical and physiological. Therefore, engineering LbL coatings, or specifically HA/PLL films, to suit the need of most diverse types of cell lines is a respectable challenge.

In general, native HA/PLL films are not suited for adhesion of cells. Low adhesion to native films was observed for chondrosarcoma cells, chondrocytes, and osteoblast.[19,121]

Myoblast cells grown on native HA/PLL films differentiate into myotubes faster when grown on stiffer 1 µM thick $(HA/PLL)_{12}$ films.[18] The group of Discher tested adhesion of smooth muscle cells on covalently crosslinked 4 µM thick $(HA/PLL)_{20}$ which are 15x stiffer than non-crosslinked films - the spreading of cells on stiffer films was 5x higher.[122] Zisch and coworkers also report that native HA/PLL are not suitable for adhesion of mesenchymal stem cells (MSC) despite high surface density of preadsorbed fibronectin which improves adhesivity of the surface.[123] Interestingly enough, MSC have shown high level of adhesion to cross-linked HA/PLL films and their proliferation was faster. However, to maintain cells on the surface of films during a few weeks necessary for differentiation, fibronectin had to be covalently attached. Furthermore, the MSC were capable of differentiating into osteocytes and chondrocytes upon addition of differentiation-inducing factors. The behavior of embryonic stem cells (ESC) on HA/PLL films has also been investigated. Unlike MSC, ESC exhibited a better potential for differentiation on native HA/PLL films than on cross-linked ones.[124] Using the same films, Tezcaner observed that photoreceptor cells exhibit good viability on HA/PLL, without any stiffening through cross-linking and fibronectin attachment.[125]

It is also noteworthy that cell-repellent properties of HA have already been described. Hydrogels composed solely from HA were too soft for adhesion of any cell type and needed modification of the surface to improve adhesion and spreading of cells.[126] Two more studies also showed that embedding hyaluronic acid in LbL films prevented seeding of peripheral blood mononuclear cells, which once again confirms the property of HA to prevent cells from spreading on the surface.[127,128]

Since it is well known that L929 cells prefer stiffer surfaces,[129] this cell line was used as an indirect method for the assessment of the stiffness of the HA/PLL films in the previously described study of Schmidt[46]. The results were quite fascinating, as L929 mouse fibroblasts not only adhered to the AuNPs-coated films, but the adhesion of the cells improved as *γ* increased (Fig. 2.5B-C). Moreover, the negative effects of AuNPs (e.g. toxicity) on spreading and growth of L929 fibroblasts were not observed, though this parameter was not studied separately. Not only does the AuNPs coatings reinforce the films, it makes them more susceptible for cellular adhesion as well.

As presented in this section, the diversity of cellular behavior is great. In order to use as many cell lines as possible for biomedical purposes, suitable LbL films have to be carefully designed and properly engineered.

2.2.4 Biodegradation

Stability of HA/PLL films in physiological condition, especially in contact with cells, is an issue that requires additional consideration. Degradation of film polymers in physiological conditions by changes in pH, ionic strength, or temperature, or by enzymes can be both a perspective and a hindering property of the film degradability. It depends primarily on the desired application of the film – if the application is towards drug delivery based on film

decomposition, or if LbL film should decompose after a certain time, degradation is a necessity. On the other hand, if endurance is required, degradation is not a welcomed property.

HA/PLL films have been given certain attention in this field as well. The main points of interest are specific enzymatic reactions for the hydrolysis of polymers. For example, a study by Ren and coworkers[130] shows that apart from being a polycationic component in PLL/DNA films, PLL plays a second role in release. The film is exposed to the α–chymotrypsin which digests PLL, and thus loosens the structure of the film which decomposes and releases DNA (Fig. 2.6A). In another research, adding a topical layer of PLL was shown to increase resistance of PLL/PGA films to enzymatic degradation as it most probably modulates the access of hydrolytic enzymes to PGA providing a barrier to digestion.[131]

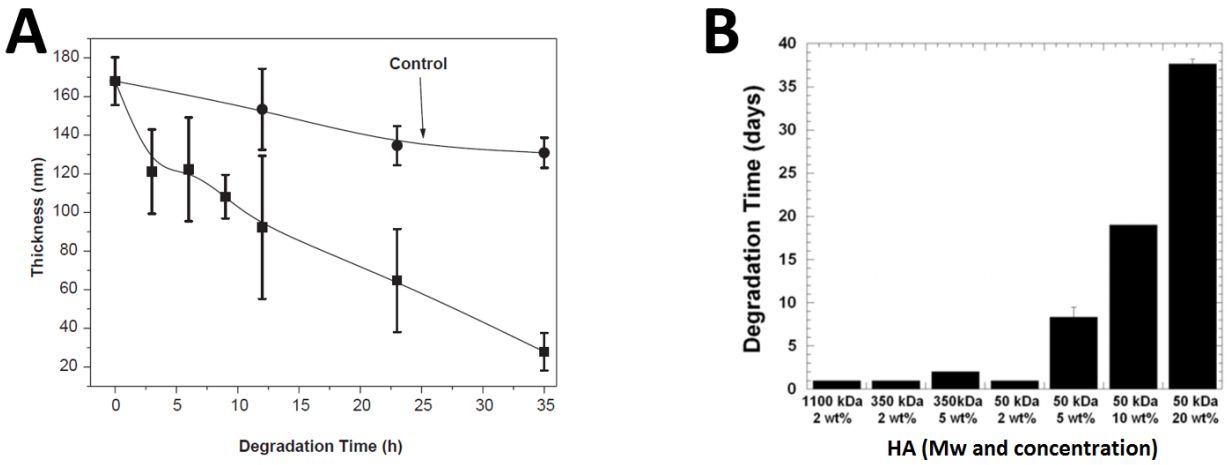

Figure 2.6. Biodegradation of PLL and HA. (**A**) The thickness of PLL/DNA films as a function of PLL degradation time. The upper curve represents the control curve of incubation in PBS without α–chymotrypsin where degradation is reduced. The lower curve represents degradation in PBS with 5 U/mL α–chymotrypsin. Reproduced from [130]. (**B**) Time for complete degradation of HA of different molar masses with 100 U/mL hyaluronidase in PBS, where the hyaluronidase was replenished every other day. Reproduced from [132].

Hyaluronic acid is a substrate for hyaluronidase which is capable of digesting HA even in polymerized films (Fig. 2.6B).[132] A study by Garza and coworkers showed that bone marrow cells degrade HA/PLL films, and even the PLL chains confined in this reservoir (Fig 2.7) are internalized by cells.[133] Apart from these few studies enlisted, information about biodegradation of HA/PLL films is rather limited. These aspects have to be addressed in order to achieve full potential of HA/PLL films for application in cellular stimulation and tissue engineering.

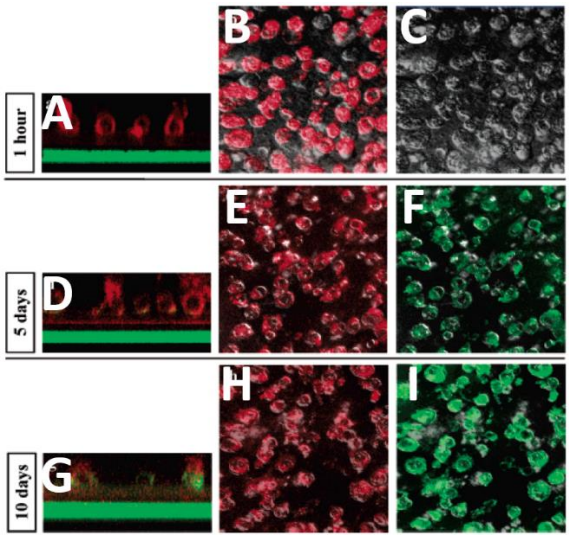

Figure 2.7. CLSM images of bone marrow cells growing on $(PLL/HA)_{30}/PLL^{FITC}/PLGA/(PLL/HA)_{30}/PLL^{Rho}$ films labeled with PLL^{FITC} (bottom part of the film) and PLL^{Rho} (upper part of the film). (**A**-**C**) 1 hour, (**D**-**F**) five days and (**G**-**I**) ten days after seeding. (**A**, **D**, **G**) Lateral view with overlapping green and red channels for visualization of PLL^{FITC} and PLL^{Rho} respectively. (**B**, **E**, **H**) Top view, red channel and (**C**, **F**, **I**) top view, green channel. After 1 h of contact between the cells and the film most of the bone marrow cells have already internalized red PLL^{Rho} located in the upper compartment. No green labeled PLL is internalized by the cells after 1 h despite its presence in bottom parts of the film. After 5 days of contact, the cells start to internalize green PLL^{FITC}. After 10 days both green and red colors are located in the cells. Adapted from [133].

2.3 ATP as an extracellular messenger

The preservation of inner homeostasis is the main prerequisite of a living cell. To do so, a cell must acquire biochemical and physical signals (both internal and external), analyze them, and act correspondingly. The same applies to multicellular tissues and further to all levels of organization of a living system. Intricate molecular relations based on specific binding of signaling molecules to intra- and extracellular receptors induce complex intracellular signaling cascades that converge to regulate gene expression, regeneration, secretion, differentiations etc.[83] The dynamics and versatility of the extracellular signaling is no less astonishing than the versatility of the signaling within a cell. Not only are these two tightly related to each other, but they rather often share same molecular and ionic species. Although each and every signaling molecule originates within a cell, its function may vary depending on its internal or external location. An excellent example is the adenosine triphosphate (ATP), to whose biological role and research application this section is dedicated.

2.3.1 Physiological role

ATP (Fig 2.8), is a nucleoside triphosphate and a ubiquitous compound in all living cells. It is often called the “energy currency” cells - in a process of enzymatically-catalyzed

transfer of one or two of its phosphate groups it provides energy for numerous metabolic reactions.[134] After the reaction, ATP is converted into its precursor and has to be constantly recycled in the cell with the help of ATP-synthase located in the mitochondrial membrane.[135]

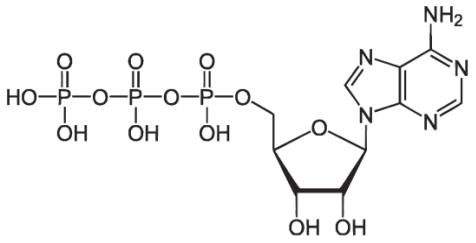

Figure 2.8. The structure of ATP.

Apart from being the main energy source for a variety of biochemical reactions, ATP is involved in signal transduction as a substrate for adenylate cyclases and kinases.[136,137] However, it was also shown that ATP is a crucial signaling species in the extracellular matrix in both plants[138–141] and animals[142–144] alike - this ATP is referred to as the "extracellular ATP" and is involved in numerous cellular processes such as immune response, cell growth, neurotransmission, cell death, motility, secretion, etc.[145] This came as no surprise as purine and pyrimidine nucleotides such as ATP, which contains a purine base adenine, represent a primordial and ubiquitous class of intracellular chemical messengers[146] - when exposed to osmotic shock, mechanical stress, hypoxia etc. cells secrete nucleotides including ATP into surrounding milieu.[147] In mammalian cells two families of P2 nucleotide receptors located in the plasma membrane bind ATP (as well as other nucleotides) released from nearby cells – the family of ligand-gated ion channel P2X and the P2Y family of G-protein-coupled receptors[148,149] The P2 receptor network regulates signaling duration and intensity over a wide range of extracellular ATP by modifying and controlling the concentration of intracellular secondary messengers, primarily intracellular Ca^{2+} (iCa^{2+}).[150] The high sensitivity and broad range of detectable ATP concentrations is facilitated by seven subtypes of the P2X family ($P2X_{1\text{-}7}$) and eight subtypes of the P2Y family ($P2Y_{1,2,4,6,11\text{-}14}$), from which all have different binding affinities for ATP.[150]

2.3.2 Ca^{2+} signaling

The accurate coordination of Ca^{2+} signal between cells in a multi-cellular system is crucial for the efficacy and synchronization of tissue and organism functions.[151] Thus, the propagation of increased intracellular calcium concentration, [iCa^{2+}], between neighboring cells occurs widely among animal cell lines and tissues.[152–155] A part of [iCa^{2+}] increase is due to the reaction cascade started by the binding of extracellular ATP to membrane-localized P2 receptors.[150] Extracellular ATP binds to ionotropic P2X receptor and alters the conformation of the P2X protein, which enables influx of Ca^{2+} from outside into the cell through the ion channel that is a part of the P2X receptors.[149] On the other hand, after binding of extracellular ATP to the P2Y family of receptors, the G-protein that is bound on the cytosolic side of the seven-transmembrane-domain P2Y receptor is activated.[148] The recruitment of

heterotrimeric G-protein and phospholipase C (PLC_β) triggers a cascade of cytoplasmic signaling reactions that finally leads to the release of Ca^{2+} from the endoplasmic reticulum into the cytosol and increase of [iCa^{2+}].[148] The schematics of calcium signaling network stimulated by extracellular ATP is given in Fig. 2.9.

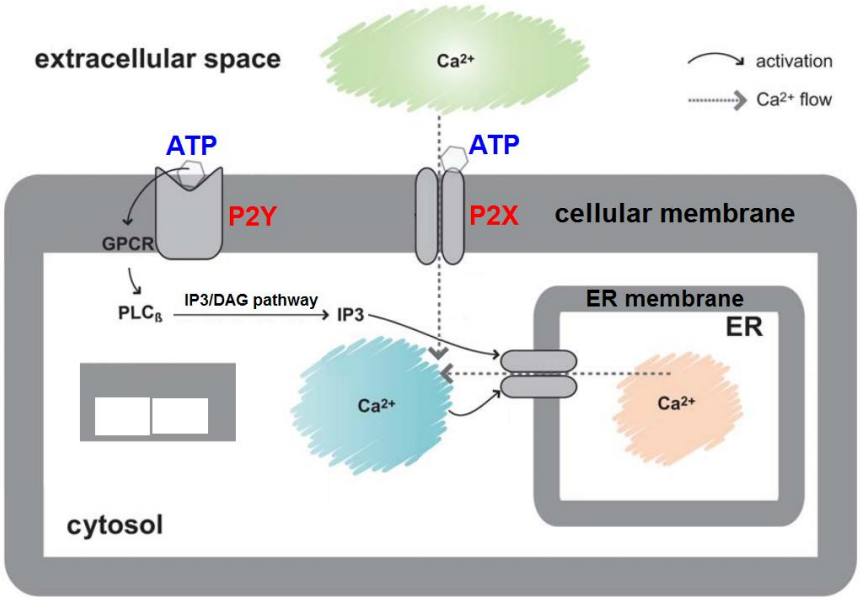

Figure 2.9. Schematics of calcium signaling network evoked by extracellular ATP. Intracellular calcium can be increased either by Ca^{2+} influx from the extracellular surrounding or by the release from endoplasmic reticulum (ER) which is the intracellular storage of calcium ions. From the surrounding milieus, Ca^{2+} enters the cell through P2X family of ligand-gated cation channel after binding of extracellular ATP to P2X receptors. At the same time, extracellular ATP binds as well to P2Y receptors, which are G-protein-coupled receptor (GPCR), activating membrane-bound phospholipase C (PLC_β). After the onset of PLC_β a complex biochemical pathway called IP3/DAG pathway is activated to finally produce inositol triphosphate (IP3) which triggers the opening of ion channels in the ER membrane and subsequent release of Ca^{2+} into cytosol. Adapted from the work of Song and Varner.[156]

The omnipresence of Ca^{2+} as a secondary messenger and the wide span of biochemical reactions it is involved in make it a perfect, both direct and indirect, indicator of cellular processes. The importance of understanding the role of Ca^{2+} ions in cellular signaling is fundamental for comprehending the integrity of a living cell. Thus the determination of iCa^{2+}, using fluorescent calcium-specific dyes in the first place, has since long been considered a standard biochemical method.[157]

2.3.3 Caged ATP

Caged compounds belong to the group of light-sensitive compounds that contain a functionally inactivated biomolecule.[158] This inactivation is usually achieved through a photolabile covalent bonding of the biomolecule of interest with a caging molecule. Upon irradiation the bond breaks, allowing the biomolecule to retrieve its activity and fulfill its biological role. The whole concept was developed by exploiting photomanipulation of cellular chemistry in order to ease the delivery of many second messengers that do not

readily enter the cell (e.g. IP3, Ca^{2+}, cAMP, nucleotides, peptides, nucleic acid).[158] Furthermore, the idea came quite convenient for stimulation of neuronal cells with neurotransmitters and hormones. Thus, numerous bioactive species have been caged so far: peptides,[159,160] enzymes,[161–163] mRNA and DNA,[164,165] inositols,[166] nucleotides,[167,168] and calcium[169,170].

Being a very import extracellular messenger ATP was one of the first biomolecules inactivated by caging to be used. One of its first application was as a substrate for Na^+:K^+ pump in red blood cells.[167] It all started as the terminal phosphate group of ATP was coupled to 2-nitrobenzyl or 1-[(2-nitro)phenyl]ethyl groups (NB-ATP and NPE-ATP) and the resulting bond was unstable when irradiated with light.[167] This instability was exploited as a mechanism of activation of ATP locked within caged ATP species (cATP) (Fig. 2.10.). Since then caged ATP species found their application in chemical, biochemical, biological, and immunological fields of research. To fully exploit the potential of caging chemistry and biological photomanipulation numerous new caged ATP species were synthetized and employed. ATP was coupled to the 2-(4-hydroxyphenyl)-2-oxo]ethyl group (pHP-ATP) and used as rapid on-demand activator of Na^+:K^+-ATPase.[171] Furthermore, NPE-ATP has been shown to be very useful for the study of vesicular adsorption,[172] conformational changes in proteins,[173] interactions among neuronal cells,[174,175] etc. For the inhibition of contraction speed in muscle fibers the ester of 3',5'-dimethoxybenzoin and ATP (DMB-ATP) was used.[176,177] ATP esters with [7-(dimethylamino)coumarin-4-yl]methyl (DMACM-ATP),[178] desyl (desyl-ATP),[171] and P^3-(1-(4,5-dimethoxy-2-nitrophenyl)ethyl) (DMNPE-ATP)[179,180] have also been used as light sensitive sources of ATP.

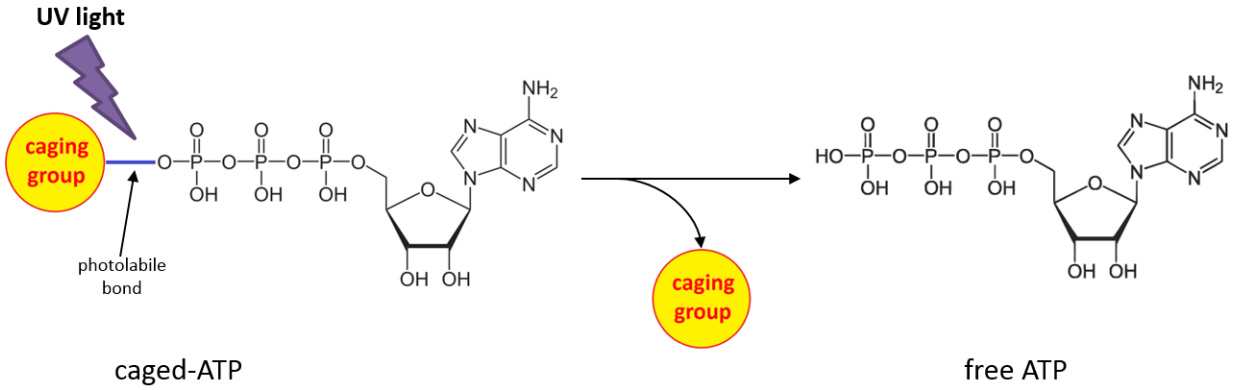

Figure 2.10. Structure of caged ATP and the mechanism of the uncaging. Caging group is bound to the terminal (tertiary or *γ*) phosphate group of ATP through an ester linkage. In this manner ATP loses its biological role as the hydrolysis of terminal phosphate, the main carrier of ATP bioactivity, is hindered. After the UV light-induced cleavage of the photolabile ester the ATP molecule recovers its bioactivity. Details about the variety of caging groups are given in the main text above.

The light-induced uncaging process, i.e. the release of ATP from its caged form is basically identical for all cATP compounds, as most caging groups are derivatives of the aromatic 2-nitrobenzyl group or its structural analogues.[181] Near-UV light (340 nm – 405 nm) is required for the heterolytic cleavage of the bond, depending on the exact

electronic properties of the caging compound.[167,178,181] Most of uncaging experiments use either lasers which deliver exact wavelength required for the bond cleavage, or flash lamps such as pulsed mercury and xenon arc lamps.[158] Despite their disparate bioapplication in the last few decades, a strong feeling prevails that the complete potential of caged ATP compounds is yet to be discovered and utilized in the fields of biosciences and bioengineering of cells and tissues.

2.4 Approaches for light triggered release

The constantly developing techniques for the manipulation of cells and tissues require inventive approaches as boundaries are being pushed every day. However, in spite of all progress made in this field certain challenges remain, especially when it comes to the non-invasive stimulation of cells. The term “low-invasive stimulation” here implies the delivery of bioactive molecule from a carrier, either extra- or intracellular, in a manner that will produce solely the anticipated effect, evading non-desired outcomes, with minimum or no interference with a cell which must remain intact and non-damaged. These challenges are met by introduction of different drug carriers such as LbL films and capsules[63] that withhold the stored drug until a highly specific stimulus changes physicochemical properties of the carrier, upon which the bioactive drug is released and made available to the cell. As well, it is to bear in mind that most drug carriers are based on polymers, liposomes, and/or their hybrid counterparts which contain metal ions.[182]

The simplest method used was the degradation of the carrier. The erosion of the polymer film or liposome carrier is hydrolytically driven and the hydrolysis is either the consequence of inherent properties of carrier constituents or is induced by changes in the surrounding milieu.[54,62,183] For example, enzymes such as pepsin can erode alginate films.[184] Capsules for intracellular drug delivery assembled from HA and PLL were also reported to be biodegradable.[185] Changes in ion concentration and pH affect charged groups of polyelectrolytes, weakening interpolymer interactions and changing the way stored molecules interact with the charged groups of the carrier.[27,186–188] Furthermore, changes of electric field as well as of temperature have been applied as drug release stimuli.[73,189]

All the methods developed so far necessarily introduce changes in the surrounding medium and none of them is non-invasive. Special attention should be paid to approaches that neither alter the medium nor affect cells. In this aspect, features of light and the feasibility of application of light as a non-invasive stimulus for drug release and stimulation of cells are considered in this section.

2.4.1 Light as a release stimulus

Nowadays considerable efforts are exerted in order to design more efficient and non-invasive systems for drug delivery to cells. Using light to achieve spatiotemporal control over chemistry and to photomanipulate biological systems has revolutionized the field of bioscience. Light-responsive carriers[190–193] offer the option to control the availability of any biomolecules they carry. The control is achieved without the need for modification of either medium or the structure of the carrier. A versatile tool like this provides infinite potential to deepen the fundamental understanding of physiological processes and to design novel technologies for highly coordinated and controlled drug release.

Light-sensitive techniques must offer application of electromagnetic radiation that does not affect cells in harmful way. Generally, near-IR and UV light is applied to release the drug to cells, thus providing a method for controlled release at locations which would otherwise be hardly achievable by other means such as pH, salt, temperature, etc.[194]

The mechanism of near-IR triggered release is based on heating. Incorporated metal nanostructures are good candidates for generating heat after irradiation with IR - the heat loosens the surrounding polymer matrix rendering it porous and permeable for the release of therapeutics.[195,196] For example, AuNPs embedded in the liposome or capsule absorb near-IR and convert it to heat which alters the permeability of liposome membrane, allowing the content to diffuse out.[197] This concept allows further variations such as remote near-IR-triggered release of DNA from PEM containing AuNPs (Fig 2.11).[198] It has also been shown that if AuNPs are not uniformly distributed, but are rather dispersed heterogeneously in form of aggregates, at distances less than few tens of nanometers from the irradiation point temperatures decreases readily to the levels prior to the experiment.[199] However, this approach remains controversial due to toxicity of metal nanostructures and due to generation of harmful amounts of heat.[200–202]

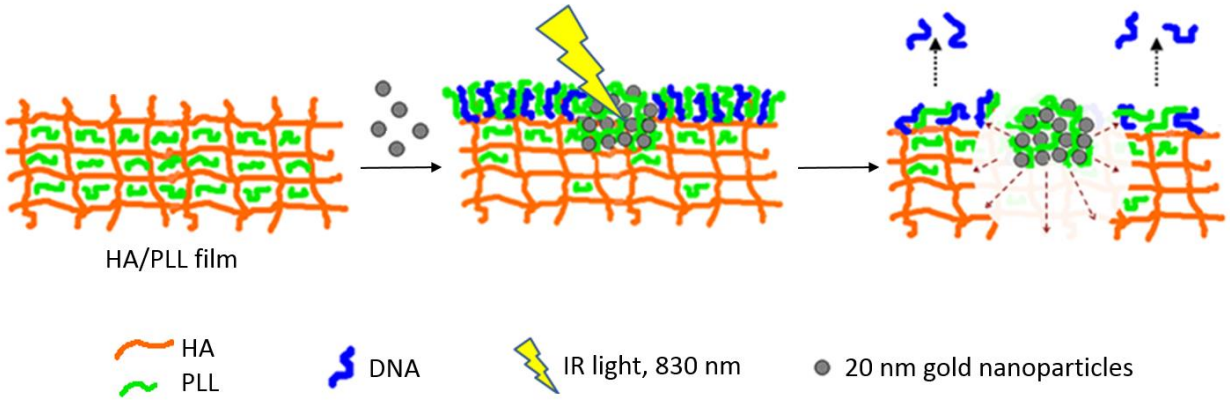

Figure 2.11. Schematics of the proposed IR-induced release of stored payload (DNA) from the films composed of HA and PLL. Adapted from a recent review of Volodkin *et al.*, 2014.[63]

As an alternative, carriers are assembled from IR light-sensitive components which after irradiation with IR light undergo chemical changes such as dimerization, bond cleavage,

oxidation, and isomerization.[190,203] Even this approach is not deprived of drawbacks, as due to low energy of near-IR light both high-power pulsed lasers and simultaneous two photon absorption are required which often results in biological damages far beyond the regeneration point.[204,205] In a recent paper[206] authors suggested that near-IR-induced heating of confined water in non-light-sensitive polymeric particles allows controlled release of payload from particles (Fig. 2.12), albeit uncompromised biocompatibility has not been shown. Another method overcomes the problematic IR activation by using upconverting nanoparticles that absorb photons and convert them into lower wavelength-higher energy UV photons.[206,207] UV light is then used to uncage and release bioactive compounds. The main limitation is toxicity, as upconverting nanoparticles contain heavy metal ions.[208] As a conclusion, the field of near-IR-triggered release unfortunately still has many challenges and is applied primarily for capsules and micelles, but not for native PEMs.

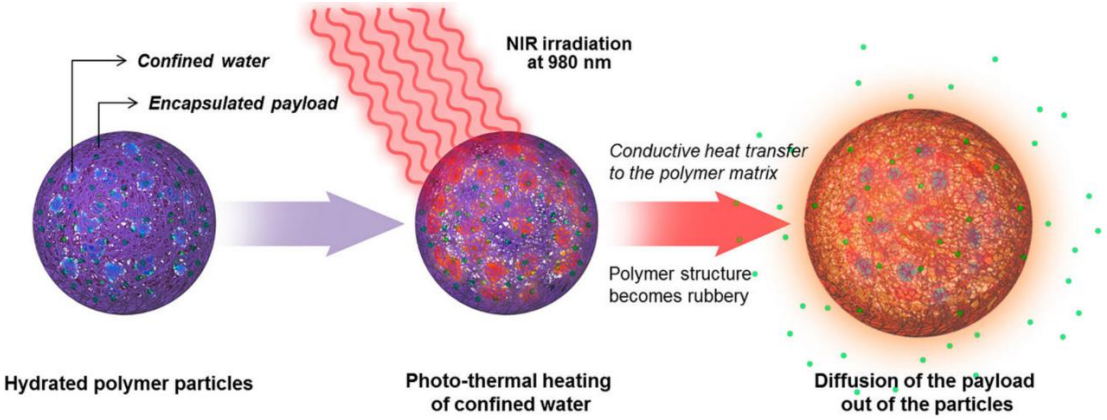

Figure 2.12. Release of encapsulated payload following photothermal heating of water droplets inside the polymer particles. Adapted from the work of Viger *et al.*, 2014.[206]

On the other hand, the application of UV light for remote drug delivery to cells is only scarcely exploited due to its harmfulness to cells and tissues and is thus limited only to photosensitive chemical reactions. The application of UV light for drug release has so far been limited to UV light-induced destruction of capsules[209], degradation of polymers through bond cleavage[210–212], increase of carrier's pore size,[213] and *cis-trans* isomerization of polymers containing azobenzene groups or some other photoisomerization chromophores followed by consequential bursting of capsules.[214,215] Another strategy for implementation of UV light is uncaging of caged compounds which are added to the bulk and subsequently uncaged. However, these approaches bear the jeopardy of damaging cells, as UV-sensitive drug carriers are ubiquitous in the supernatant and thus the whole system, including cells, has to be irradiated in order to deliver drugs.

2.4.2 Stimulation of cells using light-triggered drug release

Apart from a single report[216] about light-triggered drug release using light in the visible range, near-IR and UV light remain the most exploited areas of the electromagnetic spectrum for triggering drug release and stimulating cells. Based on the location of drug

reservoir methods could be divided into two groups: methods for intracellular delivery and methods for extracellular delivery.

Intracellular drug delivery is based on cellular internalization of drug carriers and subsequent remote-controlled release of drug using biofriendly near-IR light. Capsules composed from PDADMAC and PSS were absorbed by cells and have released their cargo upon irradiation with near-IR; near-IR caused local disruption of capsules resulting in leaking/release of stored molecules into the cytosol.[217] Similarly, combination of PSS and poly(allylamine hydrochloride) (PAH) allows formation of capsules that deliver fluorescently labeled dextrans intracellularly (Fig. 2.13).[218] Furthermore, transfection (gene delivery to cells) was achieved with gold nanoparticles-doped HA/PLL films by application of 825 nm IR light.[111] Nonetheless, in spite of their attractiveness, these methods fail to offer localized extracellular delivery.

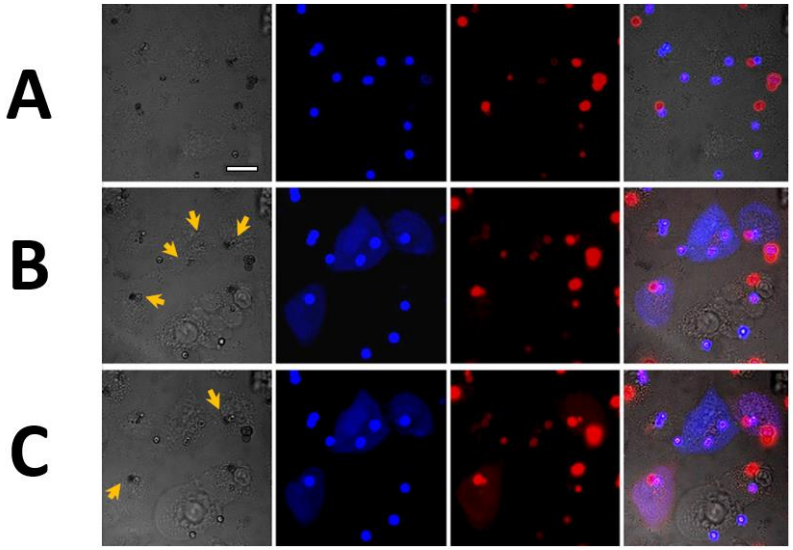

Figure 2.13. Phase contrast, fluorescence and overlay images (from left to right) of A549 cells (**A**) before, (**B**) after the opening of $(PSS/PAH)_2/Au/(PSS/PAH)_2$ capsules loaded with 10 kDa Cascade Blue-dextran, and (**C**) after the opening of capsules loaded with dextran-tetramethylrhodamine. Capsules had Au nanoparticle agglomerates embedded within their walls. They were illuminated with an 830 nm laser during few seconds. Both cargo molecules (blue and red fluorescence modified dextran) were released in the cytosol. The scale bars represent 20 µm. Arrows mark irradiation points. Adapted from [218].

Extracellular drug delivery implies that the drug carrier is located outside the cell. Due to its toxicity towards cells and tissues UV light cannot be applied for intracellular delivery, but is on the other hand readily exploited for drug carriers outside cells. Especially in the field of neurosciences, application of UV light has made a breakthrough in extracellular uncaging and release of neurotransmitters.[216,219] Ligands for acetylcholine receptors,[220] glutamate analogues,[221] glutamate and other neuroactive amino acids,[222] and caged nucleotides,[178] etc. have already been used to stimulate cells by increasing iCa^{2+} after the UV-light has been applied (Fig. 2.14).

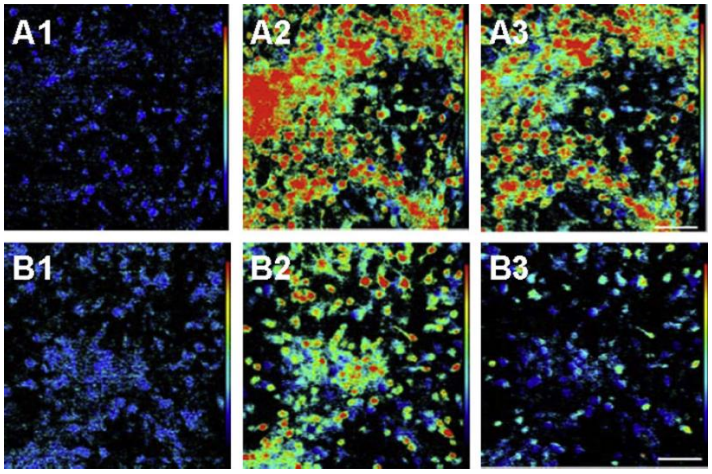

Figure 2.14. Activation of NMDA receptors (glutamate sensitive receptors) by UV-triggered photolysis of caged glutamate is crucial to the increase of [iCa^{2+}] and neuronal death in the flashed area. (**A, B**): Representative images of changes of [iCa^{2+}] at three different time points: 10 s before the exposure to UV (**A1, B1**), and 10 s (**A2, B2**) and 30 s (**A3, B3**) after the flash. (**B1–B3**) show changes in [iCa^{2+}] when the co-cultures were treated with 100 µM inhibitor of NMDA receptors. [iCa^{2+}] increases from dark blue to red through yellow (the color bar on the right represents the relative intensity scale). The scale bar is 100 µm. Adapted from [223].

However, all these extracellular techniques are based on uncaging and release from the bulk, meaning that there extracellular delivery cannot be controlled in terms of concentration,[224] and cannot provide sufficient, if any, spatio-temporal precision.[223] At the same time, since caged compounds are in the bulk and UV-light must be irradiated above whole sample, there is a considerable chance of cell damage.

Considering all the facts presented so far, a challenge remains to develop a comprehensive cell stimulation assay that in the first place combines 1) cell-growth support that acts as a local reservoir for drugs (ECM mimic) and 2) light-triggered delivery of drugs stored in the reservoir. At the same time, the assay should be non-harmful to cells and should provide highly localized delivery with a possibility of single cell stimulation. The overall control of spatio-temporal characteristics of the cell stimulations is another challenge. Thus, this study is dedicated to the design of LbL films with the reservoir capacity and with the option for controlled extracellular light-triggered release.

3 MATERIALS AND METHODS

3.1 Materials

Chemicals

Poly(ethyleneimine), 750 kDa	Sigma-Aldrich, Germany	181978
Sodium-hyaluronate, 360 kDa	Lifecore Biomedicals, USA	H500K
Poly-L-lysine hydrobromide, 15-30 kDa	Sigma-Aldrich, Germany	P7890
Poly-L-lysine hydrobromide, 150-300 kDa	Sigma-Aldrich, Germany	P1399
Poly-L-lysine - FITC labeled, 15-30 kDa	Sigma-Aldrich, Germany	P3543
Dextran - FITC labeled, 10 kDa	Sigma-Aldrich, Germany	FD10S
Dextran - FITC labeled, 70 kDa	Sigma-Aldrich, Germany	FD70S
Dextran - FITC labeled, 500 kDa	Sigma-Aldrich, Germany	FD500S
5(6)-carboxyfluorescein	Sigma-Aldrich, Germany	21877
Rhodamine 6G	Sigma-Aldrich, Germany	R4127
Hydrochloric acid fuming, 37 %	Merck Millipore	100317
Trizma base (Tris)	Sigma-Aldrich, Germany	T1503
Sodium chloride	Sigma-Aldrich, Germany	S5886
Gold colloid, diameter 5 nm (gold nanoparticles) conc. 0.01 %, stabilized with Na-citrate.	Sigma-Aldrich, Germany	G1402
Adenosine-triphosphate (ATP)	Sigma-Aldrich, Germany	A2383
DMNPE-caged ATP	Life Technologies, Germany	A-1049
NPE-caged ATP	Life Technologies, Germany	A-1048
DMB-caged ATP	Biorbyt, UK	orb63984

Cell lines

L929	Mouse fibroblasts (subcutaneous)	ACC 2, DSMZ, Germany
SH-SY5Y	Human neuroblastoma	ACC 209, DSMZ, Germany
HEK-293	Human embryonic kidney	ACC 305, DSMZ, Germany
3T3	Mouse fibroblasts (embryo)	ACC 173, DSMZ, Germany
HeLa	Human cervix carcinoma	ACC 57, DSMZ, Germany

Cell culturing media, buffers, kits, and solutions

Dulbecco's Modified Eagles' Medium (DMEM) HEPES modification	Sigma Aldrich, Germany	D6171
Foetal Bovine Serum (FBS)	Biochrom, Germany	S0115
L-alanyl -L-glutamine (200 mM), low endotoxin	Biochrom, Germany	K0302
Trypsin/EDTA solution	Biochrom, Germany	L2143
Phosphate-buffered saline, PBS, (Dulbecco) without Ca^{2+}, Mg^{2+}	Biochrom, Germany	L1820
Phosphate-buffered saline, PBS, (Dulbecco) with Ca^{2+}, Mg^{2+}	Roth, Germany	9131.1
Penicillin / Streptomycin (10,000 U/ml /10,000 µg/ml)	Biochrom, Germany	A2212
Propidium iodide in physiological saline	Merck, Germany	537059
ATP determination kit (luciferase assay)	Life Technologies, Germany	A22066

Miscellaneous

Round coverglass, 12 mm and 14 mm	Marienfeld, Germany	0111520, 111540
Sterile syringe, Luer Lock Solo 10 mL	B. Braun, Germany	461 7100 V
Sterile syringe filter (0.45 µm)	Corning, Germany	431225
Sterican 0.40 x 20mm needle	B. Braun, Germany	4657705
Hellmanex II	Hellma Analytics, Germany	9-307-011-4-507
CSC 12 tipples cantilever	Mikromasch, Estonia	
OMCL-AC160BN-A2 cantilever	Olympus, Japan	
Nunc 2-well chamber	Nunc, Germany	155380
Thoma Neubauer chamber	Carl Roth GmbH & Co. KG, Germany	
Polystyrene cuvettes 10x10x45 mm	Sarstedt, Germany	67.654

Instruments

Layer -by-layer deposition robot	Riegler and Kirstein GmbH, Germany
NanoWizard 1 AFM	JPK Instruments AG, Germany
LSM 510 Meta Confocal Laser Scanning Microscope	Carl Zeiss Microimaging GmbH, Germany
LS55 fluorometer (luminescence spectrometer)	Perkin Elmer, UK
DM IL - inverted phase contrast microscope	Leica Microsystems, Germany
PALM Comby system	Carl Zeiss, Germany
NanoWizard I AFM microscope	JPK Instruments AG, Germany
FLUOstar Omega	BMGlabtech GmbH, Germany
Blue point UV lamp	Hoenle, Germany
Plasma cleaner	Harrick Plasma, USA
CO_2 incubator	Binder GmbH (VD 23), Germany
Gamry eQCM 10M	Gamry Instruments, USA
Zetasizer Nano ZS	Malvern Instruments Limited, UK

Software

LSM Image Browser (Version 4.2)	Carl Zeiss Microimaging GmbH, Germany
ImageJ (Version 1.46r)	National Institute of Health, USA
Image Pro Plus (Version 4.1.0.0)	Media Cybernetics, USA
OriginPro (Version 9.1G)	Origin Lab, USA
Gwyddion (Version 2.34)	Czech Metrology Institute, Czech Republic
JPK Data Processing	JPK Instruments AG, Germany

3.2 Film preparation and characterization

3.2.1 Film assembly by LbL dipping technique

HA/PLL films were prepared using an automated dipping robot. Stock solutions of polyelectrolytes (PLL, HA, PEI) were prepared at a concentration of 5 mg/mL in a Tris buffer which consist of 10 mM Tris, 15 mM NaCl, pH 7.4. Dry HA was dissolved by heating its solution at 60 °C for 15-20 min under constant stirring in order to completely dissolve it; dissolution of PLL and PEI did not require heating. Solutions were filtered through a 0.45 µm

syringe filters to remove impurities and stored at -20 °C. Polymer solutions for deposition were obtained by 10 x dilution in Tris buffer of stock solutions to get a final concentration of 0.5 mg/mL.

Glass slides (12 mm or 14 mm) used for the film deposition were inserted into a specially designed Teflon holder which accommodates eight glass slides. They were cleaned by subsequent incubation in 2 % Hellmanex, then two times in 1 M HCl, and finally two times in water to remove remaining detergent and acid. Each step was done at 60 °C under constant stirring for 20 min.

Fabrication of the films was done at ambient conditions (22 °) by alternating dipping of cleaned glass slides into solutions of positively charged PLL and negatively charged HA for 10 minutes, with intermediate rinsing thrice with Tris buffer (3 minutes each, totally 9 min of washing) until desired number of bilayers (bL) was achieved. Before the actual start of the HA and PLL deposition, a precursor layer of PEI was deposited (as glass is slightly negatively charged), followed by a repetitive sequence of HA and PLL depositions. HA/PLL films composed from 12, 24, and 96 bL were produced.

Majority of the experiments were done with films terminated with PLL, however some experiment required HA as the terminating layer, so the film architecture was either $(HA/PLL)_n$, or $(HA/PLL)_n/HA$, where *n* represents the number of bL.

Films were stored in Tris buffer at +4 °C and were stable for at least one week as proven by the optical analysis.

3.2.2 Film labeling with PLL^{FITC}

To prepare fluorescently labeled films, commercially available FITC-labeled PLL 15-30 kDa (PLL^{FITC}, FITC : amino group label ratio 1 : 100) was added to PLL solution reaching 2 % of unlabeled polymer by mass.

3.2.3 Coating with gold nanoparticles

Coating with 5 nm colloidal gold (gold nanoparticles, AuNPs) was done as described elsewhere [46]. Briefly, 24 h incubation of films with AuNPs dispersion was conducted at ambient conditions, followed by rinsing and storage in the Tris buffer.

Different concentrations of AuNPs were used for coating, resulting in different amounts of AuNPs deposited on the film surface – the amount is expressed as number of monolayers (γ) and one monolayer is required to fully cover the surface of the film assuming that the nanoparticles are closely packed.[46] To achieve $\gamma = 1$ for the film (14 mm diameter), 200 µL of dispersion is required; for $\gamma = 1.5$ and $\gamma = 3$, 300 µL and 600 µL of dispersion were used, respectively.[46]

3.2.4 Introducing the scratched area

A scratched area was introduced manually using a Sterican 0.40 x 20 mm needle. An X-shaped pattern was introduced on assembled films, and it was done before AuNPs coatings as doing it afterwards results in rupturing of the whole film.

3.2.5 Microscopic observation

Films were optically analyzed using Leica DM IL - inverted phase contrast microscope, or with LSM 510 Meta Confocal Laser Scanning Microscope (CLSM) in case they were labeled or loaded with fluorescent molecules.

3.2.6 Thickness measurement

NanoWizard I atomic force microscopy (AFM) head mounted on the Olympus IX51 optical microscope was used for determination of the film thickness. A part of the HA/PLL film was scratched with a needle to produce X-shaped scratched area. The scratched area was analyzed in Tris buffer using an OMCL- AC160BN-A2 cantilever in tapping (AC) mode. The size of the scan was varied, and the scan rate was 1 Hz. Film thickness was calculated using cross sections of the AFM micrographs. AFM imaging was done in triplicate at different positions in the middle area of the film.

3.2.7 Analysis of the mechanical properties using colloidal probe AFM

AFM was used for the thickness measurement. The method described in the paper of Schmidt and coworkers[46] was used. Briefly, native HA/PLL films without scratched area were mapped in Tris buffer by a series of AFM force-distant curves for the determination of elastic modulus. An uncoated Mikromasch CSC 12 silicon cantilever (nominal spring constant of 0.2 N/m) with a silica probe particle (diameter 20 µm) attached to the apex of the cantilever was used. Hertz-Sneddon Force-Deformation theory was used for the evaluation of the force curves. Prior to the measurement, the cantilever with the attached colloidal probe was rinsed with ethanol and water, followed by plasma cleaning. Scans were done in multiplicate on different points on the film and the size of the scan area, as well as the grid size were varied, 10 x 10 – 100 x 100 μm^2 and 8 x 8 – 32 x 32 data points, respectively.

3.3 Loading and release of molecules

3.3.1 Loading of SCM

Loading of small charged molecules (SCM) was done by incubation of HA/PLL films assembled on 14 mm round glass slides in 1 mL of 5(6)-carboxyfluorescein (CF), rhodamine 6G (Rho) or adenosine-triphosphate (ATP) solution in Tris buffer. Concentrations of the SCM were varied depending on the requirements of the experiment from 1 µM to 100 µM.

Incubation was done in wells of 24-well plates for 24 h at ambient temperature. As a control, a bare glass slide was incubated under the same conditions to check potential adsorption by a glass slide and/or a well. After incubation, the supernatants containing non-loaded SCM were preserved at +4 °C for determination of SCM concentration.

3.3.2 Release of SCM

After loading, HA/PLL films were washed by brief dipping three times in Tris buffer to remove traces of loading solutions from the film. Upon washing, films were immersed in 1 mL of Tris buffer to monitor release. At predefined time points, the whole supernatant (1 mL) was collected and preserved at +4 °C for later determination of SCM concentration and new 1 mL portion of Tris buffer was added. Normally, buffer was replaced a few times during the first 90 minutes of the release and once every 24 h afterwards. By constant buffer replacement perfect sink conditions can be simulated, i.e. as if administered drug molecules were distributed throughout an organism/present *in vivo* were simulated.

3.3.3 Determination of the SCM

The loaded amount of SCM was calculated as the difference between amounts of the SCM left in the loading solutions for the bare glass slide and the film after 24 h incubation:

$$n_{loaded} = \frac{(C_0 - C_f) - (C_0 - C_{cg})}{V}, \quad \text{or simplified} \quad n_{loaded} = \frac{C_{cg} - C_f}{V},$$

where n_{loaded} represents amount (in moles) of the SCM loaded into the film; C_0 (mol/dm^3) represents initial loading concentration; C_f is the SCM concentration in the loading solution after the loading; C_{cg} is the concentration in the glass slide-loading solution after loading; V is the loading volume, 1 mL.

Loading efficiency (LE in the formulae below) is expressed as ratio of the loaded SCM amount against initial SCM amount in the loading solution and is calculated as:

$$\mathrm{LE} = \frac{n_{loaded}}{n_{total}}, \text{ and since volume is identical } \mathrm{LE} = \frac{C_{cg} - C_f}{C_0}$$

Amount of the released SCM was measured in the aliquots collected for each time point of the release. The total release at a certain point in time was presented as the sum of the amounts released in all time point before and including this certain point.

CF determination - CF exhibits fluorescence with the excitation peak at 492 nm, and the emission peak at 512 nm, thus allowing direct determination using a fluorometer. 200 µL samples were added to the 96-well plate and analyzed using the FLUOstar Omega fluorometer, excitation filter 485 nm, emission filter 520 nm. Tris buffer was used as a control. If the expected concentration of CF in the sample was above 5 µM, the samples were diluted to max 2.5 µM in order to maintain CF concentration in the linear part of the calibration curve.

Rho determination - Similarly to CF, rhodamine 6G is fluorescent (excitation at 526 nm, emission at 515 nm) and can be determined directly. 200 µL samples were added to the 96-well plate and analyzed using the FLUOstar Omega fluorometer, excitation filter 526 nm, emission filter 590 nm. Tris buffer was used as a control.

ATP determination - Unlike CF and Rho, ATP is not a chromophore and can be determined only indirectly, measuring luminescence that is produced during ATP consumption by a luciferase. Mechanism of reaction includes oxidation of luciferin catalyzed by luciferase which produces light at the cost of consumption of one ATP molecule:

$$\text{Luciferin} + \text{ATP} + O_2 \xrightarrow{\text{Luciferase, } Mg^{2+}} \text{oxyluciferin} + \text{AMP} + \text{pyrophosphate} + CO_2 + \text{light}$$

Commercially available luciferase assay is used to determine ATP. Briefly, standard reaction solution consisting of the reaction buffer (Tricine, $MgSO_4$, EDTA, Na-azide, pH 7.8), dithiothreitol, D-luciferin, and firefly luciferase is added to samples containing ATP. After 15 min incubation in the dark at ambient conditions, the luminescence is measured using luminescence mode of the FLUOstar Omega fluorimeter.

For each CF, Rho, or ATP measurement a new calibration curve with 12 concentration points was measured.

3.3.4 Real time monitoring of ATP and cATP loading using QCM

$(HA/PLL)_5$ films were prepared in Hettich eCell T with Gamry eQCM 10M. Quartz crystal microbalance (QCM) chips used as a substrate for polymer deposition were cleansed by rinsing with 10 % EtOH, then with 2 M NaOH and MilliQ water, followed by 60 min of O_2 plasma cleaning. Prior to use, they were additionally rinsed with 2 M NaOH and then with Tris buffer in the QCM chamber. The microfluidic system of the QCM was cleaned with 2 M NaOH, followed by MilliQ water, and then purged with air.

The deposition of films was done as described in the Table 3.1. (note that Tris buffer was always being pumped, either at a “rinse” flow rate or a “deposition” flow rate). After deposition of the film, 1 µM ATP or 1 µM DMNPE-ATP was passed through the system at a flow rate of 45 µL/min along with 5 µL/min Tris buffer until a mass plateau was reached (film saturated).

Table 3.1. Parameters for deposition of HA/PLL films and loading of ATP and cATP in a QCM chamber.

step	duration	Tris buffer flow rate	polymer	polymer flow rate
1. washing	4 min	50 µL/min	/	
2. PEI deposition	12 min	5 µL/min	PEI	45 µL/min
3. washing	8 min	50 µL/min	/	
4. HA deposition	4 min	5 µL/min	HA	45 µL/min
5. washing	8 min	50 µL/min	/	
6. PLL deposition	4 min	5 µL/min	PLL	45 µL/min
7. washing	8 min	50 µL/min	/	
steps 4.-7. are cyclically repeated until desired number of HA/PLL bilayers is deposited				

3.4 Analysis of the CF - film interaction

3.4.1 Measurement of the CF spectra

Excitation and emission spectra of 1 µM, 10 µM, and 100 µM CF solutions in Tris buffer were taken. Furthermore, excitation and emission spectra of CF loaded in $(HA/PLL)_{24}$ films were determined by placing the films sidewise in the cuvette, making sure the light beam goes directly through the film (Fig. 3.1A). The films were loaded with CF by incubation in 1 µM, 10 µM, or 100 µM CF solutions, as described above. As the control, non-loaded $(HA/PLL)_{24}$ were used. Spectra were recorder using a LS55 luminescence spectrometer.

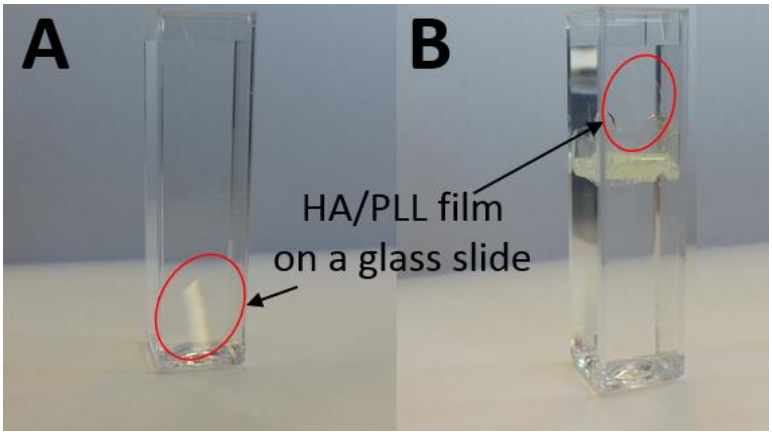

Figure 3.1. Position of a HA/PLL film deposited on a 12 mm glass slide (A) on the bottom and (B) in the upper part of a cuvette.

Furthermore, spectra of CF in CF solutions containing PLL were measured. Concentration of CF was kept fixed at either 5 µM or 300 µM, and PLL concentration was varied to obtain different ratios between number of the lysine monomer units (Mr = 209) in PLL and CF molecules. 5 µM CF solutions with the following PLL : CF ratio were made: 957, 478, 191, 96, 48, 19, 9.6, 4.8, 1.9, 1, 0.5, 0.2. 300 µM CF solutions with the following PLL : CF ratio were made: 42, 10, 5, 2, 1, 0.5, 0.2, 0.1.

3.4.2 Real time observation of CF loading into the film

The upper half of a 10 x 10 x 45 mm polystyrene cuvette was modified in order to accommodate 14 mm glass slides - the light beam of the fluorimeter did not have any obstacles while passing through the cuvette (Fig. 3.1B). Fresh $(HA/PLL)_{24}$ films deposited on 14 mm glass slides were placed in the cuvette with 4 mL of Tris buffer. At regular predefined time points 150 µL of the solution from the cuvette was removed and kept for subsequent analysis, and 150 µL of CF stock solution (20 µM in Tris buffer) was added to the cuvette. The process was repeated until the final CF concentration in the cuvette was near to 10 µM - 18 steps were required to achieve 9.95 µM. The process of loading was monitored in real time - measurements of the fluorescence of the solution in the cuvette were taken every 6 s (excitation 492 nm, emission 512 nm; excitation slit 12.5, emission slit 2.5). The solutions were under continuous stirring. The experiment was done in triplicate. As the control experiment, a 14 mm glass slide was used, also in triplicate. CF in the collected aliquots was determined as described above. The amount of CF loaded in the film was determined as previously described in Section 3.3.3.

3.4.3 Measurement of spectra of CF loaded in the film

Fresh $(HA/PLL)_{24}$ films were loaded with CF by incubation in 1 µM, 10 µM, and 100 µM CF solutions. After loading, films were washed with Tris buffer and placed into a cuvette with Tris buffer to determine spectra of CF loaded in the film (excitation at 492 nm). The measurement was done 1 min and 60 min after immersion of the loaded films into the Tris buffer in the cuvette - immersion moment is considered as the start of the release.

3.4.4 Dynamic light scattering (DLS)

DLS measurements of hydrodynamic diameter and ζ-potential of CF and PLL molecules were performed using a Zetasizer Nano ZS. Measurements of CF and PLL solutions were done in Tris buffer or in water. Moreover, measurements of mixtures of CF and PLL were conducted also at different molar ratios. PLL concentrations were 1, 5 and 10 mg/ml; concentrations of CF were 0.18 mg/ml, 0.9 mg/ml and 0.45 mg/ml. 0.18 mg/mL CF (500 µM) is saturated solution of CF. All the DLS measurements were performed at 25 °C using disposable folded capillary cells for ζ-potential determination and disposable 70 µl UV-cuvettes for size measurements.

3.4.5 Study of molecular diffusion into the films

Diffusion of charged molecules of different sizes - Diffusion rate of small CF (376 Da) and large PLL^{FITC} (15-30 kDa) into non-coated $(HA/PLL)_{24}$, $(HA/PLL)_{24}$/AuNPs γ = 1.5, and $(HA/PLL)_{24}$/AuNPs γ = 3 films was studied using the CLSM. The film was put in 1 mL of buffer in a well of a 2-well Nunc chamber and CF or PLL^{FITC} were added to a final concentration of 1 µg/mL and 100 µg/mL, respectively. 100-fold difference in concentration was made in order to obtain similar fluorescence intensity from CF and PLL^{FITC}, since one in hundred lysine

residues in PLL is labeled with FITC. Using the Z-slicing mode of the CLSM the focus was positioned in the middle of the height of the film. Fluorescence images were taken before addition of the fluorescent molecules, and at predefined time points afterwards (1, 3, 5, 7, 10, 15, 20, 30, 60 min). The integral fluorescence of each image was used as a measure of the amount of CF or PLL^{FITC} accumulated in the film. Fluorescence was normalized to the value of the highest fluorescent intensity in the series and plotted as a function of time to show speed of diffusion in the film.

Diffusion of large non-charged molecules of different sizes - Determination of diffusion rate of 10 kDa, 70 kDa, and 500 kDa FITC-labeled dextrans ($dextran^{FITC}$) was carried out the same way as for CF and PLL^{FITC}.

3.4.6 Estimation of the relative diffusion rate of small and large molecules into the film

The diffusion coefficient and the amount of immobile fraction were evaluated by fluorescence recovery after photobleaching (FRAP). Glass slides with HA/PLL films loaded with either PLL^{FITC} or CF were mounted into a holder, covered by a layer of appropriate buffer for protection from drying and placed into the CLSM. Using a 63x/1.4 objective the sample was bleached by full laser power (Ar-Ion, 488 nm) or scanned by highly attenuated laser. Scanning area spanned 73.12 µm x 73.12 µm (512 pix x 512 pix) and bleached area spanned 73.12 µm x 2.14 µm (512 pix x 15 pix). A proper z-position was found as the position with the highest fluorescence signal. The sample was primarily scanned twice, bleached (by scanning the laser fifty times over the bleached area resulting into dip of the fluorescence signal) and was finally scanned thirty times. Time span between successive images was 10 s, scanning time per pixel was 3.2 µs.

Recorded image stacks were averaged along one dimension (using ImageJ) to result in raw FRAP profiles. Further data processing was performed in MS Office Excel. These profiles were corrected for the spatial fluorescence inhomogeneity and unwanted bleaching by reference measurements. The following evaluation procedure was based on an analytical solution of Fickian diffusion.[225] Evaluation of immobile fraction amount is based on relation between dip depth of the fluorescence profiles and time. All measurements were done at least in triplicates. The raw images from FRAP experiment are cropped (to limit the edge effect) and averaged in perpendicular direction to the diffusion direction to obtain a one dimensional FRAP profile. The set of FRAP profiles resulting from one FRAP measurement are normalized afterwards to pre-bleach fluorescence intensity, corrected for inhomogeneity of local fluorescence, corrected for unwanted bleaching and edge effects in other dimension.

The FRAP curves are afterwards fitted by a Gaussian curve defined as:

$$I(x,t) = I_0(t) - A(t) \cdot \exp\left(-\frac{x^2}{2w^2}\right) \qquad \text{Eq1}$$

where $I(x,t)$ is the fluorescence intensity at distance from dip x and time point after bleaching t, $I_0(t)$ is the fluorescence intensity of background (ideally, its value is constant and

close to 1), $A(t)$ is the depth of dip at time point t, w describes the width of the Gaussian curve between inflexion points. All four parameters are free for fitting with every separate FRAP profile. After fitting the Gaussian function into FRAP profiles, the diffusion coefficient D is evaluated as half of the slope of w^2/t plot:

$$D = \frac{d(w^2)}{2d(t)} \qquad \text{Eq2}$$

Only the first three points of this plot are used for slope evaluation, because this plot tends not to be precise when more fractions (immobile fraction) are present. The slope is influenced by multifractionality already from the beginning of recovery process and thus resulting D shows a kind of average diffusion coefficient.

The relative amount (percent) of the immobile fraction K_{rel} is evaluated from the time development of the dip depth $A(t)$ by fitting the following function:

$$A(t) = \frac{M}{(4\pi D(t+t_0)^{d/2}} + K \qquad \text{Eq3}$$

where $A(t)$ is the depth of the dip at time point t, M is amount of bleached molecules, D is the diffusion coefficient, t is time after bleaching, t_0 is time shift, d is dimensionality of diffusion and K is partial depth of dip attributed to immobile fraction. D and d are taken from previous evaluation and fixed during fitting. Unfortunately, these values are already influenced by presence of the immobile fraction, but their presence during fitting is essential for a good approximation of the immobile fraction. The minimum d value used here is limited to 1. Logically, the values lower than 1 cannot reflect reality. The deviations of d and D to lower values are caused by the presence of the immobile fraction. M, t_0 and K are free fitting parameters. The input values $A(t)$ are acquired directly from FRAP profiles, not from the parameters of Gaussian function fitting, because the evaluation of immobile fraction is intended to be as much independent on evaluation of D as possible. Afterwards the K_{rel} is obtained by relating K to the depth of the dip just after bleaching:

$$K_{rel} = \frac{K}{A_0(t)} \qquad \text{Eq4}$$

where K_{rel} stands for the relative amount of the immobile fraction, K represents the depth of the dip attributed to the immobile fraction resulting from Eq3, $A_0(t)$ represents the depth of the dip just after bleaching ($t = 0$). Such an approach for the evaluation of immobile fraction amount requires that only two fractions are present in the sample – a single mobile fraction wit a certain D and an immobile fraction.

3.5 Cell culturing

Various cell lines - L929, SH Sy5y, HEK, 3T3, HeLa - were used for the examination of cell-film interactions. After initial testing of cellular adhesion to the film, two cell lines, HeLa

and 3T3, were tested for optimal response to ATP stimulation, and HeLa cells were stimulated by light-triggered delivery of the small bioactive molecule ATP from the film. The cells were always used in rather early stages of their passages, not more than 30 passages after reactivation from the stock at -170 °C.

3.5.1 Maintaining and sub-culturing of cells

Cells were maintained in an incubator at 37 °C and 5 % CO_2, in 25 mL tissue culture flask containing medium. After reaching about 80 % confluence cells were sub-cultured - the medium was removed, cells were rinsed twice with PBS w/o Ca^{2+} and Mg^{2+}, trypsin-EDTA solution was added and cells were incubated for 5-8 min, depending on the cell line. The trypsin was deactivated by addition of 5 mL of fresh medium, cells were counted using a Thoma-Neubauer-chamber and further used for either establishing a new passage or for experiments.

Details about maintaining and sub-culturing of cells are given in Table 3.2, and details about number of cells used for different purposes in Table 3.3.

Table 3.2. Media composition and culture conditions for cell lines used in the study

Cell line	Medium used	Trypsin/EDTA (w/v)	Trypsinisation time (37 °C)
SH-SY5Y	DMEM + 15 % FBS + 4 mM L-alanyl -L-glutamine + 1 % penicillin/streptomycin	0.25 % / 0.02 %	8 min
L929, HEK, 3T3, HeLa	DMEM + 10 % FBS + 4 mM L-alanyl -L-glutamine + 1 % penicillin/streptomycin	0.05 % / 0.02 %	5 min

Table 3.3. Number of cells used for sub-culturing and seeding on the films

	Small tissue flask	Glass slide 14 mm
Surface (cm^2)	25	1.54
Medium volume (mL)	5	1
Cells	10^5	10^4

3.5.2 Monitoring cellular response

Cell spreading - Growth and adhesion of cells were monitored optically using the microscopic analysis. Images were taken either with a Leica optical microscope or with a CLSM microscope at time points defined by the requirements of the experiment.

Cell viability - Propidium iodide (PI) test: The PI exclusion test was used to assess the viability of the cells. 10 µg/mL PI in PBS with Ca^{2+} and Mg^{2+} was used for the test. After removing the medium, the cells were twice washed with PBS. 200 µL of PI solution was added to cover the cells, followed by 8 min incubation. The dye was removed, residual dye

was washed away by rinsing with PBS, and the sample was observed under a fluorescence microscope to identify dead cells which are stained red.

3.6 Caged ATP

Three commercially available cATP were used (Fig. 3.2):

- NPE-ATP (adenosine-5'-triphosphate-P^3-(1-(2-nitrophenyl)ethyl)-ester)

- DMNPE-ATP (adenosine-5'-triphosphate-P^3-(1-(4,5-dimethoxy-2-nitrophenyl)ethyl)-ester)

- DMB-ATP (adenosine-5’-triphosphate-P^3-(1-(3’,5’-dimethoxyphenyl)-2-oxo-2-phenyl-ethyl)-ester).

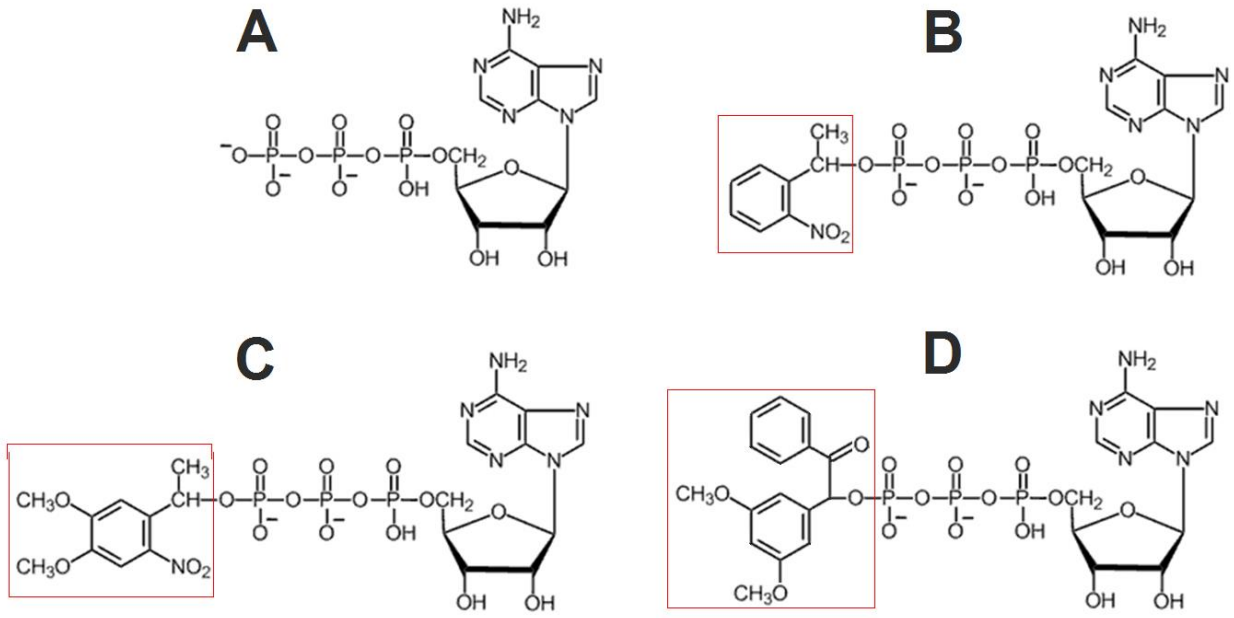

Figure 3.2. Structures of caged ATP compounds used in the study. (**A**) ATP, (**B**) NPE-ATP, (**C**) DMNPE-ATP, and (**D**) DMB-ATP. Red squares mark the caging group.

3.6.1 Stability of cATP at ambient conditions

The stability of cATP in laboratory conditions (22 °C, daylight and/or artificial ambient light) was examined by storing 1 µM solutions of cATP in transparent Eppendorf tubes on the laboratory desk not protected from light. Samples were collected after defined periods of time and the concentration of ATP was determined to estimate the rate of spontaneous decomposition of caged compounds. As a control, 1 µM solutions of cATP were exposed to 16 W/cm^2 UV light from a UV lamp for 1 min to ensure complete uncaging and it was considered that the determined concentration of ATP in the samples afterwards represents completely uncaged cATP.

3.6.2 Interference of cATP with the luciferase assay

To assess if cATP can interfere with the enzymatic determination of ATP, 2 µM ATP, 2 µM cATP, and 1 µM ATP + 1 µM cATP stock solutions were made and a series of dilutions of these stock solutions was made. Using the luciferase assay the concentration of ATP in each solution was determined and compared to the initial (known) ATP concentration in each solution. If the two concentrations were not the same, it would mean that cATP affect the luciferase assay.

3.6.3 Light-triggered uncaging of cATP

To estimate the rate of the uncaging process a series of solutions of cATP was exposed to 16 W/cm^2 UV light. During the irradiation samples were taken at different time points to determine ATP and to observe the rate of cATP uncaging.

3.6.4 Determination of cATP

The procedure for the determination of loading was identical to the one used for other SCM (Section 3.3.1). The determination of the cATP release was conducted in the same way as the determination of the release of other SCM (Section 3.3.2). However, irradiation of collected samples was required in order to fully uncage cATP to obtain ATP whose concentration is measured. In addition, ATP concentrations were determined in the samples before the irradiation to check for spontaneous decomposition of cATP. The difference of ATP concentrations determined before and after irradiation indicates the amount of released cATP.

3.7 Light-triggered release of ATP for extracellular stimulation of cells

Photoactivated localization microscopy (PALM) is a method that allows controlled irradiation with either IR or UV light. Options for adjusting power and focusing of the UV laser have been exploited in this study. The PALM combi system used was assembled by Carl Zeiss Microimaging GmbH, Germany and is composed of a Zeiss inverted microscope, an UV laser CryLaS FTSS 355-50, a XCite Series 120 EXFO fluorescence lamp, shutter, and a main controller (Fig. 3.3)

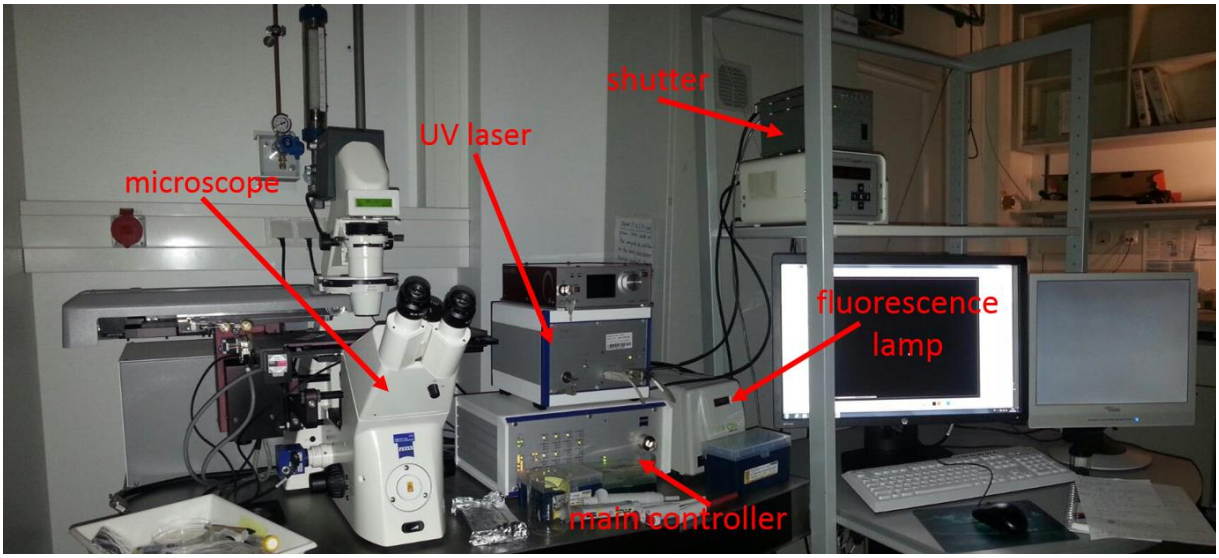

Figure 3.3. Main components of the PALM system used in the study. Details are given in the text above.

3.7.1 Optimization of UV laser for affecting $(HA/PLL)_{24}$ films

UV light from a CryLaS FTSS 355-50 UV laser with the maximum power of 60 kW/cm^2 was applied for the irradiation of the film. The laser is an integral part of the PALM system. To optimize laser intensity and focus, different laser intensities and foci were tested, since inappropriate laser power can readily cut and/or burn the polymer film depending on the position of the focus of the laser beam.

In order to focus light spot exactly into the film, the area near the area of interest (for further affecting) was irradiated with the lowest intensity. The intensity was then increased until the film was visually affected (cut) by UV light (bubble of gas is formed). Afterwards the focus of the laser was altered until the sharpest cutting of the film was achieved. The sharpest cutting of the film indicates the best focus and the laser intensity above optimal. The laser intensity was then decreased until no cut was present (the focus was not changed). In this way it was ensured that the energy delivery does not destroy the film, while substantial UV light is still applied. Optimal relative laser power that was used varied among experiments and was between 47 % and 55 %.

3.7.2 Determination of ATP released from cATP stored in $(HA/PLL)_{24}$ films

To assess the amount of ATP that is released from cATP stored in the HA/PLL film, $(HA/PLL)_{24}$ film was loaded with 1 µM cATP and placed in a well of a 2-well Nunc chamber filled with 2 mL of Tris buffer. The holder with the Nunc chamber was placed under the microscope which is part of the PALM system (Fig. 3.3). UV light from the laser was applied by automatically moving the laser beam over the predefined spiral-patterned pathway (Fig. 3.4) with a total size of 40 x 30 µm^2 during about 45 s. Three spots on the film were affected, each in a different quadrant. Immediately after the irradiation, 50 µL samples were collected

above the irradiation zone. This was done in order to collect all of released ATP. The fourth sample was taken from the last quadrant without previous irradiation. It was used to check if ATP has enough time to diffuse into the whole buffer, and if it is completely collected after irradiation. Both ATP and cATP concentrations were determined in collected samples. The schematics of the positions of the irradiated zones on a $(HA/PLL)_{24}$ film and the spiral irradiation pathway are shown in Fig. 3.4.

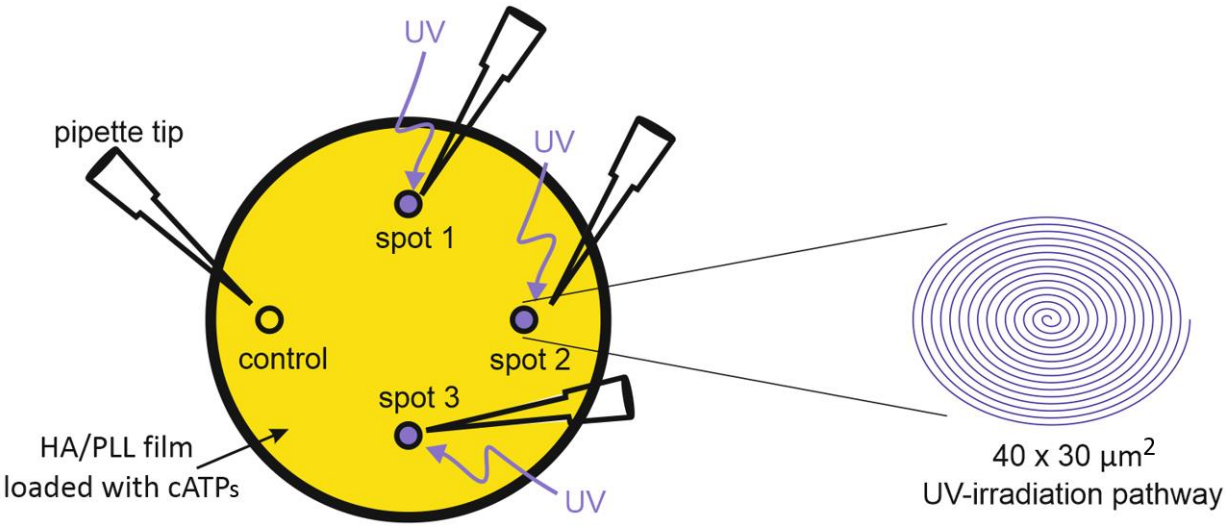

Figure 3.4. The schematics of the positions of the irradiated zones on a $(HA/PLL)_{24}$ film and the spiral irradiation pathway. Three spots were irradiated and immediately after irradiation 50 µL sample was collected above the irradiation zone. The fourth sample (control) was taken at the end in the same manner as previous three, only without prior irradiation. The spiral irradiation pathway (right) of the UV laser covered a total area of 40 x 30 μm^2 and a single irradiation lasted for 45 s. All experiments were done in triplicate.

3.7.3 Ca^{2+} staining

The increase of the concentration of intracellular calcium ($[iCa^{2+}]$) in cells seeded on HA/PLL films was visualized and assessed using Ca^{2+}-sensitive fluorophores: Fluo-3 and Oregon Green 488 BAPTA-2 (OG). The stock solutions of the fluorophores were prepared according to the producer's manual. The cells were washed with PBS Ca^{2+} and Mg^{2+} and 10 µM Oregon Green BAPTA 2 or Fluo-3 in serum free DMEM medium was added; the volume corresponded to the size of the sample, enough to cover the whole sample surface with 3-4 mm of the staining solution. After incubation for 15 minutes in an incubator at 37 °C and 5 % CO_2, the staining solution (in 10 % medium) was replaced with 100 µL PBS with Ca^{2+} and Mg^{2+}. If kept in an incubator, stained cells are viable and responsive to external stimuli for up to 2 h. Images were taken using Carl Zeiss inverted fluorescence microscope of the PALM system. FITC filter 495 nm/517 nm was used.

3.7.4 Stimulation of cells using light triggered-release of ATP

Cells are seeded onto a 14 mm $(HA/PLL)_{24}$ film preloaded with 1 µM cATP, left overnight to adhere and stained with 10 µM OG or Fluo-3. Films were placed in a holder and

placed under the microscope. Power and focus of the UV light were optimized as described in Section 3.7.1. A region on the film without cells was chosen as an irradiation zone. Irradiation was conducted in the same manner as for the monitoring of ATP uncaging – the UV laser followed the spiral pathway covering a total area of 40 x 30 μm^2 and a single irradiation lasted for 45 s. The fluorescence of cells was monitored up to 10 min from the onset of irradiation by taking fluorescence images of stained cells every 2s. The fluorescence of cells was quantified afterwards using the ImageJ software and further analyzed using Microsoft Office Excel and Origin Lab software.

4 RESULTS

4.1 HA/PLL film assembly

The physico-chemical properties of the HA/PLL films must be understood in detail, as these multilayer assemblies occupy the central position of the study. Their stability, morphological properties, internal charge balance, and behavior of polymer components are crucial factors for adequate implementation of these films as reservoirs for molecules (Sections 4.2 and 4.3) and as substrates for cellular adhesion and growth (Section 4.4).

4.1.1 Film fabrication and stability

$(HA/PLL)_{24}$ films have been prepared on glass coverslips using an automated dipping protocol based on the alternating deposition of HA and PLL until a required number of bilayers is deposited. Removing a portion of the film by scratching represents a simple and rapid patterning method for providing film-free areas. Scratched areas were introduced with a sharp needle to enable the investigation of the film's consistency and stability, as well as the investigation of the cellular response to bare glass in the scratched area. The bare glass in direct vicinity to the examined film was a control for the cellular response to the film.

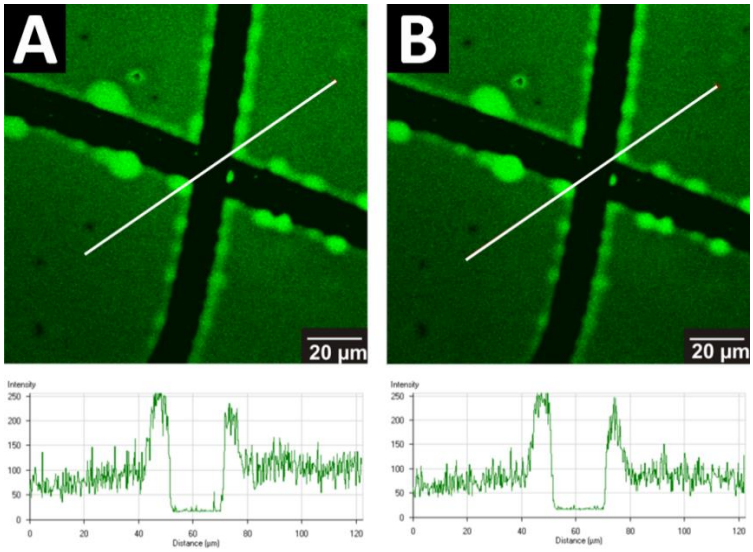

Figure 4.1. CLSM images of $(HA/PLL)_{24}$ films stained with 10 µM PLL^{FITC}. After incubation in Tris buffer the films maintain their stability even after 24 h (**A**) and 72 h (**B**). Fluorescence profiles are placed below the corresponding CLSM images. Black regions are places where the HA/PLL multilayer was removed by scratching. Films were deposited and stored in Tris buffer.

The first experiment was to study film stability at preparation conditions, because the high dynamics of polymer interaction in HA/PLL films may result in changes of the film structure during storage. For stability study, fluorescence of PLL^{FITC} stained films was monitored after different storage time – 24 h and 72 h in Tris buffer. A prominent feature of the films is their morphological uniformity (smooth surface) as seen in Fig. 4.1. Furthermore

the scratched area did not shrink or deform in any way as concluded by the analysis of the film profiles – it kept its width at around 20 µm. The overall stability of deposited films judged by fluorescence intensity after three days of storage (Fig. 4.1B) indicates no spontaneous degradation or disassembly.

4.1.2 Film characterization: thickness and mechanical softness

To understand the interaction between HA and PLL that greatly determines the structure and stability of the film, and especially the effect of PLL length (HA is immobile due to its size[103]), $(HA/PLL)_{24}$ films were assembled with 15-30 kDa PLL (PLL_{short}) or 150-300 kDa PLL (PLL_{long}). The chains of PLL_{long} are considerably longer compared to the chains of PLL_{short}, which means that PLL_{long}, unlike PLL_{short}, can form coils within the film.[226] The assumption is that the length and the coiling of the PLL_{long} could decrease its mobility within the film.

To examine physical characteristics of these two types of films, atomic force microscopy (AFM) was employed. Softness, i.e. Young's modulus (E_0) was analyzed (Fig. 4.2). Young's modulus of $(HA/PLL_{short})_{24}$ and $(HA/PLL_{long})_{24}$ are fairly the same, 2.41 ± 0.18 kPa and 2.84 ± 0.35 kPa, respectively, indicating rather soft structures.

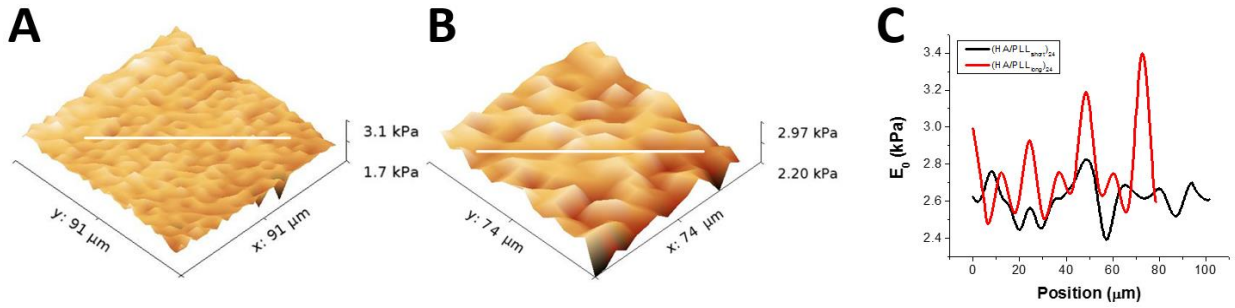

Figure 4.2. Maps of the Young's modulus of (**A**) $(HA/PLL_{short})_{24}$ and (**B**) $(HA/PLL_{long})_{24}$ films; (**C**) Young's moduli for both films. White lines in A and B mark the line at which profiles shown in C were taken.

Furthermore, the thickness of the $(HA/PLL)_{24}$ films is analyzed (Fig. 4.3). The thickness is determined by AFM as the difference in height between the film and its glass support. Unlike E_0, height varies almost by a factor of two. PLL_{short} film have an average thickness of 1.7 ± 0.3 µm (Fig 4.4A-B), whereas PLL_{long} films are 0.9 ± 0.2 µm thick (Fig. 4.3C-D). Both films have smooth surfaces, with the exception of rim around the scratched areas that were inflicted during the scratching procedure.

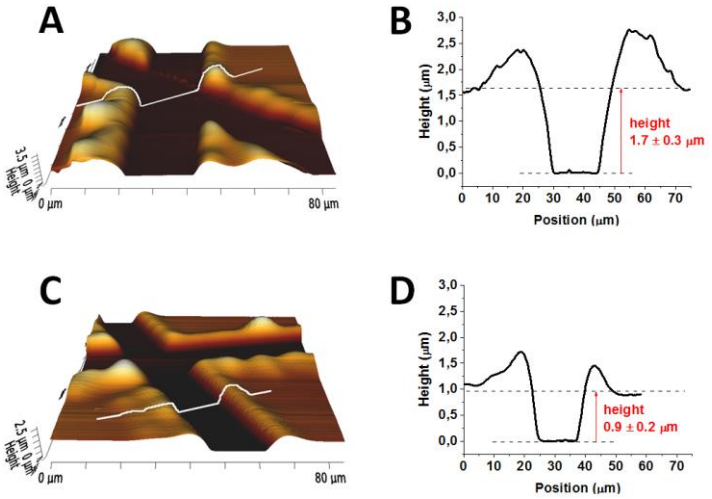

Figure 4.3. AFM images of the surfaces of (**A**) $(HA/PLL_{short})_{24}$ and (**C**) $(HA/PLL_{long})_{24}$ films with scratched area in the middle - white line marks the position at which the representative height profile was taken; Representative height profiles of (**B**) $(HA/PLL_{short})_{24}$ and (**D**) $(HA/PLL_{long})_{24}$; average height values are given.

Effect of the PLL chain length on film properties. Additionally, it was assumed that PLL_{short} and PLL_{long} chains have different mobility, i.e. that there are both mobile and immobile fraction of PLL in the film. To test this assumption, which could explain different thicknesses of the film, a series of FRAP experiments is conducted and results are given below in Fig. 4.4. FRAP experiments were conducted in friendly cooperation with David Šustr, Fraunhofer IZI-BB, Potsdam.

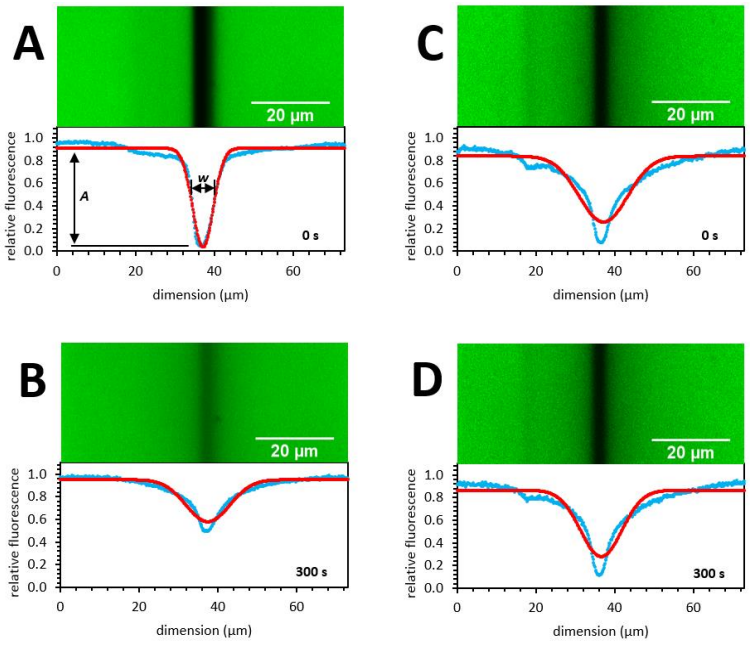

Figure 4.4. CLSM images (**A**) and (**C**) were recorded 0 s after bleaching and images (**B**) and (**D**) 300 s after bleaching. Images A and B correspond to $(HA/PLL_{short})_{24}$ during FRAP measurement. Images C and D correspond to $(HA/PLL_{lobg})_{24}$ during FRAP measurement. Top part of every image shows a raw image, bottom part shows the corresponding FRAP profile taken along the image (in blue) and fitted Gaussian function[225] (in red).

Primarily, the diffusion coefficient *D* of PLL is evaluated from every FRAP measurement (Fig. 4.5A). The value of *D* is an apparent value, because it comprises overall contributions of all fractions of different mobility. High deviations of the resulting *D* are observed. In addition, the contribution of the immobile fraction is evaluated from FRAP measurements (Fig. 4.5B). The value of the parameter *D* shows the fraction of PLL that seems to be immobile within the time scale of measurement (diffusion coefficient below 0.01 µm²/s).

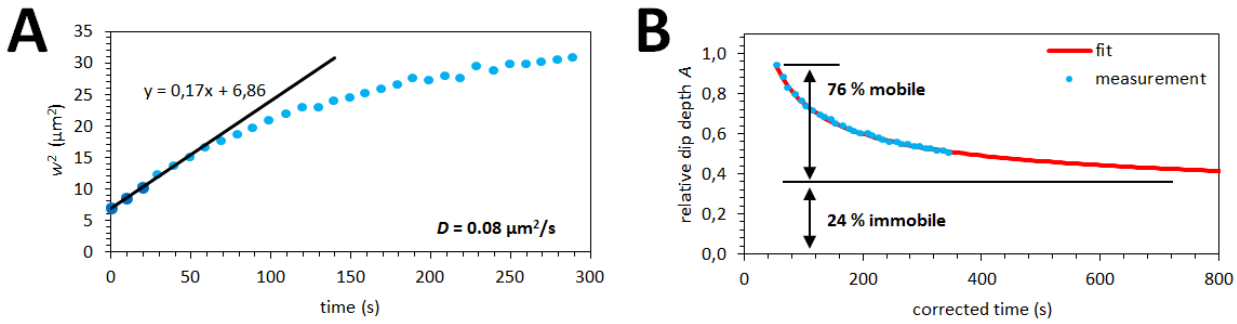

Figure 4.5. (**A**) A typical evaluation procedure of the diffusion coefficient (*D*) is based on a graph as shown. *D* is determined as a half slope at the origin of plot w^2/t (squared width of dip versus time). At later time the curve starts to deviate from its initial trend because of the presence of a immobile fraction.[225] (**B**) A typical evaluation procedure of the immobile fraction is shown on the graph. Afterwards a function describing this relationship (red) is fitted to measured data (blue) and the extrapolation for infinite times is calculated. From the known dip depth at the beginning of diffusion and the dip depth at the infinite time the amounts of mobile and immobile fraction are calculated.

The FRAP data evaluation showed that in case of PLL_{short} the average apparent diffusion coefficient of the mobile fraction is 0.17 ± 0.10 µm²/s and amount of immobile fraction is about 29 ± 6 %. In case of PLL_{long} an evaluation showed that practically all PLL is immobile (92 ± 2 %). Obviously, the mobility of PLL chains is related to the length of the polymer chains.

4.2 Reservoir properties of the HA/PLL films

After having characterized the films and the effect of the length of PLL on film properties, the reservoir capacity of the films is described. The method is based on the indirect determination of the amount of the SCM stored in the films by incubation of the films in the solution of SCM. The amount of stored SCM was calculated as the difference in SCM amount in the loading solution before and after incubation.

4.2.1 Loading of small charged molecules

Structural formula of small molecules used in this study (CF, Rho, ATP) are given in Fig. 4.6. pKa values of CF, Rho, and ATP are 6.4,[227] 7.5,[228] and 6.5,[229] respectively. Fluorescent dyes CF and Rho are used as model compounds for loading into the $(HA/PLL)_{24}$

films. ATP is a significant biologically active compound that serves not only as the main energy source, but as an extracellular secondary messenger, and as well as a precursor of another secondary messenger cAMP. CF has two carboxylic groups and Rho is positively charged. ATP carries three negatively charged phosphate groups. Small molecular weight compounds used are expected to bind to the film by electrostatic interactions with polyelectrolytes. Loading of CF, Rho, and ATP was done by incubation of the films in 1 µM solution of the corresponding compound in Tris buffer.

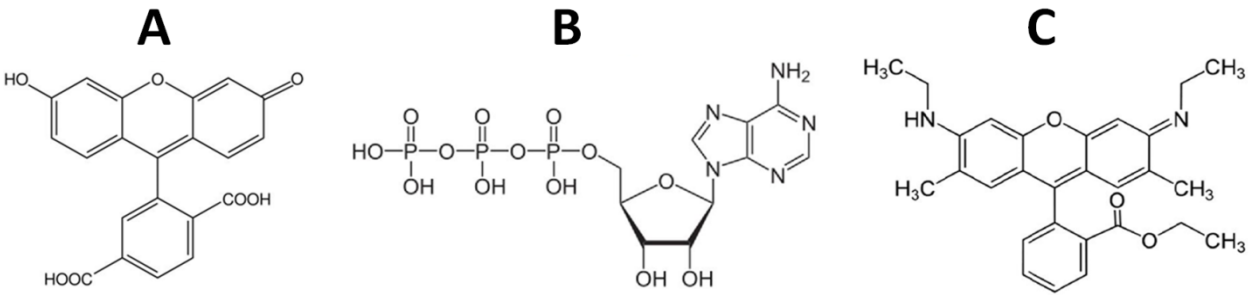

Figure 4.6. Structural formulae of (**A**) CF, (**B**) ATP, and (**C**) Rho.

The loading efficiency, defined as the ratio (in percentage) between the SCM amount loaded into the film and the initial amount of SCM used for the loading, was found to be high for all examined species. The loading efficiency was calculated to be ~30 % for CF, ~35 % for Rho, and ~90 % for ATP (Fig. 4.7). The loading efficiency of CF depends on the last deposited layer of the film. In case of PLL terminated film - $(HA/PLL)_{24}$ - the CF loading was found to be higher than that of HA terminated one - $(HA/PLL)_{24}/HA$. For Rho and ATP loading no dependence on the last deposited layer has been found.

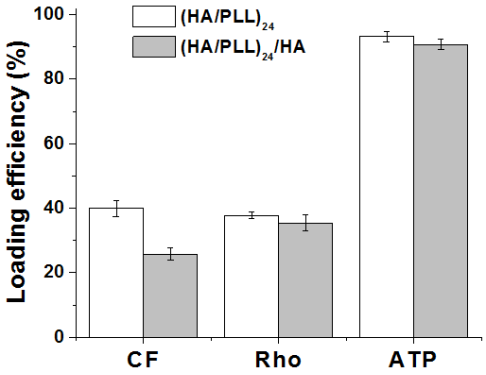

Figure 4.7. Loading efficiency of CF, Rho, and ATP in $(HA/PLL)_{24}$ or $(HA/PLL)_{24}/HA$ after overnight incubation. Concentration of the dyes and ATP in stock solutions in Tris buffer is 1 µM.

High loading efficiencies shown in Fig. 4.7 demonstrates high reservoir capacity of the films. The thickness of $(HA/PLL)_{24}$ film is 1.7 ± 0.3 µm as determined from AFM imaging using the scratch approach (Fig. 4.3). Taking into account that 40 ± 3 % of CF from 1 mL 1 µM CF solution has been adsorbed into PLL-terminated films, the concentration of CF inside the film, made on round 12 mm glasses, is rather high (~2.4 mM). Since the CF concentration in the supernatant at these conditions is 0.6 µM, 2.4 mM CF in the film corresponds to the

partitioning coefficient p = 4 x 10^3. A similar partitioning coefficient is obtained for Rho (4 x 10^3), and ATP has even a higher affinity for the film (4 x 10^4).

4.2.2 Interactions of CF in the film

The binding of small charged molecules in HA/PLL films is driven by the charge of both the polymers and the binding species.[230] Thus, the following part of the study is devoted to the elucidation of the binding mechanism of CF, which is taken as a model compound as it has a similar molecular weight as ATP and is negatively charged. In addition, it allows direct determination of its concentration through its fluorescence.

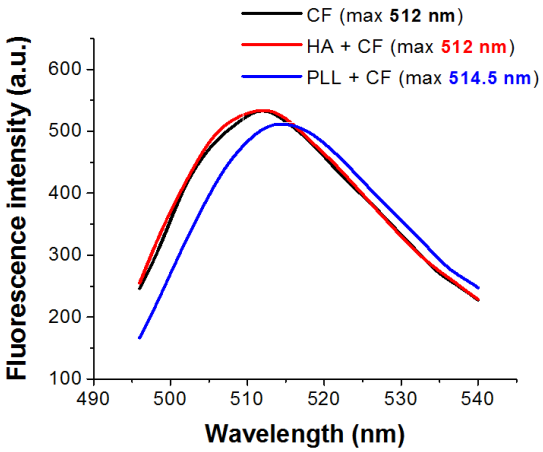

Figure 4.8. Emission spectra of 20 µM CF in Tris buffer (black), or in Tris buffer containing 0.5 mg/mL HA (red) or 0.5 mg/mL PLL (blue).

In CF along with its π-electrons there are two carboxylic groups, which are deprotonated at physiological pH and represent a potent source of negative charge of a CF molecule. Thus, it is expected that it will preferentially interact with positively charged polymers such as PLL. Fig. 4.8 shows the emission spectra of CF in solution containing HA or PLL. From the spectra it is obvious that CF in the combination with HA has the identical emission peak as pure CF, whereas PLL induced a shift of CF emission. The solutions were buffered at the pH 7.4.

To determine the exact state of CF in the film, emission spectra of 1 µM CF in solution, CF loaded in the film, and CF released from the film are taken. Emission peaks of these spectra are compared and taken as a measure of CF aggregation and/or CF-PLL and CF-film interactions. The state of CF in the film at the beginning of the release process and after one hour of the release is analyzed. From Fig. 4.9A it is clear that CF molecules stored in the film have identical emission peaks regardless of the time point of release they were taken at, which are 516 nm, in comparison to 512 nm of CF that has been released from the film. 512 nm is the position of the emission peak of 1 µM CF in solution as well, meaning that released CF and CF in buffer are in the same state, while CF at a concentration of 500 µM has its emission peak at 525 nm (Fig. 4.9B). In Fig. 4.9C the shift of the emission peak as a function of CF concentration in solution is presented. Increasing concentration of CF in

solution leads to the corresponding increase of the emission peak of CF fluorescence, and it might be the consequence of aggregation. As CF concentration approaches 500 µM the emission peak tends to reach a plateau at 525 nm. Beyond a concentration of 500 µM CF the solution turns into a colloidal solution.

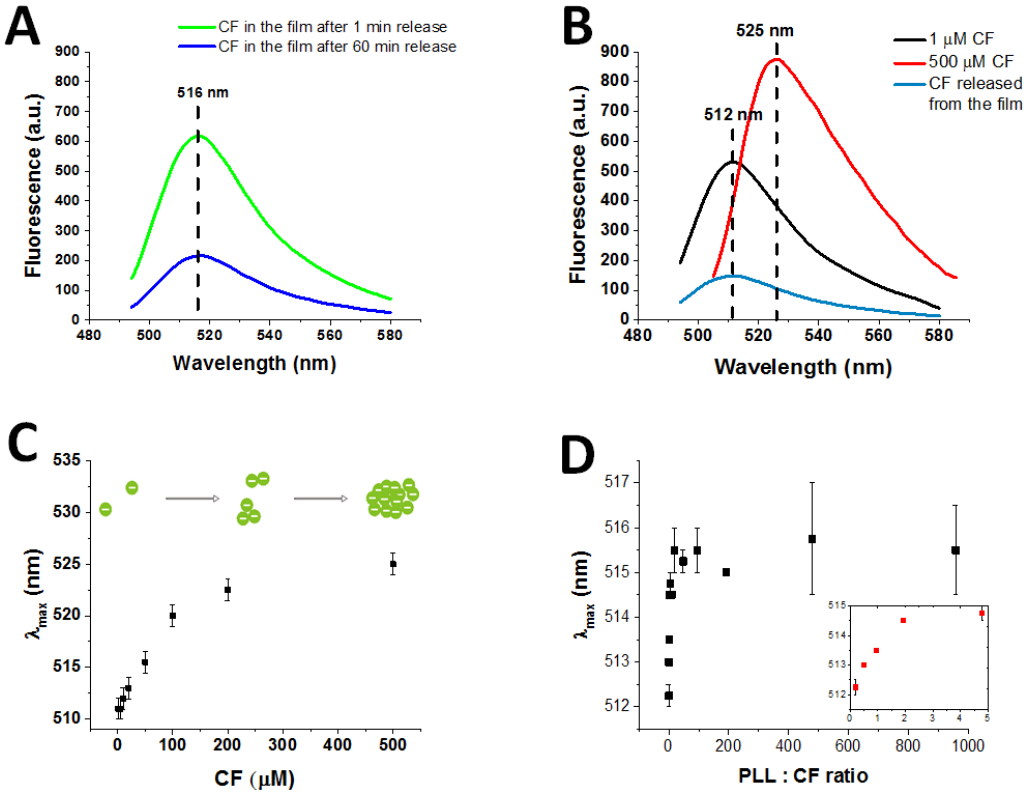

Figure 4.9. (**A**) Spectra of CF loaded into the film 1 min and 60 min after the beginning of the release; (**B**) Spectra of 1 µM CF, 500 µM CF, and the CF released from the film; (**C**) Peaks of the emission spectra (λ_{max}) as a function of CF concentration (schematic of the assumed concentration-dependent aggregation of CF is given as well); (**D**) λ_{max} of 5 µM CF in Tris buffer pH 7.4 containing PLL at different concentrations. The inset shows the first five data points of the main graph.

If PLL is stepwise added to a solution of low CF concentration (e.g. 5 µM), a red shift of about 4 nm takes place and the CF emission peak increases until 516 nm (Fig. 4.9D). Moreover, the shift is dependent on the PLL : CF ratio, and the maximum shift of 4 nm is achieved at a PLL : CF ratio 5 - further increasing of the PLL content does not yield an increase of wavelength (Fig. 4.9D). Furthermore, it was observed that the addition of PLL to 300 µM CF solution induces much higher emission shift (Fig. 4.10A).

The emission peak of 300 µM CF in Tris buffer is slightly above 525 nm. Addition of PLL causes additional red shift of CF which depends on the PLL : CF ratio (black curve in Fig. 4.10A). The highest emission peak (547 nm) occurs at a PLL : CF ratio of 5. Above this PLL : CF ratio emission peak of CF decreases. The opposite trend is noticed for the fluorescence intensity at the emission peak (red curve in Fig. 4.10A). As the PLL : CF increases, fluorescence intensity of CF decreases up to the point where the PLL : CF ratio is 5. Once again, above this ratio the effect is reversed – fluorescence intensity increases along with PLL

concentration. DLS experiments conducted with generous help from Alena Sergeeva (Fraunhofer IZI-BB, Potsdam) have shown that the size of CF and CF-PLL aggregates depends on their total concentration and ratio (shown in Fig. 4.10B).

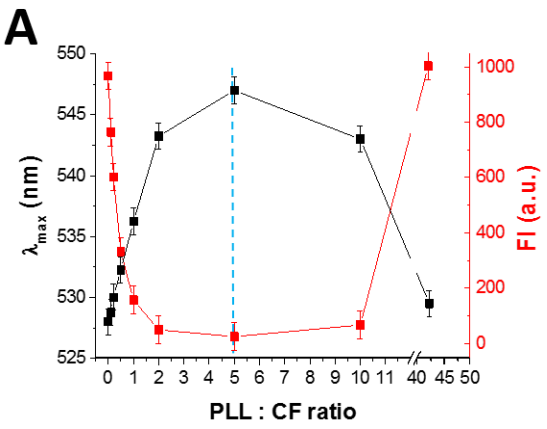

B

PLL : CF	size	λ_{max}
only CF	40-80 nm	525 nm
5 : 1	6-10 nm	547 nm
42 : 1	4-9 nm	516 nm

Figure 4.10. (**A**) Dependence of the fluorescence emission peak (λ_{max}) and fluorescence intensity (FI) at λ_{max} on PLL : CF ratio (CF kept constant at 300 µM). Dashed vertical blue line represents the threshold at which spectral features are reversed. (**B**) A table showing the emission peak and the size of the particles in 300 µM CF solution containing PLL at different PLL : CF concentration ratios.

Another aspect of the CF state in the film is its mobility. To check the mobility of CF in the film a series of FRAP experiments was conducted. Diffusion coefficient and the amount of the immobile fraction were estimated from these experiments in the manner previously described for PLL (Fig. 4.4). The immobile fraction accounts for the CF molecules which are immobile on the timescale of the experiment ($D < 0.01$ µm^2/s). The diffusion coefficient of CF loaded in PEM was measured to be about $D = 1.26 \pm 0.64$ µm^2/s and the amount of the immobile fraction is about 9 ± 10 % of total CF presented in PEM.

4.2.3 CF-PLL interaction – mechanism of CF loading in the film

After the behavior of CF in the film was studied, the focus was moved to the loading of CF into $(HA/PLL)_{24}$ films. The loading of CF from solutions of CF concentrations up to 10 µM in real time was monitored (Fig. 4.11), as parallel experiments have shown that the same amount of CF (~13 ± 2 mM in the film) is stored when films were incubated with either 10 µM or 100 µM CF.

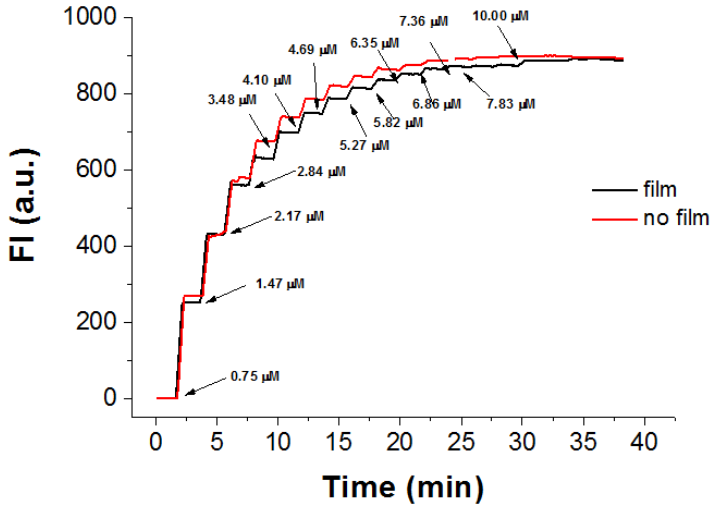

Figure 4.11. The graph shows the dependence of CF fluorescence intensity (FI) in the solution on time during which CF concentration was gradually increased. The arrows indicate time points at which the concentration of CF in the solution was increased to the designated value, assuming that no adsorption of CF took place. Data are obtained during real-time monitoring of CF loading into the $(HA/PLL)_{24}$ film (black curve). The control experiment was done without the film (red curve). The aliquots of loading solutions were taken after every increase of CF concentration. The difference in CF concentrations between supernatant of the loaded film and the supernatant of the control sample at each step was used to calculate the amount of CF stored in the film.

Adsorption kinetics of CF into the film was analyzed. Three kinetic models – Langmuir, Brunauer–Emmett–Teller (BET), and Freundlich - were applied to the data of CF loading to construct the best adsorption isotherm and to predict the loading behavior of the model compound CF in $(HA/PLL)_{24}$. These three models were chosen as they cover all possible scenarios of molecular interaction in the loaded films: monolayer adsorption (monoadsorption) of CF onto the film and exclusively CF-film interaction (Langmuir model); polyadsorption, which assumes only CF-CF interactions in the film, since CF-film interaction is considered negligible (BET); polyadsorption with both CF-CF and CF-film interactions, i.e. non-uniform distribution of adsorption affinities in the film (Freundlich) - basic assumptions of these three models are given in Table 4.1. Previously it was shown that the maximum CF concentration in the film does not exceed 13 mM, and maximum of 500 µM CF is dissolvable in Tris buffer.

Table 4.1. Comparison of the three kinetic models used. C_{sol} is concentration of CF in the solution, C_{film} is the CF concentration in the film, $C_{filmmax}$ and C_{solmax} are the maximum amounts of CF that can be stored in the film and buffer, respectively, *K* represents the binding constant, and *1/n* is a parameter of the Freundlich function.

Langmuir[231-234]	**BET**[235]	**Freundlich**[236-238]
$C_{film} = \frac{C_{filmmax} * K * C_{sol}}{1 + K * C_{sol}}$	$C_{film} = \frac{C_{filmmax} * K * C_{sol} * C_{solmax}}{(C_{solmax} + (K-1) * C_{sol}) * (C_{solmax} - C_{sol})}$	$C_{film} = K * C_{sol}^{\frac{1}{n}}$
Reversible adsorption and no chemical reaction between CF and the film are assumptions of all three models		
- Monoadsorption - only one monolayer of CF forms; - All binding sites in the film are equivalent; - No steric hindrance; - Homogenous adsorption.	- Polyadsorbtion - Multiple CF molecules can be adsorbed to each site and each adsorbed CF provides a site for the adsorption of the molecule in the layer above it; - All binding sites on the surface are equivalent;	- Each adsorbed molecule provides a new site for the adsorption; - Non-uniform distribution of adsorption affinities in the film; - The amount adsorbed is the sum of adsorption on all sites, with the stronger binding sites occupied first.

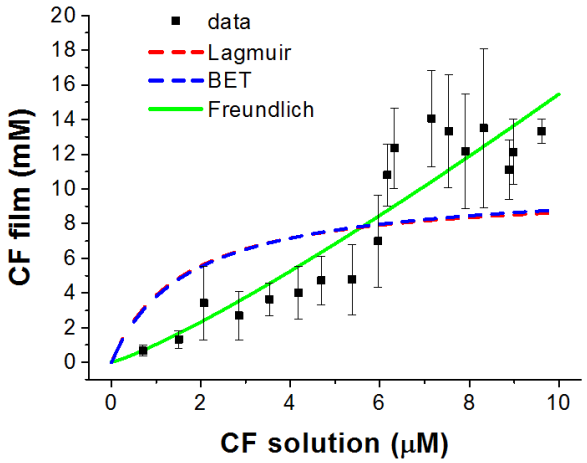

Figure 4.12. A graph showing fitting of Langmuir, BET, and Freundlich models to the data of CF loading into $(HA/PLL)_{24}$. Langmuir and BET curves (red and blue dashed curves) overlap to a high extent. The Freundlich curve, which is the best fit (Table 4.2), is presented by a full line.

Fig. 4.12 shows adsorption isotherms obtained by fitting the three different models to the experimental data. Data used for fitting were obtained from the average of quadruplicate measurements. Curves of each model that fit the best to the experimental data are presented. The coefficient of determination (R^2) was used as a measure of the quality of the fit. R^2 is calculated as:

$$R^2 = 1 - \frac{SS_{res}}{SS_{tot}},$$

where SS_{res} is the sum of squared residuals, $SS_{res} = \sum_i (y_i - f_i)^2$. It represents the parameter to be minimized during the fitting procedure. *y* stands for input data values, *f*

stands for fit values. SS_{tot} is the total sum of squares, $SS_{tot} = \sum_i (y_i - y_{av})^2$. y stands for input data values, y_{av} stands for the average value of variable y of the data. This parameter is proportional to the variance of y.

R^2 for all three models is given in Table 4.2. The results reveal that the best fit by far is the Freundlich model indicating that the loading of CF into $(HA/PLL)_{24}$ films corresponds to the assumptions on which Freundlich model is based upon.

Table 4.2. Coefficient of determination (R^2) for fitting of three different adsorption curves.

	Langmuir	**BET**	**Freundlich**
R^2 (average ± SD)	0.32 ± 0.08	0.34 ± 0.08	0.72 ± 0.05

The data fits the Freundlich adsorption isotherm with more than twice higher coefficient of determination than it fits the Langmuir or BET models (R^2~0.8 vs. ~0.4 for the other two models). The shape of the curve implies cooperativity, which is a property of the Freundlich model.

4.3 Release capability of the films

4.3.1 Examination of the release mechanism of loaded SCM

Having studied the loading of SCM in $(HA/PLL)_{24}$ films, the release from these films was examined. The amount of released CF was determined by measurements of CF fluorescence in the supernatant above the films after certain incubation times. About 70 % of CF has been released during 90 min of incubation in Tris buffer at room temperature, regardless of the last deposited layer (Fig. 4.13A). Release profiles of Rho and ATP look similar to that of CF, though ATP is released more slowly probably due to its higher charge density (Fig. 4.13B-C). This rather fast release kinetics is surprising because very high p (10^3-10^4 as mentioned in Section 4.2.1) indicates strong interaction of CF with the film. CF strongly binds to the film and one should expect that its release is very slow or does not even take place at all.

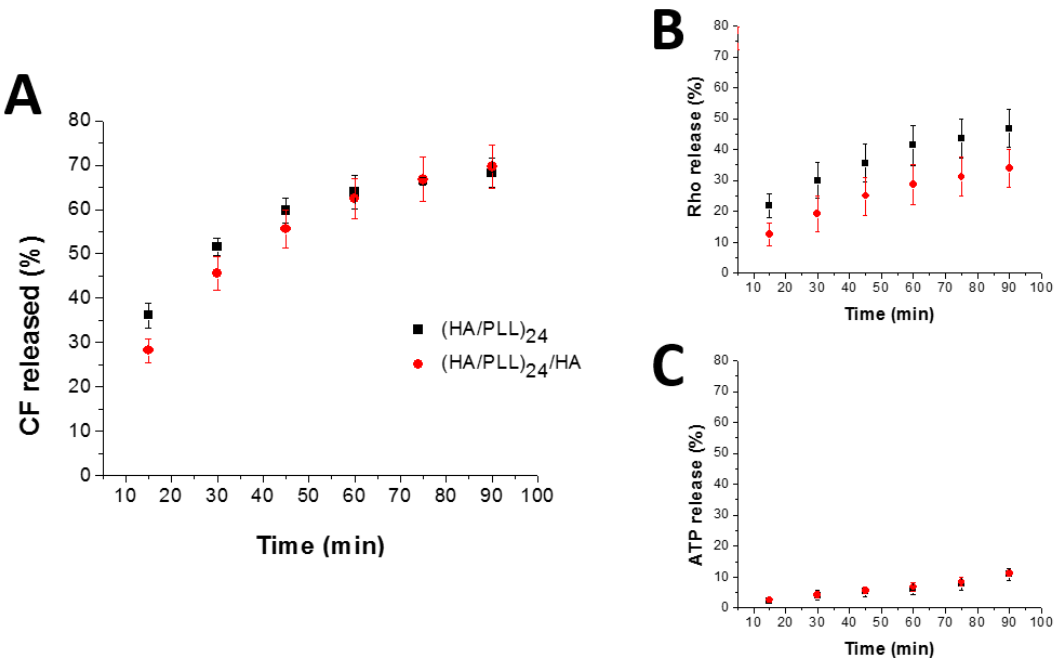

Figure 4.13. Release profiles of (**A**) CF, (**B**) Rho, and (**C**) ATP from $(HA/PLL)_{24}$ (black) and $(HA/PLL)_{24}/HA$ (red) films in Tris buffer.

To further invastigate the mechanism of binding and release of SCM from HA/PLL films, the influence of the film thickness on the release kinetics was examined. AFM imaging has shown that the thickness of a $(HA/PLL)_{96}$ film is 3.8 ± 0.2 µm against 1.8 ± 0.3 µm for a $(HA/PLL)_{24}$ film. For better comparison, the last layer (PLL) was the same in both cases. The $(HA/PLL)_{96}$ and $(HA/PLL)_{24}$ films were loaded by incubation in 1 µM CF. The loading efficiencies were 78.6 ± 1.2 % and 35.4 ± 1.2 %, respectively, and the release during 90 min from both films was similar (Fig. 4.14). The calculated ratios between $(HA/PLL)_{96}$ and $(HA/PLL)_{24}$ film thicknesses and the loaded amounts of CF are 2.1 and 2.2, respectively. This demonstrates that the film loading capacity is directly proportional to the film thickness.

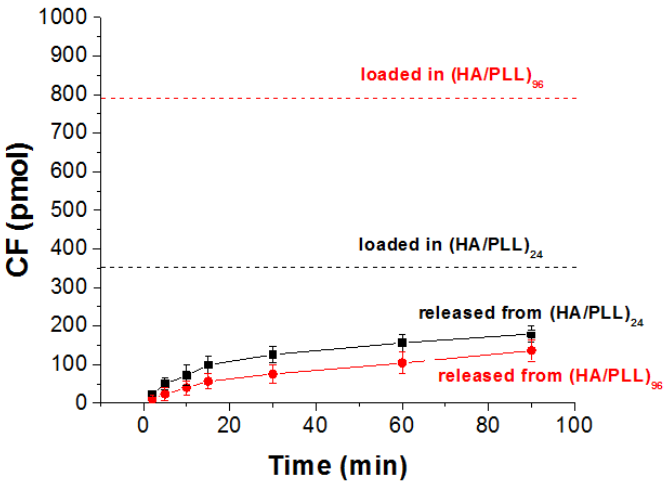

Figure 4.14. Amount of CF loaded and released from $(HA/PLL)_{24}$ (black) and $(HA/PLL)_{96}$ (red) films. The interrupted black and red lines represent the amount of CF loaded in $(HA/PLL)_{24}$ and $(HA/PLL)_{96}$, respectively.

Furthermore, the release of CF was analyzed. Various kinetic models were applied to the release data to predict drug release mechanism. Higuchi, Hixson Crowell, and First order model are three models that are conventionally used[240] for drug release modeling (Fig. 4.15). Comparative features of these three models are given in Table 4.3.

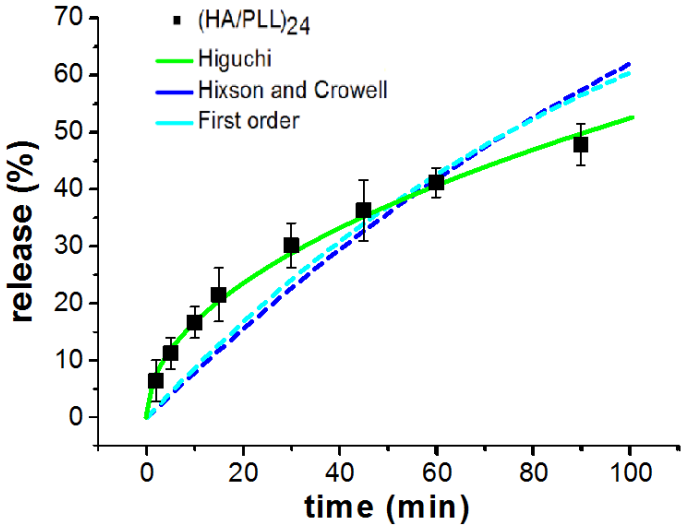

Figure 4.15. A graph showing modeling of CF release from $(HA/PLL)_{24}$ using Higuchi, Hixson Crowell, and First order models.

Table 4.3. Comparison of the three kinetic models used. C_{sol} is concentration of the released CF, t is time, and a describes the rate constant of the function.

Higuchi[241,242]	**Hixson-Crowell**[240,243,244]	**First order**[240,244]
$C_{sol} = a * \sqrt{t}$	$C_{sol} = 100 * (1 - (1 - a * t)^3)$	$C_{sol} = 100 * (1 - e^{-a*t})$
Planar systems (films), liquid medium, and perfect sink conditions are assumptions of all three models		
- The initial CF concentration in the film is much higher than the solubility of CF in buffer; - Mathematical analysis is based on one-dimensional diffusion (e.g. only through surface). Edge effects are negligible, meaning that the thickness is much smaller than the surface of the film; - The CF is much smaller in diameter than the thickness of the system; - One population of CF. - Swelling or dissolution is negligible.	- Dissolution occurs perpendicular to the surface; - Release is uniform over the whole surface; - Diffusion coefficient of the drug is constant; - The film retains relative ratio of dimensions but not its absolute size i.e. it can degrade or swell;	- Release of the drug is proportional to the amount of drug remaining in the film. Thus, the released amount diminishes in time;[245] - Although good for prediction of doses in time, this mechanism is difficult to conceptualize on a theoretical basis – its physical meaning is not yet fully understood.

From the comparison of R^2 values for all three fitted functions presented in Table 4.4 it is obvious that CF release kinetics follows the Higuchi equation (R^2 ~0.99 vs. < 0.7 for the other two functions).

Table 4.4. Functions of different release models fitted to the release data and corresponding coefficient of determination.

Film	Models	Mathematical equation	R^2
$(HA/PLL)_{24}$	Higuchi	$C_{sol} = 5.2493 * \sqrt{t}$	0.98 ± 0.07
	Hixson-Crowell	$C_{sol} = 100 * (1 - (1 - 0.0028 * t)^3)$	0.64 ± 0.05
	First order	$C_{sol} = 100 * (1 - e^{-0.0093 * t})$	0.70 ± 0.11

4.3.2 Adjustment of the release kinetics by AuNPs coatings

The application AuNPs as an additional layer upon HA/PLL films was shown to change surface properties of the film such as roughness and stiffness, leading to improved adhesion of cells.[46] The question remains, however, if the deposition of AuNPs alters storage and release properties of the film. To answer this question, loading and release of CF and ATP from plain $(HA/PLL)_{24}$ films and from films coated with AuNPs, $(HA/PLL)_{24}$/AuNPs, was examined. Different concentrations of AuNPs were used for coating, resulting in different γ. $(HA/PLL)_{24}$ films were coated with γ = 3 by 24 h incubation in AuNPs solution. Afterwards the films were loaded with either CF or ATP, and for comparison non-coated $(HA/PLL)_{24}$ films were used. The loading efficiency is given in Fig. 4.16A.

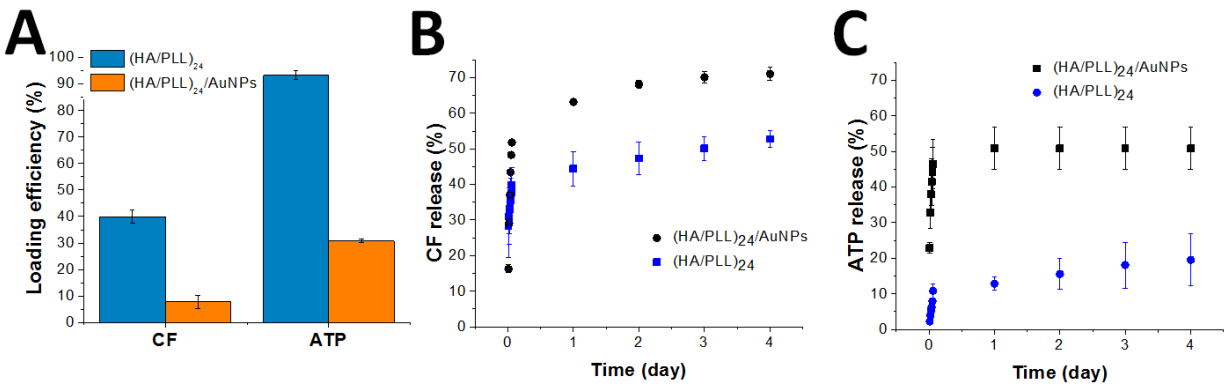

Figure 4.16. (**A**) Loading efficiency of CF and ATP into $(HA/PLL)_{24}$ (blue) and $(HA/PLL)_{24}$/AuNPs (γ = 3) films (orange). Films were loaded by 24h incubation in 1 mL 1 µM CF or ATP. Release of (**B**) CF and (**C**) ATP from the films.

As seen in the graph above, loading efficiency for CF was 39.9 ± 2.5 % and 7.9 ± 2.5 %, and for ATP 93.2 ± 1.6 % and 30.6 ± 0.6 % for $(HA/PLL)_{24}$ and $(HA/PLL)_{24}$/AuNPs films, respectively. The presence of AuNPs coatings reduces the reservoir capacity of the films by roughly 5-fold for CF and 3-fold for ATP (Fig. 4.16A). Surprisingly, AuNPs increase the rate of released CF by 40 % (Fig. 4.16B) and the rate of released ATP by three times (Fig. 4.16C). Although the initial concentration of CF and ATP in the coated films is lower than in the non-coated ones, the release rate is significantly higher. Release profiles look similar in all cases, with both CF and ATP being released rather intensively within the first 90 min and then very slowly afterwards.

4.4 Cell-film interaction and protection from degradation

4.4.1 Cellular adhesion to films

To get an insight into cell behavior on 24 bL films, cells that can be found *in vivo* in either soft or hard environments (neuroblastoma SH-SY5Y and fibroblast L929 cells, respectively) are seeded onto $(HA/PLL)_{24}$ films. L929 cells can distinguish between 24 bL film and bare glass which is present both in control and in scratched areas of 24 bL films (Fig. 4.17). It is obvious that L929 cells follow scratch patterns of 24 bL films, showing higher adhesion preferences for the scratched area than for the film. Interestingly, SH-SY5Y cells remained unattached to a $(HA/PLL)_{24}$ film and rather non-spread, and even avoided scratched areas that L929 readily inhabited. Not only did neuroblastoma cells not spread, but they aggregated to a very high extent on the film surface as well. They do not adhere and show preference for intracellular interactions.

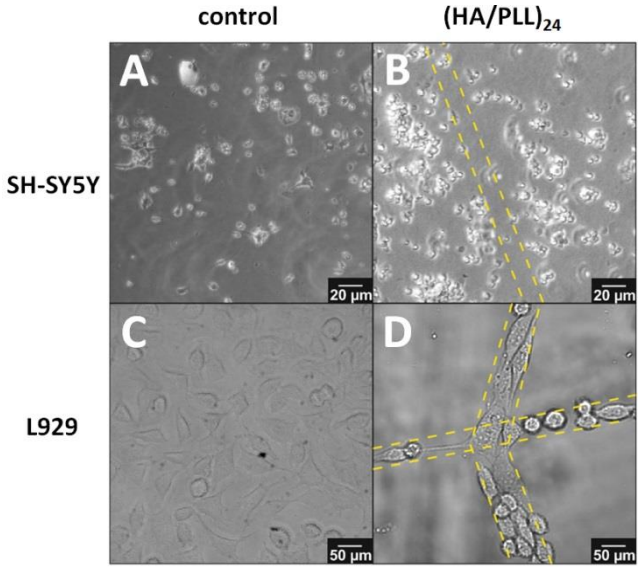

Figure 4.17. Phase contrast images of neuroblastoma SH-SY5Y (upper row) and L929 mouse fibroblast cells (lower row) grown on bare glass as a control (**A, C**) and on $(HA/PLL)_{24}$ film (**B, D**), respectively. All cells were seeded at a concentration of 10^4 cell/cm^2. Scratched areas are marked by the dashed yellow lines.

It is crucial to establish a system which will have high storage capacity for small molecules and still be attractive and not repellent to as many cell types as possible. To achieve this, $(HA/PLL)_{24}$ films were coated with AuNPs according to the recently established protocol.[46] Different cell types (L929, HEK, and HeLa) have been examined for adhesion to the AuNPs coated and non-coated $(HA/PLL)_{24}$ films. All cell lines have spread in the scratched area of non-coated films (Fig. 4.18, middle column). However, the areas distant from the scratched area remained fairly unpopulated meaning that cells do not spread on the film. Cell spreading into the scratched areas leads to the increased density of L929 cells

(Fig. 4.18B). $(HA/PLL)_{24}$ induce considerable aggregation of HEK cells in the scratches, as can be seen in Fig. 4.18E.

On the other hand, all cell lines with exception of HEK settled on AuNPs stiffened films, which is in accordance with the earlier findings that the mechanical softness of HA/PLL assemblies plays an important role in their repellent properties. HeLa cells can easily discriminate between scratched areas, coated and non-coated films. It is clear that AuNPs improves cellular adhesion of two out of three tested cell types. Table 4.5 gives an overview of cell adhesion and growth on the studied films according to the results shown in Fig. 4.18.

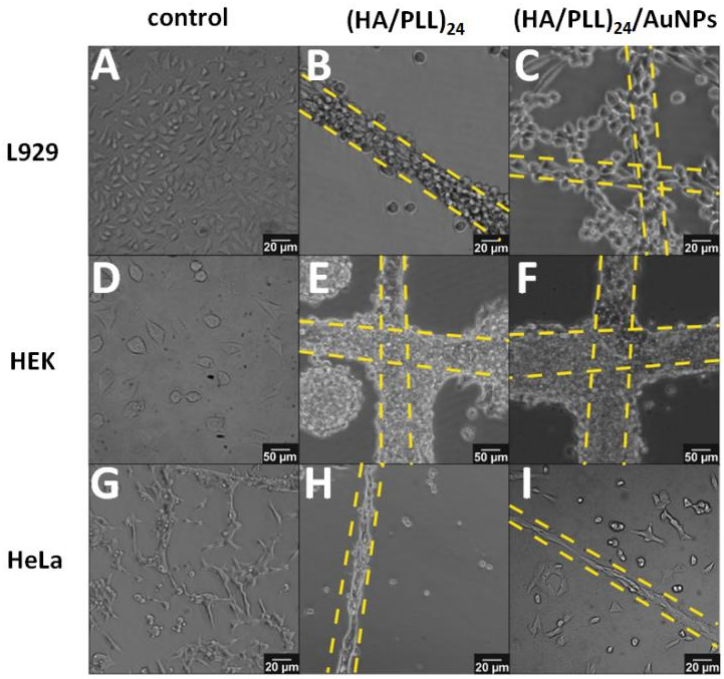

Figure 4.18. Phase contrast images of cells seeded on $(HA/PLL)_{24}$ films and corresponding films coated with AuNPs. Cell lines are L929 (**A**-**C**), HEK (**D**-**F**), and HeLa (**G**-**I**). The cells were seeded on bare glass slides for control (left column), on $(HA/PLL)_{24}$ films (middle column), and on $(HA/PLL)_{24}$/AuNPs films (right column). Cells were seeded at a concentration of 10^4 cell/cm^2. The scratched areas are marked by dashed yellow lines. Brightness and contrast of images are adjusted.

Table 4.5. Summarized cell adhesion on coated and non-coated HA/PLL films.

Cell line line	$(HA/PLL)_{24}$		$(HA/PLL)_{24}$/AuNPs	
	scratch	film	scratch	film
L929	+	-	+	+
HEK	+	-	+	-
HeLa	+	-	+	+

Another observation of the cell adhesion experiment shown in Fig. 4.19 is appearance of irregular fiber-like structures on the non-coated film. This does not appear on AuNPs-coated films and they also do not appear when films are incubated only in Tris buffer. To examine whether cells induce the formation of these structures, non-coated and coated films were incubated overnight with cell growth medium. Surprisingly, these structures

appeared again only on the non-coated films (Fig. 4.19A), while coated ones remained as they were (Fig. 4.19B). This means that components of the cell culture medium but not cell-expressed molecules are responsible for the formation of the observed structures. As almost 50 % of PLL in HA/PLL represents the mobile fraction with a high diffusion coefficient of up to 1 $\mu m^2/s$,[246] it is possible that, when diffusing, PLL reaches the film surface it interacts with negatively charged components of the cell culture medium such as serum proteins (10 % by weight) and forms insoluble complexes (the observed structures). At the same time, a rationale for this not taking place with coated films could be that AuNPs prevent mobile PLL fraction to be in direct contact with the medium. Moreover, they hinder PLL to diffuse out of the film and to form the insoluble complex.

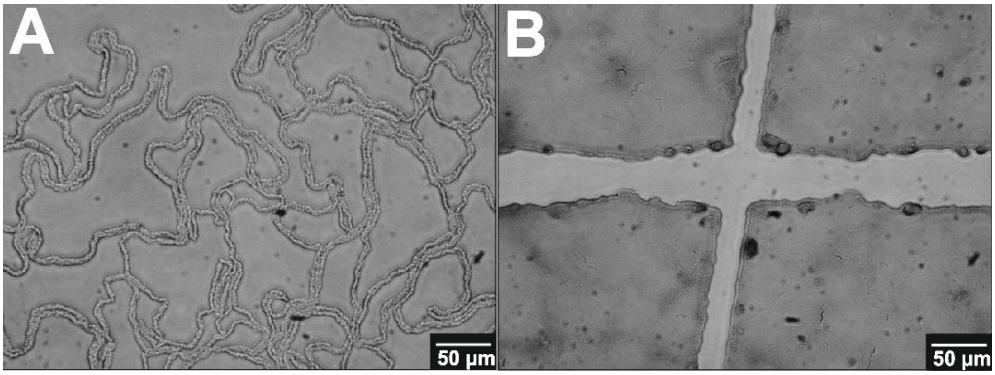

Figure 4.19. Phase contrast images of $(HA/PLL)_{24}$ and $(HA/PLL)_{24}$/AuNPs films incubated for 24 h in 10 % FBS DMEM cell growth medium. When incubated with cell growth medium, (**A**) the morphology of the non-coated film is significantly changed and (**B**) the morphology of the coated film is unchanged.

4.4.2 AuNPs coatings as a barrier for diffusion

To test the hypothesis of AuNPs being a sort of barrier for PLL to diffuse out of the film, transport of molecules of different sizes and charges into the AuNPs-coated films has been examined. Small fluorescent molecule CF and large positively charged PLL^{FITC} (15 - 30 kDa) have been employed. The probes have been brought in contact with the film and fluorescence from the film has been monitored to examine the diffusion kinetics. The films coated with γ = 1.5 and γ = 3 AuNPs were further used.

After exposing both non-coated and AuNPs-coated films to solution of small CF molecules, the diffusion of CF into the film occurs almost instantaneously, regardless of the value of γ (not shown). The fluorescent signal coming from $(HA/PLL)_{24}$/AuNPs films in contact with CF solution reaches its maximum in 10 min and does not change significantly afterwards. However the situation is essentially different with the large molecule. While PLL^{FITC} saturates the bare film within 20-30 minutes, its diffusion into AuNPs-coated films is considerably slowed down by γ = 1.5 and totally blocked if γ = 3 (Fig. 4.20). Diffusion of PLL^{FITC} and CF cannot be compared quantitatively, but the very fact that the film becomes saturated with CF rather fast indicates a fast diffusion rate of CF into the film.

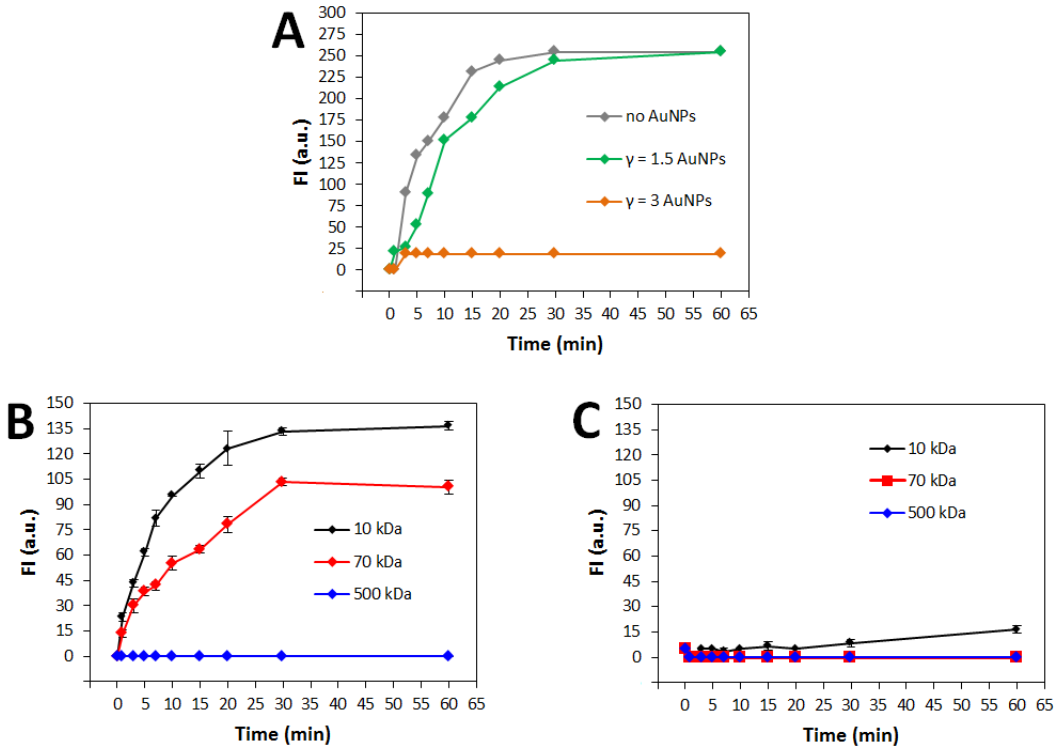

Figure 4.20. (**A**) Fluorescence intensity (FI) of $(HA/PLL)_{24}$ film and $(HA/PLL)_{24}$/AuNPs films (γ = 1.5 or γ = 3) during incubation with PLL^{FITC}. (**B**) Fluorescence intensity of $(HA/PLL)_{24}$ and (**C**) $(HA/PLL)_{24}$/AuNPs films (γ = 3) in the presence of 10 kDa, 70 kDa, and 500 kDa FITC-labeled dextrans.

Diffusion of charged molecules, CF and PLL^{FITC}, has been examined. However, the question remains what will be the behavior of non-charged molecules. Therefore, non-charged molecules - dextrans - of various molecular masses (10 kDa, 70 kDa, and 500 kDa) have been employed to evaluate the impact of molecular masses to permeability of the AuNPs coatings. Fig. 4.20B shows a cut-off for non-coated films between 70 kDa and 500 kDa. Diffusion of 500 kDa dextran is fully hindered and 10 kDa and 70 kDa dextrans can rather easily penetrate into the film saturating it after 30 min of incubation (Fig. 4.20B). A similar time is necessary to saturate the film with charged PLL (15-30 kDa) (Fig. 4.20A). This is another confirmation that the mesh size of the polymer network of the film plays a significant role for diffusion of macromolecules into the film. To evaluate how AuNPs affect molecular transport, dextran diffusion into the film has been examined for the films with γ = 3 (Fig. 4.20C). The coated film is almost impermeable even for the shortest dextran (10 kDa).

4.4.3 Enzymatic degradation of films by cells

Since the AuNPs can prevent even the smallest of tested dextrans to enter the film, it could mean that AuNPs can as well prevent other large molecules, such as those of the family of hyaluronidase enzymes (Mw ~ 54 kDa) and proteases (Mw ~ few tens of kDa) from entering and affecting the film. The focus is on protection of HA/PLL films from enzymatic degradation. The L929 cells were seeded on non-coated and AuNPs-coated $(HA/PLL)_{24}$ films comprising scratches each (width of about 20 µm). Fig. 4.21A-B demonstrates the enzymatic

degradation potential of L929 fibroblasts which significantly widens the scratched area up to 100 µm after 3 days of culturing the cells on the films. The dimensions of the scratch before and after incubation with L929 cells are marked in red and yellow, respectively. The fluorescence of the film (the film was labeled with PLL^{FITC}) has decreased after incubation with cells (Fig. 4.21A), which is most probably caused by film degradation. Fluorescence from the rims of the film can be observed (green in Fig. 4.21A). The rims are formed due to the mechanical compression of the film[110] caused by the scratching procedure. Denser or/and thicker rims can be visually identified in Fig. 4.21B. Another reason for reduced film fluorescence might be due to quenching of PLL^{FITC} by DMEM cell culture medium, which contains 10 % of serum proteins from FBS (Fig. 4.22F). It is noteworthy that the films incubated either in Tris buffer or in cell culture medium during 3 days without cells do not degrade as there is no change of width of the scratched area (Fig 4.22A-E).

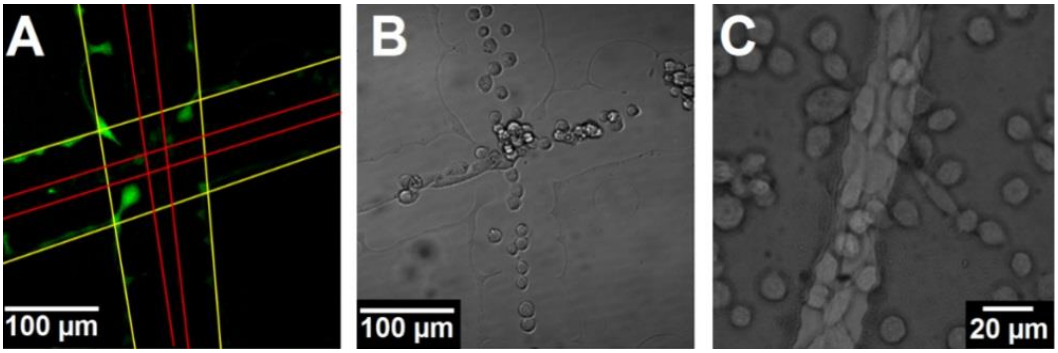

Figure 4.21. (**A**) Fluorescence and (**B**) transmission images of L929 cells on $(HA/PLL)_{24}$; The film was labeled with PLL^{FITC}. (**C**) transmission image L929 cells on $(HA/PLL)_{24}$/AuNPs (γ = 3). Red lines in A present initial position of the scratched area, and yellow lines after three days of cellular growth. L292 cells were seeded at 5 x 10^4 cells/cm^2 and films with cells were incubated in 10 % FBS DMEM medium at 37 °C and 5 % CO_2. Cells were not fluorescently labeled. Images were taken after 3 days.

Fig. 4.21C shows a transmission image of the $(HA/PLL)_{24}$/AuNPs (γ = 3) with L929 cell growing on the film for three days. Improved cellular adhesion correlates well with the previously described results (Section 4.4.1), which showed that the coating with nanoparticles enables the cells to adhere to the film by increasing stiffness of the film. One can see that the film is cell-adhesive and the width of the scratched area is unchanged, which proves the resistance of the films to enzymatic degradation. The width of the scratched area in $(HA/PLL)_{24}$/AuNPs was 20 µm before seeding the cells, as well as after a 3-day period, which would suffice for cells to hydrolyze non-coated $(HA/PLL)_{24}$ films.

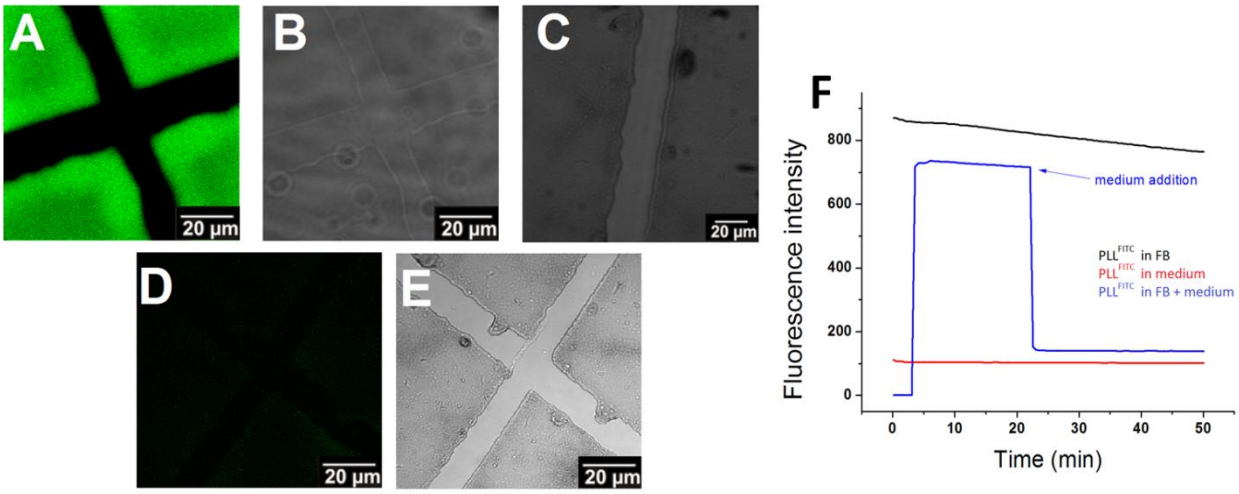

Figure 4.22. (**A**) Fluorescence and (**B**) transmission images of an X-shaped scratched area in a $(HA/PLL)_{24}$ film labeled with PLL^{FITC}, and (**C**) **|**-shaped scratched area in a $(HA/PLL)_{24}$/AuNPs film, all in Tris buffer. (**D**) Fluorescence and (**E**) transmission images of the X-shaped scratched area in a $(HA/PLL)_{24}$ film labeled with PLL^{FITC} in cell culture medium with 10 % FBS. All images were taken after three days of incubation, and the width of the scratched areas (~20 µm), as well as the overall geometry have not changed. Fluorescence intensity and width remained stable even after seven days in Tris buffer, which indicate that there is no spontaneous decomposition of the film. The film is stable in medium as well as in Tris buffer, but the fluorescence intensity is low due to (**F**) quenching of FITC fluorescence by medium (DMEM with 10 % FBS).

4.5 Caged ATP as a source of ATP

Model molecules such as CF, Rho, and ATP were used to examine mechanisms of SCM storage and release, as they can be determined rather simply. It was done in order to understand the potential of HA/PLL films to act as reservoirs for SCM. After having described the cellular adhesion onto the films, the next step was made towards their functionalization. Here, the stability and light-triggered uncaging of cATP and their loading and release from $(HA/PLL)_{24}$ films were studied. Loading $(HA/PLL)_{24}$ films with cATP was the main approach to obtain the light-sensitive drug delivery system for localized extracellular stimulation of cells.

4.5.1 Stability and light activation

Structures of cATP (NPE-ATP, DMNPE-ATP, DMB-ATP) used in the study are given in Fig. 3.2. Their main feature is that they are comprised of ATP covalently bound to a caging group which blocks bioactivity of ATP. This covalent bond is photosensitive and cleaves upon absorption of UV photons. The stability of cATP and their sensitivity to ambient light in laboratory conditions were tested (Fig. 4.23A-B) by storing 1 µM cATP solutions in the laboratory without any protection from light. In addition, the rate of uncaging and the release of free ATP from polyelectrolyte layers was examined by exposing 1 µM cATP solutions to 16 W/cm^2 UV light (Fig. 4.23C). The uncaging efficiency was determined by measuring released ATP using the luciferase assay. As a control, it was shown that 1 min of

irradiation completely uncages cATP, with the exception of DMB-ATP, and the uncaging yield is 98.6 ± 1.5 %.

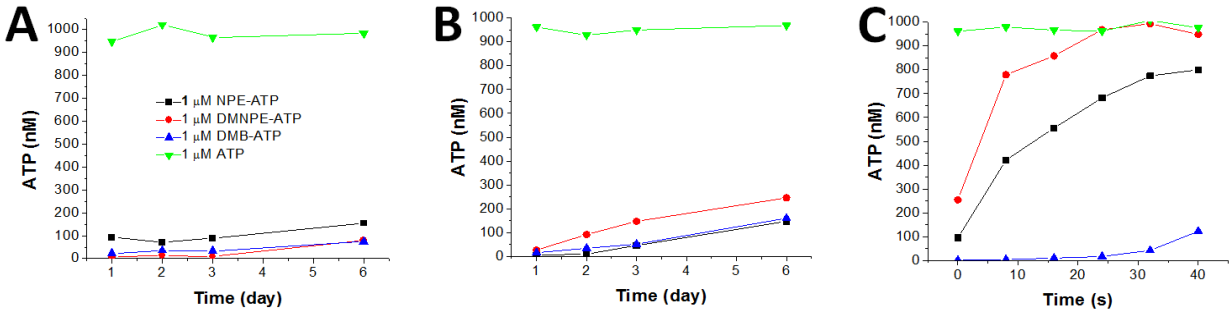

Figure 4.23. Spontaneous uncaging of cATP in solution (**A**) in dark (protected from light) and (**B**) in ambient light conditions during six days. (**C**) Uncaging of cATP in solution during exposure to 16 W/cm^2 UV light from a lamp. As a control of ATP stability, ATP was treated the same way as its caged counterparts in all experiments. ATP was determined using the luciferase assay.

Ambient light does not significantly increase the uncaging of cATP in solution compared to dark conditions during six day period (Fig. 4.23A-B). On the other hand, when UV light from a lamp is applied, the uncaging occurs on a time scale of few tens of seconds (Fig. 4.23C). ATP is readily released. DMNPE-ATP is completely uncaged after only 25 s. NPE-ATP gives 15 % lower yield in comparison to DMNPE-ATP, whereas DMB-ATP turned out to be rather poor donor of ATP, as it was uncaged even after 30 min of irradiation.

Since cATP contain ATP, it was essential to assess if cATP can act as a substrate for the luciferase assay. Thus, the solution containing ATP, or DMNPE-ATP, or equimolar amounts of ATP and DMNPE-ATP were analyzed using the luciferase assay. The results given in Fig. 4.24 show that 2 µM ATP solution exerted the highest fluorescence, whereas DMNPE-ATP showed zero reactivity with the assay. The equimolar solution of ATP and DMNPE-ATP had 50 % of the luminescence of pure ATP solution. These finding confirm that cATP do not interfere with the luciferase assay, and that only ATP, but not cATP, acts as a substrate for luciferin.

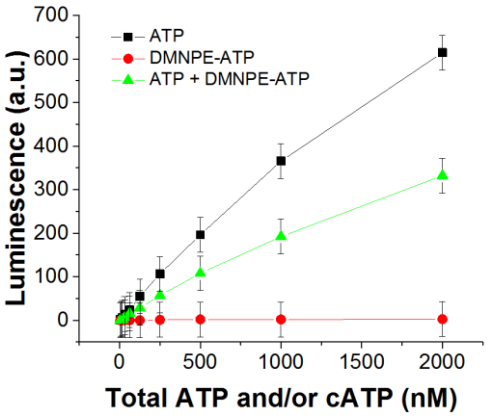

Figure 4.24. Luminescence of ATP (black), DMNPE-ATP (red), and equimolar ATP + DMNPE-ATP (green) solutions during the luciferase assay.

4.5.2 Loading into and release from the films

Loading of cATP. After checking the stability and uncaging kinetics of cATP, these molecules were loaded into $(HA/PLL)_{24}$ films by incubation. The loading efficiency was 38.6 ± 7.3 %, 39.2 ± 6.3 %, and 36.1 ± 7.4 % for NPE-ATP, DMNPE-ATP, and DMB-ATP, respectively. The calculated mass of ~2 μm thick $(HA/PLL)_{24}$ film on a 12 mm glass slide with the density of 1 g/cm3 the film is $3.1x10^{-4}$ g, which means that the relative increase of the film mass after loading with DMNPE-ATP was 0.06 ± 0.02 %, and after loading with control ATP was 0.14 ± 0.03 %.

Real-time observation of ATP and cATP loading. QCM measurements were done with kind help from Guy Guday, Fraunhofer IZI-BB, Potsdam. QCM was employed for the observation of real time loading of ATP and DMNPE-ATP. Initially, $(HA/PLL)_5$ films were assembled on a QCM chip using solutions of the same concentration as for the dipping method. Afterwards 1 μM ATP or DMNPE-ATP solution is passed until the film was saturated and then washed with Tris buffer until the new plateau is achieved. The increase of the film mass after loading of DMNPE-ATP was 0.12 ± 0.05 %, and after loading with ATP was 0.07 ± 0.01 %. Interestingly, when the solution of dissociated DMNPE-ATP (contains DMNPE and ATP in equimolar amounts) was passed, the saturation of the film after washing was achieved when the mass increase was 2.0 ± 0.2 %.

By comparison of the loading efficiencies of the two methods, it is obvious that the increase of the mass of the $(HA/PLL)_{24}$ film during incubation-loading with DMNPE-ATP is 0.06 ± 0.02 % is in line with the 0.07 ± 0.01 % obtained during loading in the QCM chamber. In the case of ATP, the mass of the film increased 0.14 ± 0.03 % and 0.12 ± 0.05 % for incubation-loading and QCM-loading, respectively. These results indicate that both loading methods lead to the saturation of the films with either ATP or DMNPE-ATP.

Release of cATP from the films. The release of cATP from $(HA/PLL)_{24}$ films is shown in Fig. 4.25. NPE-ATP and DMNPE-ATP are released at the same relative rate, few times faster than ATP, again most probably due to the lower charge density which decreases the ability to interact with the film. After 90 min around 18 % of both NPE-ATP and DMNPE-ATP are released from the film, with the tendency to form a plateau, which would leave total of roughly 80 % of stored cATP in the film (320 pmol or 1.4 mM).

The measurement of released cATP is indirect and requires uncaging ATP from cATP using UV light. Since it has been shown previously that DMB-ATP is not susceptible to uncaging during reasonable time, all further experiments were conducted with DMNPE-ATP, which although has the same relative release profile as NPE-ATP, has a higher uncaging yield (Fig. 4.23).

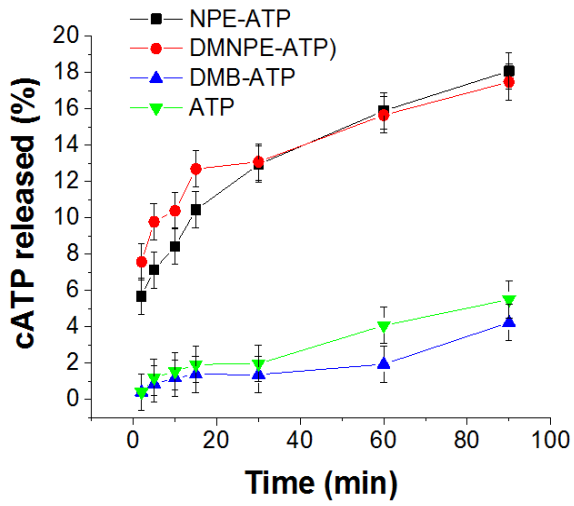

Figure 4.25. Release of cATP from $(HA/PLL)_{24}$ films.

4.5.3 UV-triggered release of ATP from cATP stored in the film

Release of ATP from cATP stored in the film. After having characterized the uncaging dynamics and loading of the films with cATP, a method for localized release of ATP from film loaded with cATP was established. The approach was based on the application of an UV-laser over a 40 x 30 μm^2 area of the loaded film for 45 s. The supernatant above the irradiated zone is immediately collected and saved for further ATP concentration determination. An additional aliquot was collected above non-irradiated zone of the film as a control. The scheme of the experiment is given in Fig. 4.26.

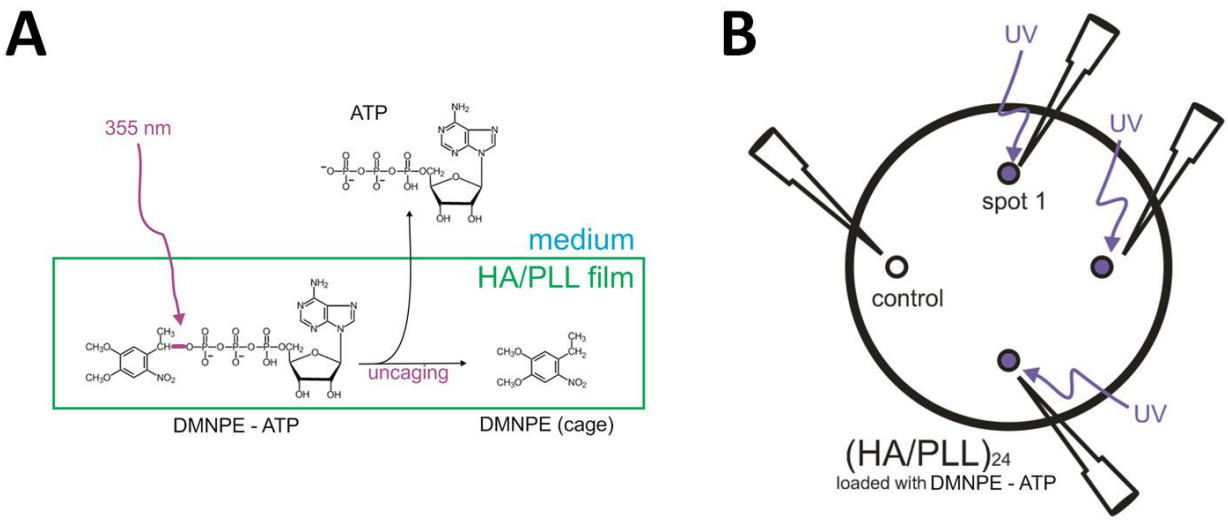

Figure 4.26. (**A**) Schematics of the method – UV light is applied to a 40 x 30 μm^2 area of the $(HA/PLL)_{24}$ film loaded with DMNPE-ATP; UV-light locally cleaves all photolabile bonds of DMNPE-ATP molecules and ATP is released from the film. (**B**) The irradiation is repeated three times in different parts of the film (purple circles) and 50 µL aliquots were collected above the areas irradiated. As a control, the fourth sample (white circle) was taken at the end in the same manner as the previous three, only without prior irradiation. Afterwards, ATP concentrations were determined in all collected aliquots. Details of the experiment are given in Section 3.7.2.

Before irradiation, the ATP in the solution above the film was not detected. After irradiation, the average concentration of released ATP determined from a 50 µL sample collected after each irradiation was 17.6 ± 7.5 nM, whereas the control, taken after three irradiations were done, contained 2.8 ± 1.5 nM of ATP. In terms of the amount, it means that every irradiation releases 0.88 ± 0.37 pmol of ATP from the film, i.e. since 320 pmol of cATP can be loaded, theoretically around 360 deliveries of ATP can be achieved from one loaded film.

4.6 Light triggered cell activation

Characterization of the loading of cATP and UV light-triggered release of ATP from cATP stored in the film was described in the previous sections. This support is thus shown to be effective for highly localized extracellular delivery of ATP, which is a bioactive compound that can stimulate cells to elicit the iCa^{2+} (Section 2.3.2). In pursuit of the development of new assays and exploitation of HA/PLL films loaded with cATP for stimulation of cells, the response of cells was examined. Here, cells are seeded on the $(HA/PLL)_{24}$ films loaded with cATP. Afterwards, UV-light is applied to locally uncage cATP stored in the film in order to release ATP. ATP would then bind to P2X and P2Y receptors on the cell membrane, which would in turn lead to the increase of $[iCa^{2+}]$. This increase would be monitored and measured indirectly by Ca^{2+}-sensitive fluorophores that were loaded into the cells prior to the experiment. After that the response of cells (fluorescence change) was quantified, which gave information required for the analysis of the effectivity of extracellular UV light-triggered ATP release and stimulation of cells.

4.6.1 Cellular response: Ca^{2+} staining and optimization

Oregon Green 488 BAPTA-2 (OG) and Fluo-3 are derivatives of Ca^{2+} chelator BAPTA. Both dyes are in the form of acetoxymethyl esters meaning that their chelating ability is blocked. However, after the dyes enter the cell through the membrane, the blocking acetoxymethyl groups are removed by cellular esterases and the dyes are able to chelate Ca^{2+}. Their fluorescence increases 14-100 x upon Ca^{2+} binding. OG and Fluo-3 are tested in order to determine which one detects changes of $[iCa^{2+}]$ more efficiently in HeLa cells. HeLa cells are chosen as they make the best distinction between $(HA/PLL)_{24}$ films and the scratched area under given conditions (Section 4.4.1).

HeLa cells seeded on glass slides were stained with different concentrations of either OG or Fluo-3 dye: 5 µM, 10 µM, and 20 µM. Afterwards, ATP was added to the sample to obtain final concentration of 5 µM, 50 µM, 500 µM, and 5000 µM. External ATP elicits iCa^{2+} which is chelated by OG and Fluo-3. Upon chelation, the fluorescence of dyes increases. Images of cell fluorescence were taken before and after addition of ATP, and the change in total fluorescence of all cells was determined. The results are given in the Table 4.6, and the representative image in Fig. 4.27.

Table 4.6. Increase of fluorescence of HeLa cells stained with OG or Fluo-3 after addition of different concentrations of ATP.

ATP final	OG			Fluo-3		
	20 uM	10 uM	5 uM	20 uM	10 uM	5 uM
5000 µM	/	27 %	13 %	35 %	8 %	/
500 µM	37 %	28 %	6 %	21 %	12 %	/
50 µM	16 %	23 %	/	24 %	12 %	/
5 µM	8 %	17 %	/	29 %	/	/

From the results above it is clear that Fluo-3 is able to provide relevant signal only when it is applied at 20 µM and 10 µM, and even in that case it is insensitive to low ATP concentration (5 µM). On the other hand, 10 µM OG increased the fluorescence by 17 % when 5 µM ATP was added. Even 5 µM OG was able to sense the change in [iCa^{2+}] when ATP was added. Since OG was shown to have higher sensitivity for low ATP concentrations, 10 µM OG was selected as dye for further experiments.

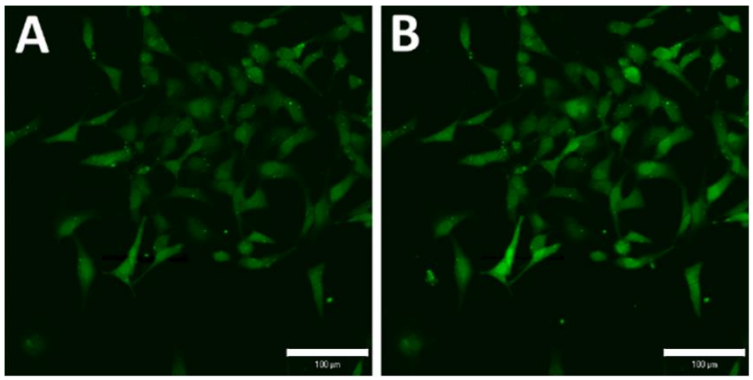

Figure 4.27. Fluorescence images of HeLa cells stained with 10 µM OG (**A**) before and (**B**) 8s after addition of 5 µM ATP (at the peak of the fluorescence intensity of cells). The increase in fluorescence intensity after ATP addition was about 17 %, as determined by measuring integral fluorescence of the images. Scale bar 100 µm.

4.6.2 Real-time monitoring of cellular response

Extracellular UV light-triggered stimulation of cells. HeLa cells were seeded on the $(HA/PLL)_{24}$ films loaded with 1 µM DMNPE-ATP and were afterwards stained with 10 µM OG. Normally, cells spread in scratched areas of the film. Samples were put under a fluorescent microscope and UV light was applied on a part of the film where no cells were spread. Results are given in the Fig. 4.28.

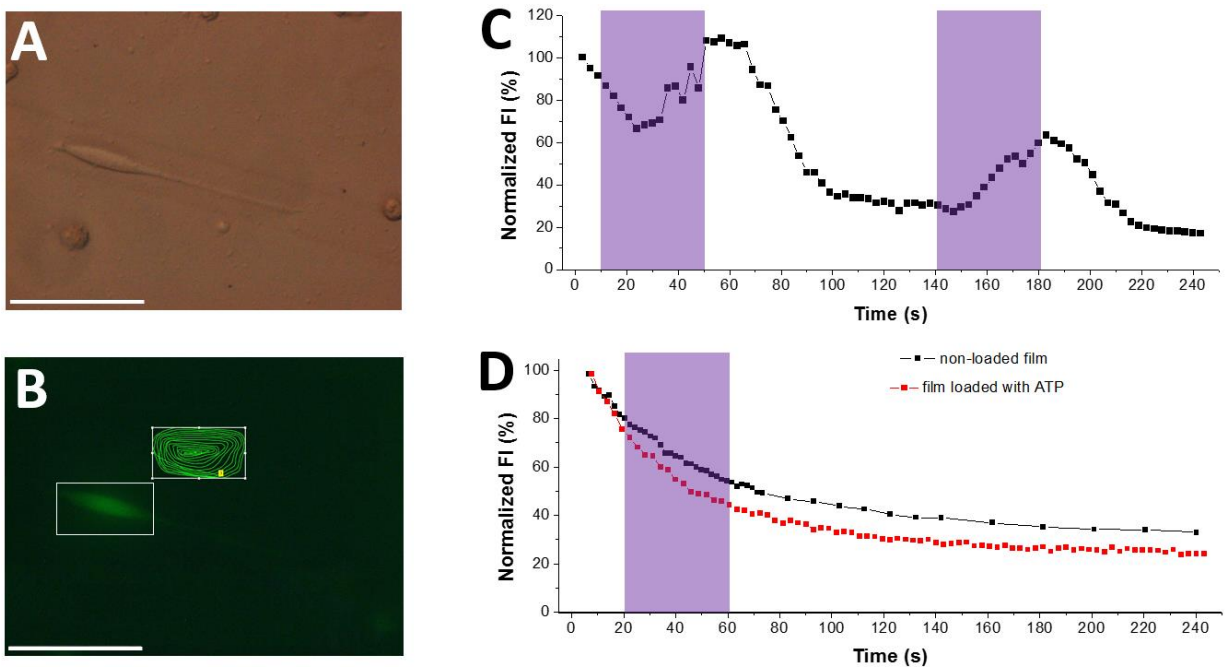

Figure 4.28. Light triggered stimulation of cells. (**A**) Transmission and (**B**) fluorescence images of a HeLa cell spread in the scratched area of a $(HA/PLL)_{24}$ film loaded with DMNPE-ATP. The white rectangle indicates the area in which the fluorescence signal from the cell has been measured; spiral green line inside the white rectangle indicates the area (40 x 30 μm^2) that was irradiated with UV light during 45 s. (**C**) Fluorescence intensity profile of the HeLa cell stained with 10 µM OG before, during and after 2 consecutive periods of irradiation with 355 nm UV light of the same area. UV light uncages ATP which diffuses out of the film and induces a cellular response. (**D**) Control experiment with cells growing on the non-loaded films and on the films loaded with ATP. Irradiation periods are marked with purple rectangles. The intensity is normalized to the highest fluorescence value of non-stimulated cells. Scale bar 75 µm.

The experiment shows that application of UV light releases ATP from its caged precursor DMNPE-ATP. ATP diffuses out of the film and affects the cells, which is proven by spikes in $[iCa^{2+}]$ shown in Fig. 4.28C. Furthermore, the effect can be repeated although the second spike represents 25 % fluorescence increase, in comparison to the 40 % increase after the first stimulation. It is important to note that third irradiation did not produce detectable signal change. Cells grown on the non-loaded films and on the films loaded with ATP were not stimulated after irradiation of these films (Fig. 4.28D).

In addition, the experiment was repeated, though this time two different places were irradiated in order to assess homogeneity of film loading, uncaging, and release (Fig. 4.29). Both regions of irradiation were chosen to be 75 µm away from the observed cell. The peaks after the first and the second subsequent irradiations represent 100 % increase of fluorescence. The irradiation of the second area caused the identical effect of the cell stimulation as did the irradiation of the first area. This means that the release from the film is localized only within the area affected by the UV laser and not from the whole film.

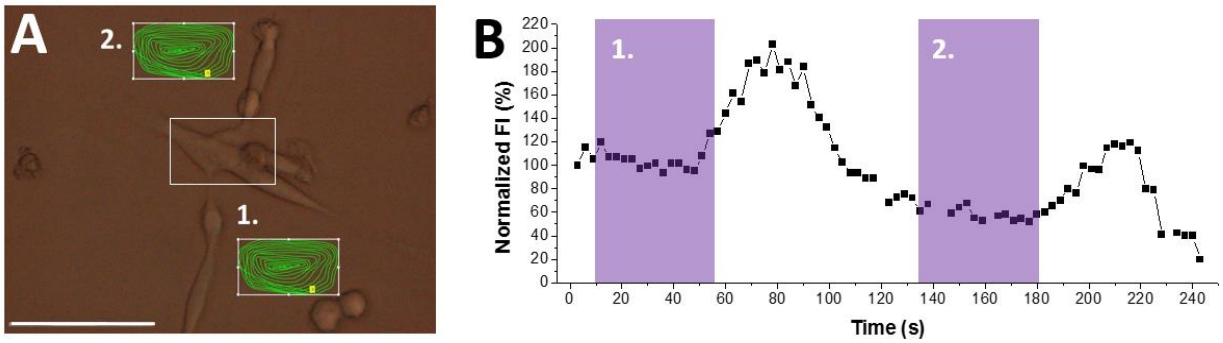

Figure 4.29. Light triggered stimulation of cells. (**A**) Transmission images of HeLa cells spread in the scratched area of the $(HA/PLL)_{24}$ film loaded with DMNPE-ATP. The white rectangle indicates the area in which the fluorescence signal from the cell has been measured; two green spirals inside the white rectangles indicate two areas marked 1. and 2. (40 x 30 μm^2) which were irradiated with UV light during 45 s. (**B**) Fluorescence intensity profile of the HeLa cells stained with 10 µM OG before, during and after 2 consecutive periods of irradiation of areas marked 1. and 2. in (A). UV light uncages ATP which diffuses out of the film and stimulates cells. Irradiation periods are marked with purple rectangles. The intensity is normalized to the highest fluorescence value of non-stimulated cells. Scale bar 75 µm.

In addition, cells, which are at equal distances of about 70 µM from the irradiation zone, respond simultaneously and with comparable intensity to ATP released from the film (Fig. 4.30). This means that diffusion of free ATP is surprisingly fast. Both cells after both irradiation periods show an increase of fluorescence intensity of roughly 50 % compared to the steady state prior to the irradiation.

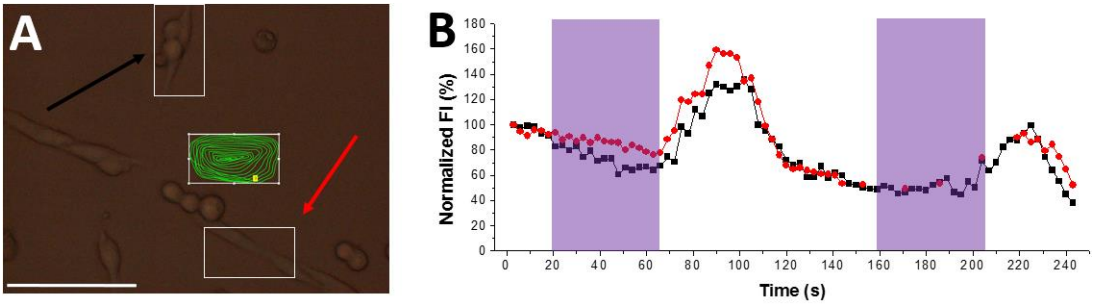

Figure 4.30. Light triggered stimulation of cells. (**A**) Transmission images of HeLa cells spread in the scratched area of the $(HA/PLL)_{24}$ film loaded with DMNPE-ATP. The white rectangles indicate the area in which the fluorescence signal from the cells has been measured; the spiral green line inside the white rectangle indicates the area (40 x 30 μm^2) which was irradiated with UV light during 45 s. Observed cells were 70 µm away from the irradiated zone. (**B**) Fluorescence intensity (FI) profile of the HeLa cells stained with 10 µM OG before, during and after 2 consecutive periods of irradiation with 355 nm UV light. UV light uncages ATP, which diffuses out of the film and induces the cellular response. Irradiation periods are marked with purple rectangles. The intensity is normalized to the highest fluorescence value of non-stimulated cells. Scale bar 75 µm.

Cell viability. Although the UV laser was used only locally, it was of high importance to check if the UV light affects the cells in the vicinity of the irradiation zone. Propidium iodide was used for the cell viability assay. Cells were not affected by UV irradiation of areas

in their vicinity (Fig. 4.31A-D), though direct irradiation of cells caused their imminent death (Fig. 4.31E-F).

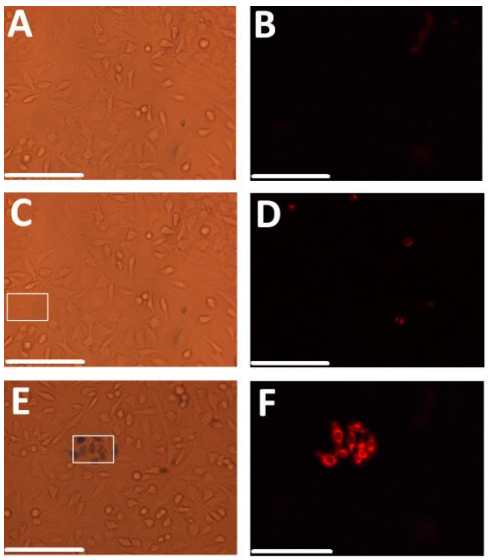

Figure 4.31. Viability of cells (**A-B**) before and (**C-D**) after irradiation of a 60 x 80 μm^2 area with UV light - no cells were directly affected. The irradiated zone was not populated with cells and is marked with a white rectangle in (C). (**E-F**) As a control, cells marked with the white rectangle in (E) were irradiated directly. (**A, C, E**) Transmission and (**B, D, F**) fluorescence images are shown. Scale bar 150 μm.

4.6.3 Spatio-temporal characteristics of activation

As shown in the previous section, cells responded to extracellular ATP released from DMNPE-ATP stored in $(HA/PLL)_{24}$ films after UV light has been locally applied. However, it is of interest to measure the level of stimulation of cells at different distances from the irradiation zone in order to examine spatio-temporal effects of the ATP release.

The time point of the onset of the cellular response is identical for all cells, regardless of their distance from the irradiation point (Fig. 4.32B). Furthermore, the fluorescence intensity decreases as the cells are further away from the irradiation zone. At distances greater than 120 μm, no change of fluorescence intensity is detected – cells at 1200 μm, 900 μm, 600 μm and 300 μm were not stimulated (Fig. 4.32C). The peak of [iCa^{2+}] after the irradiation decreases with the square distance between cells and the irradiation zone.

In addition, in a separate experiment, irradiation time was varied and the response of cells 30 μm away from the irradiation zone was observed. Results given in Fig. 4.32D suggest that the irradiation time cannot be varied significantly in order to achieve more potent stimulation of cells. Irradiation time below 30 s did not induce a significant increase in fluorescence intensity, whereas irradiation periods longer than 30 s induced the same effect as 30-35 s irradiation periods.

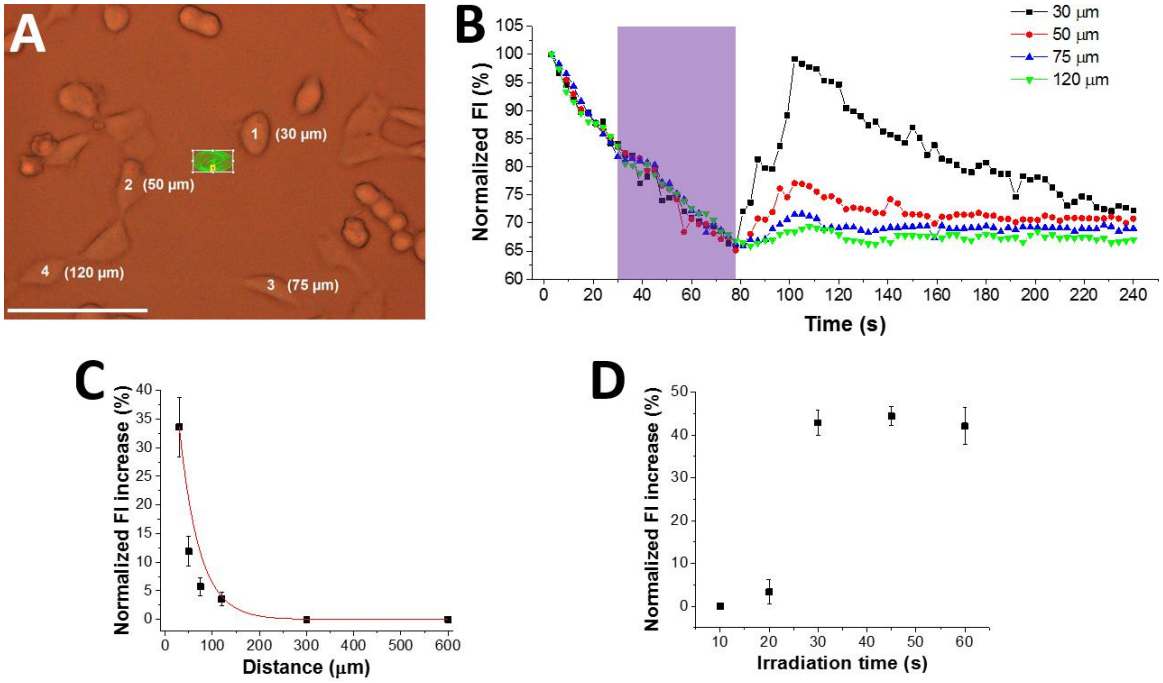

Figure 4.32. Level of cell stimulation as a function of distance from the irradiation zone. (**A**) HeLa cells are seeded on a $(HA/PLL)_{24}$ film loaded with DMNPE-ATP. The irradiation zone (40 x 30 µm^2) is marked with the green spiral line inside the white rectangle which was irradiated with UV light during 45 s. Cells at distances 30 µm, 50 µm, 75 µm, and 120 µm are marked with numbers 1, 2, 3, and 4, respectively. Scale bar 75 µm. (**B**) Fluorescence profiles of HeLa cells stained with 10 µM OG, marked 1-4 in (A), before, during and after irradiation with 355 nm UV light. The irradiation period is marked with a purple rectangle; the intensity is normalized to the highest fluorescence value of non-stimulated cells. (**C**) Cell fluorescence intensity as a function of cell distance from the irradiation zone after UV light-triggered release of ATP from the film. The fluorescence intensity after irradiation is calculated from the surface area beneath corresponding profiles. An exponential function $y = y_0 + a \times e^{b \times x}$ was fitted to the data by (red curve). (**D**) Dependence of the increase of the fluorescence signal intensity on the duration of irradiation. Observed cells are 30 um away from the irradiation zone.

5 DISCUSSION

5.1 Stability and characterization of HA/PLL films

The main topic of the study was to develop an approach for highly localized extracellular stimulation of adherent cells by light-triggered release of biomolecules. For this, multilayer films assembled from HA and PLL were employed. HA/PLL films were assembled using the modern dip coating method and the results indicate that the films had high integrity as concluded from long term stability experiments (Fig. 4.1). The films remain stable and unchanged up to seven days of storage in Tris buffer at physiological pH.

A number of analytical methods were applied to help understand the film properties and the effect of PLL length on the film properties. Since cellular adhesion is significantly influenced by mechanical properties of their surroundings, Young's modulus of the prepared films was measured. Young's moduli of $(HA/PLL_{short})_{24}$ and $(HA/PLL_{long})_{24}$ are fairly the same - 2.41 ± 0.18 kPa and 2.84 ± 0.35 kPa, respectively. This indicates a rather soft structure of the films (Fig. 4.2), which is expected since HA/PLL films are known to be immensely hydrated - water consists roughly 80 % of the film weight.[33]

The films prepared with PLL of different lengths have the same softness, which might be explained by the dominant role of HA for the film softness and rather minor contribution of PLL. HA is an extremely hydrated polymer.[112,113] Higher variation of E_0 across the films prepared using PLL_{long} have been observed (red curve in Fig. 4.2C). The changes in E_0 as a function of the position on the film surface are obviously more pronounced for PLL_{long}; the variations are observed on the scale of micrometers that is much beyond the polymer size. Thus, it is hard to conclude that polymer length can be responsible for the variation of E_0.

The thicknesses of the films prepared using PLL of different lengths are not similar and the film prepared using PLL_{long} is almost twice thinner than the film prepared with PLL_{short}(Fig. 4.3). This could be attributed to the difference in polymer mobility within the film, i.e. diffusion of short and long PLL chains. The lower the diffusion, the thinner the film because the film growth is determined by polymer diffusion.[34] However, the previous is valid only above a certain number of deposited bilayers when the film is thick enough and diffusion can start to play a role. Shorter PLL chains diffuse easily into the film[34] and throughout the whole film as they are shorter and form less contacts with immobile HA chains. On the other hand most probably significantly less mobile long PLL chains diffuse only within the upper part of the film.[34] Due to this limitation the inflow of building materials (PLL and HA molecules) into the film is lower, causing the final thickness of $(HA/PLL_{long})_{24}$ films to be smaller.

Differences in mobility of PLL_{short} and PLL_{long} were confirmed by FRAP experiments (Fig. 4.4). PLL_{short} was found to have two fractions of molecules – diffusive (D_{fast} = 0.17 ± 0.10 μm^2/s) and immobile (D_{slow} < 0.01 μm^2/s). PLL_{long} is almost fully immobile

(D_{slow} < 0.01 µm^2/s) (Fig. 4.5). The presence of two populations of molecules for PLL_{short} might be explained looking at a critical number of ion pairs formed between amino groups of PLL and carboxylic groups of HA. If this number is below the critical one, the molecule of PLL will not be in contact with HA anymore and therefore can diffuse. Otherwise, the PLL molecule is bound to immobile HA chain. Fig. 5.1 presents these two assumptions.

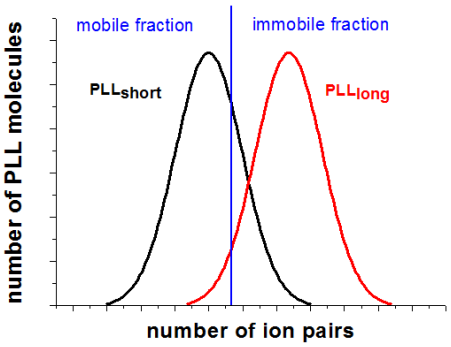

Figure 5.1. A graph showing assumed distributions of PLL_{short} and PLL_{long} molecules relative to the number of ion pairs they form with HA in the film. Vertical blue line represents a threshold left of which PLL molecules have few ion pairs with HA and are mobile (D_{fast} = 0.17 ± 0.10 µm^2/s). Right from the threshold are PLL molecules with significantly hindered mobility due to the increasing number of PLL-HA bonding – these molecules have D_{slow} < 0.01 µm^2/s and are thus considered immobile.

5.2 Reservoir properties of the HA/PLL films

5.2.1 Loading of small charged molecules

The following steps were made to understand reservoir properties of the films towards SCM. The experimental results show that HA/PLL films can readily store SCM such as CF, Rho, and ATP (Fig. 4.7), and there are prior works[56] that show the successful loading of the biologically relevant drug paclitaxel which is small and charged. However, the loading efficiencies achieved with these three species are different. Moreover, the loading efficiency of CF depends on the last deposited layer on the film. Lower CF loading in case of HA-terminated films may be explained by lower PLL content in these films due to PLL diffusion in and out of the films during its buildup.[33,43] According to this diffusion model,[33,43] PLL can diffuse into the film during PLL deposition step and diffuse out of the film during HA deposition. HA-PLL complexes are formed on the top of the film where HA is exposed to the PLL which diffuses out. Therefore, the HA-terminated films have lower content of free positive PLL charges, which means that a smaller amount of negatively charged CF could be loaded into these films in comparison to PLL-terminated films. Considerably higher loading efficiency of ATP might be explained by higher negative charge of ATP compared to CF (three phosphate groups against two carboxylic).

Rho binding to the film does not show any dependence on the last deposited layer, which may be explained by binding of positively charged Rho to negatively charged HA. It

might be reasonable that the number of free negative charges of HA does not depend on the last layer (hence no difference in Rho binding) since HA is immobile and mobile PLL can easily compensate the charges of the upcoming HA molecules.

The high CF concentration in the films is attributed to the binding of deprotonated carboxylic groups of CF to positively charged primary amino groups of polyelectrolytes. CF molecules cannot compete with strong cooperative interpolymer interactions formed by ion pairing between PLL and HA and they bind to free (uncompensated) charges of the polymer backbones.[43] Hence, such high concentration of small molecules in the film must require rather high concentration of free charges of the polyelectrolytes. The HA/PLL film contains about 80 % of water (polymer content in the film is 20 %)[33] and at this high water content the molar concentration of charges on the polymer backbone is estimated to be hundreds of mM. The high mobility of PLL molecules in HA/PLL films that has been shown in this study, points to a rather high number of free (uncompensated) charged groups of PLL and, consequentially, of HA. Thus, high concentration of CF, Rho, and ATP in the film might be explained by rather high concentrations of free charged groups of polyelectrolytes. The concentration of SCM loaded into the film is 3-4 orders of magnitude higher compared to the CF concentration in the stock solution. Such a high partitioning coefficient demonstrates high reservoir capacity of the HA/PLL films for SCM.

5.2.2 Interaction of CF in the film

The interaction of SCM with the film is crucial for understanding of the loading and release mechanisms. The assumption that CF preferentially interacts with PLL was confirmed by incubating CF with either HA or PLL and observing the CF emission spectra – CF has a shifted emission peak only in the presence of PLL in the solution (Fig. 4.8). Therefore, the predominance of CF-PLL interaction over CF-HA interaction in the film is expected. Moreover, CF could be prone to aggregation due to its core hydrophobic part. Considering the two features of CF, three models of CF binding in the film are proposed in the Fig. 5.2.

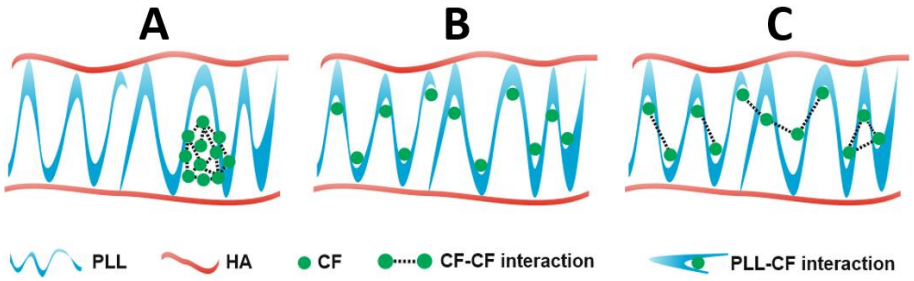

Figure 5.2. Schematic representation of three possibilities of CF binding in the film. (**A**) CF forms aggregates within the film; (**B**) CF does not form aggregates (there are no CF-CF interactions) and binds to PLL, equally distributed throughout the film; (**C**) CF is primarily bound to PLL, but CF-CF interactions are present as well.

The amount of CF that can be loaded into the film is in the range of a few mM (Section 4.2.1), which by far surpasses the solubility of CF in Tris buffer (~500 µM). Such a

high CF concentration could lead to formation of CF aggregates - hence the first model of CF binding in the film (Fig. 5.2A). Contrary to the first model, the second model (Fig. 5.2B) assumes that the energy gain of CF-PLL is higher than the one of the CF-CF interaction and suggests that no aggregate formation occurs - CF is homogenously distributed throughout the film and is bound only to PLL. The third model (Fig. 5.2C) is a combination of the previous two.

The results presented in Fig. 4.9A clearly show that although concentration of CF in the film is a few mM it has an emission peak (λ_{max}) at 516 nm. This is much below λ_{max} = 525 nm of CF in 500 µM solution. Additionally, there are no other visible emission peaks of CF stored in the film, apart from the 516 nm, indicating that only one CF population is present. It would then not be misleading to conclude that there are no CF aggregates in the $(HA/PLL)_{24}$ films. The lack of aggregates, i.e. CF population with λ_{max} = 525 nm, leads to the conclusion that the first model (Fig. 5.2A) is not feasible and that it either model B or C describe the real condition in the film.

The calculated concentration of positively charged amino groups in $(HA/PLL)_{24}$ films is about 500 mM. Since CF concentration in the film is around 2 mM, and at this concentration in solution CF is aggregated, it is logical to assume that there should still be CF-CF interactions present in the film as well. As PLL is more than two orders of magnitude more concentrated in the film than CF, it could mean that CF-PLL interaction would predominate over CF-CF interaction. Fig. 4.9A shows that the emission band of CF in the film has its λ_{max} = 516 nm, which is above λ_{max} = 512 nm of non-aggregated CF and below λ_{max} = 525 nm of assumed aggregated CF (Fig. 4.9C). In addition, as described in Section 4.2.3, the binding of further CF molecules is dependent on previously bound CF molecules. Considering the results so far, the model B has to be rejected, which confirms the model C for CF-PLL interaction in the film, since it is to expect that there will be both CF-PLL and CF-CF interactions in the film.

Fig 4.10A shows the behavior of CF fluorescence emission depending on the PLL : CF ratio in a 300 µM CF solution. The CF emission peaks as well as the fluorescence intensity varies significantly. The rationale for both could be that a PLL : CF ratio below five PLL interacts with CF aggregates in a way that it forces CF molecules to approach each other, making CF aggregates more compact. Interaction between PLL and CF is based on the interaction between the aromatic ring of CF and the amino groups of PLL.[247] At these conditions, CF molecules undergo self-quenching, and it would be higher as the molecules are closer to each other.[247] The same mechanism could be held responsible for the red shift. As CF molecules are drawing closer to each other, the interaction of their π-electrons would become stronger which would lead to a change in their spectral properties,[227,247] i.e. red shift in this case. Above PLL : CF ratio of 5 the opposite occurs - both self-quenching and red shift become less pronounced. This could be explained by the assumption that now there is enough PLL not only to interact with CF aggregates and change spectral properties of CF, but even to destroy aggregates. The evidence for the destruction of aggregates is based on the

results obtained by DLS analysis of solutions containing CF and PLL (Fig. 4.10B). These results have shown that above 300 µM CF the size of particles is 40-80 nm. With the addition of PLL until PLL : CF < 5 the size of aggregates decreases down to ~10 nm; the size is even more reduced to ~5 nm when PLL : CF > 5.

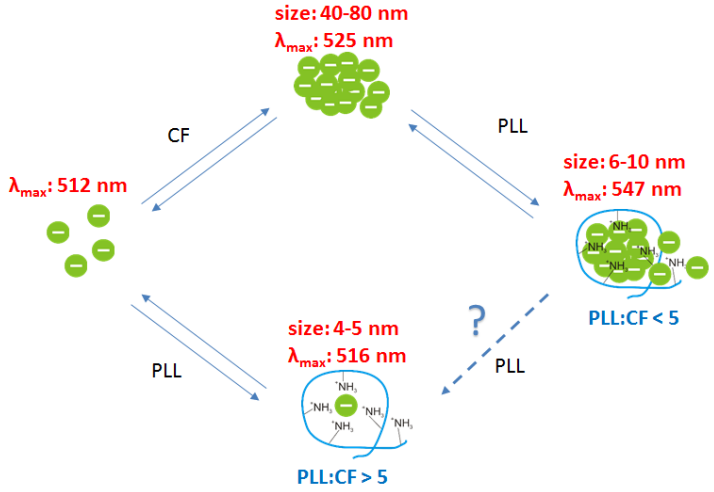

Figure 5.3. A scheme showing the suggested mechanism of CF-PLL interaction depending on the PLL : CF ratio. The emission peaks and the sizes of the aggregates determined by DLS are given for each step.

In Fig. 5.3 a diagram is shown which schematically summarizes the results concerning CF-PLL interaction in the solution. The proposed model suggests the following: if it is possible to infinitely increase PLL concentration in 300 µM CF solution (PLL : CF >> 42), it would be able to again measure 516 nm emission from CF (question mark in Fig. 5.3).

5.2.3 CF-PLL interaction – mechanism of CF loading into the film

The loading of the film with CF was observed in the real time (Fig. 4.11) and the comparison of the coefficients of determination (R^2) for the fitting of different adsorption models (Fig. 4.12 and Table 4.2) reveals that the model which best describes the loading of CF into the films is the Freundlich model. This indicates the following:

1) Cooperative binding - A bound CF molecule can act as a new binding site for upcoming CF molecules;
2) The affinity of binding sites in the film is non-uniform, meaning that there are at least two different binding sites in the film - the amount of adsorbed CF is the sum of adsorbed molecules on all sites;
3) Langmuir model's assumption that there is no adsorbate-adsorbate interaction is rejected, as well as that from the BET model that all binding sites are equal.

As far as the physical meaning of the fitting is concerned, it is realistic to expect that the first CF molecules that enter the film bind to PLL, but those that come afterwards not only bind to PLL but interact with already bound CF molecules. At this point the binding affinity at certain sites in the film is increased, and the most probable model would be that

CF reorients the polymer matrix, increasing the affinity of another CF to insert there. Since $(HA/PLL)_{24}$ films have limited capacity for CF, this cooperative binding occurs until all binding sites are occupied, both native and those formed during loading of CF.

5.2.4 Release mechanism

The literature does not provide information about the release mechanism of SCM from HA/PLL films, although there is considerable knowledge about other polymer films such as those based on hydroxypropyl methylcellulose[248]. The assumption tested in this work is that the release mechanism is related to the mobility of PLL chains as described below. PLL can diffuse within the film rather fast resulting in a diffusion coefficient of 0.17 ± 0.10 $\mu m^2/s$ (Section 4.1.2), as demonstrated in this study. This correlates well with previously reported values[33,51] of up to 1 $\mu m^2/s$. Similarly, the diffusion coefficient of CF has been found to be 1.26 ± 0.64 $\mu m^2/s$, which is in line with earlier publications[51]. The similarity between diffusion coefficients of CF and PLL might suggest that diffusion of CF may depend on diffusion of PLL. CF mobility similar to PLL mobility in the film could take place due to two possible reasons: i) CF is bound to a PLL molecule and diffuses along with it; and ii) CF is released from the complex with PLL due to formation of energetically more favorable PLL-HA ion pairs as a result of PLL migration from one HA molecule to another. In principle, both cases may take place at the same time. However, the release of CF from the film to the bulk solution is possible only if CF molecules detach from the PLL backbone, otherwise CF will stay within the film, bound to PLL as a film constituent. This means that CF release is possible only when conformational changes of PLL occur. Fig. 5.4 represents this model. It is to note that here one should consider the contribution of both PLL segment movement and movement of the whole PLL molecule. It is hard to experimentally distinguish between these two kinds of movements and it is assumed that both movements will contribute to the formation of ion pairs. The same mechanism could explain the release of ATP, which is negatively charged like CF, only with a higher charge density, and hence the ATP release is slower. Positively charged Rho molecules are bound to HA and detach upon conformational change of PLL, which has a higher affinity to HA than to Rho. Detached Rho molecules can either bind to other positions on the HA chain again or can diffuse out of the film.

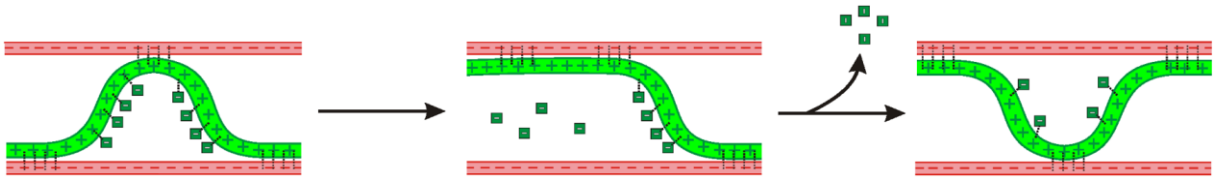

Figure 5.4. Schematics represents a unit of HA/PLL film containing an extended HA polymer chain (in red) and a flexible PLL chain (in green). PLL undergoes conformational changes that result in release of some CF molecules (green squares).

The film has always an excess of PLL - the molar charge ratio between primary amino groups of PLL and negatively charged carboxylic groups of HA is about 2, it varies depending on the number of deposited layers, but does not decrease below 1.[33] This supports the

assumption that CF release from the film is determined by the CF-PLL interaction and is affected by conformational changes of PLL, as shown in Fig. 5.4. Thus, there should be no significant effect of the terminal layer on the overall charge of the film. This is confirmed by the results presented in Fig. 4.13 which show that the release kinetics does not depend on the last deposited layer (HA or PLL). The only effect of the terminal layer is on the net charge of the surface of the film - the surface of HA-terminated films has a surface potential of about -30 mV, and that of PLL-terminated films is about +50 mV.[35]

The release data from the films of different thicknesses (Fig. 4.14) suggests that the release is limited not by CF diffusion through the whole film but rather by CF transport through the film surface.

The first proof is that if the release kinetics were limited by CF binding to the polyelectrolytes in the film, the release kinetics would strongly depend on the film thickness. According to the diffusion equation the time needed for CF molecule to travel through the film (t) is proportional to the square of the travelling distance (d), i.e. $t = d^2/2D$, where D is the diffusion coefficient of a molecule. Thus, if the film is twice thicker, the time t will be four times longer. This will result in significant changes of the release profiles. However, in the experiment shown in Fig. 4.14 the released amount of CF does not significantly depend on the film thickness.

The independence of mechanical properties of the film on the number of deposited layers (above 24 bilayers)[110] could indicate that water content in the films does not change with an increase of the number of layers. Thus, the polymer density is constant as well as the number of free charges of PLL. This would then give the second proof – since the number of free charges of PLL is constant, the capacity for CF should be proportional to the film thickness. If the film is twice thicker, the number of free charges and CF loaded amount is also twice higher, which is consistent with the results obtained from $(HA/PLL)_{24}$ and $(HA/PLL)_{96}$ films.

The film-solution interface defined by the film surface area is identical for both $(HA/PLL)_{24}$ and $(HA/PLL)_{96}$ films because the films are smooth and flat. The CF release can be explained by conformational changes of PLL molecules located on the film surface. As schematically shown in Fig. 5.5, CF released due to PLL conformational changes may either stay in the film and bind to other PLL molecules, or may be released from the film to the bulk solution – it depends on the localization of a PLL molecule. However, there might as well be additional barriers to the release of negatively charged CF, e.g. a potential well that is the result of an excess of positive charges within the film.

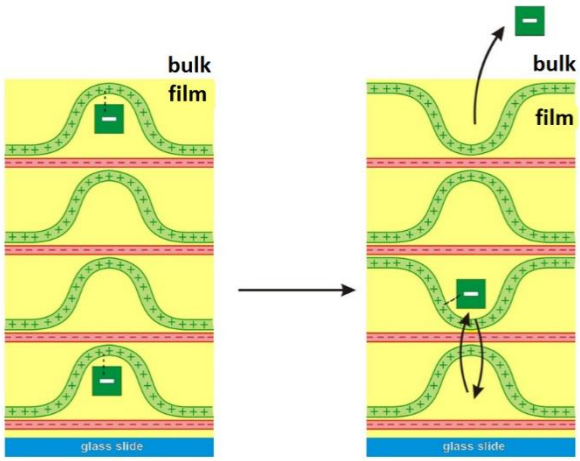

Figure 5.5. Proposed mechanism of the release of CF from the film caused by PLL conformational changes. Film - in yellow, PLL - in green, HA - in red. If the conformational changes take place in the film interior, CF stays inside the film and binds to other PLL molecules. If the PLL on the surface of the film undergoes the conformational changes, the CF molecules are released to the bulk solution.

The proposed surface-mediated release mechanism is in line with the main criteria for the Higuchi release model, which according to the R^2 describes the release of CF from the film the best (Fig. 4.15 and Table 4.3). This finding indicates the following:

1) There is one population of CF, i.e. CF does not change its state (aggregated or non-aggregated) during the process of the release;
2) CF diffuses through the surface of the film;
3) There is no swelling or degradation of the film, which is additionally confirmed by the fact that the Hixson-Crowell model does not fit well to the data.

5.2.5 Adjustment of the release kinetics by AuNPs coatings

AuNPs coatings have emerged as a powerful tool for controlling cellular adhesion,[46] though their influence on the film reservoir capacities remains unknown. As described in Section 4.3.2 CF and ATP amounts stored in non-coated films were found to be five or three times higher respectively, than that stored in AuNPs-coated ones. Most probably the reduced amount of free PLL in the film (Fig. 4.16A) - due to binding to AuNPs which contain citric acid with a high charge to mass ratio[46] - is responsible for lower loading of the negatively charged CF and ATP into the coated films.

From Fig. 4.16 it is clear that coated films provide faster release. The AuNPs coatings may reduce the positive surface charge density of the films due to their negative charge (citric acid stabilized particles). This will result in an easier access of PLL to the film surface from the film interior due to less electrostatic repulsive forces between PLL molecules on the film surface. In such way, more PLL can be provided to the bulk-film interface and more CF or ATP molecules can be released per unit of time, if the assumption is correct that the PLL conformational changes are responsible for the release (Section 5.2.4).

5.3 Cell-film interaction and the role of AuNPs

5.3.1 AuNPs coatings as a diffusion barrier

Not only can AuNPs coatings be used for the tuning of cellular adhesion on HA/PLL films of various cell lines (Fig. 4.17 and 4.18), but it was as well speculated that the coatings could prevent hydrolytic degradation of the films by cell-secreted enzymes. This can presumably be caused by diffusion limitations for large molecules such as enzymes to enter the film. From the results shown in Fig. 4.20 one can assume that AuNPs coatings behave as a size-exclusion semipermeable barrier that does not present diffusion limitations for small molecules such as CF. Diffusion of macromolecules with the mass of tens of kDa is significantly reduced and depends on γ. Moreover, diffusion of charged molecules such as CF and PLL can depend not only on the size of molecules but also on the molecule interaction with the film.

In contrast to the charged molecules used for the examination of the permeability of the coating, dextrans are not charged. However, there was no significant effect of the charge of the diffusing species on diffusion. AuNPs prevented even the shortest 10 kDa dextran from entering into the film.

In conclusion, the diffusivity through the AuNPs coatings might be tuned by adjusting the amount of AuNPs in the coatings and is independent on the charge of used molecules. Serum proteins with a molecular mass comparable to PLL most probably face the same limitation as PLL^{FITC} and do not diffuse into the AuNPs-coated film, which leads to protection against interaction of film components with serum proteins (Fig. 4.19). This is the first time that the diffusivity in/out from the film was put under the control using non-polymer capping layer and at the same time it demonstrates that the coating with AuNPs may open new opportunities to tune transport of molecules of interest.

5.3.2 Enzymatic degradation of films by cells

The feasibility of the AuNPs coatings to hinder even 10 kDa dextran to enter the film could mean that AuNPs can as well prevent hydrolytic enzymes secreted by cells, such as hyaluronidases and proteases with molecular weights of few tens of kDa, from coming into the contact with the film and degrading it. The focus was on protection of $(HA/PLL)_{24}$ films from enzymatic degradation. Fig. 4.21 clearly shows that the presence of AuNPs on the film seeded with cells prevents any change in the film morphology and geometry, while non-coated films are degraded. The width of the scratched area in which cells were growing increased 4-5 times when there were no AuNPs present. The hydrolytic effect of cells was obviously blocked by the presence of the AuNPs coatings.

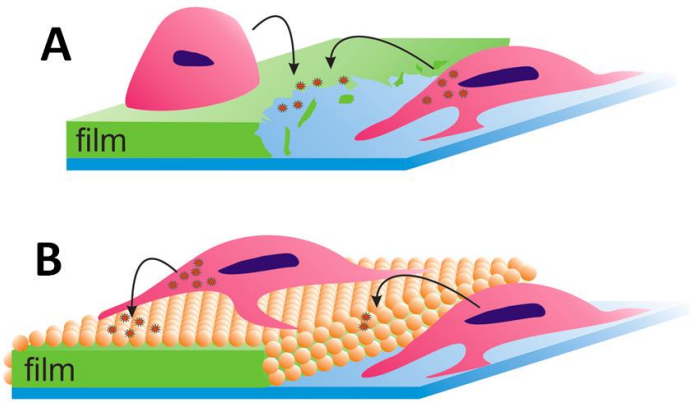

Figure 5.6 Schematics of adhesion of cells on (**A**) non-coated and (**B**) AuNPs-coated $(HA/PLL)_{24}$ films. Cells enzymatically degrade bare films which results in increased cellular adhesion, but cannot degrade AuNPs-coated films. At the same time, AuNPs coatings enhance adhesion of cells.

Fig. 5.6 presents schematics of the interaction of L929 fibroblasts with non-coated and AuNPs coated $(HA/PLL)_{24}$ films. Cells do not adhere well on the native films and can spread within the scratched area made by mechanical removal of the film (Fig. 5.6A). After a few days of growth the cells express and secrete enzymes, which degrade the film in the vicinity (Fig. 5.6A). However, AuNPs coated films are cell-adhesive and are not degraded enzymatically (Fig. 5.6B). Furthermore, AuNPs coatings present not only a protective layer against hydrolytic enzymes but also a size-exclusion diffusion barrier on the film surface with a cut-off tuned by the *γ* value. Such multifunctional properties of these coatings make them very attractive for the design of biomaterials with adjustable degradability and the possibility of controlled release for drug delivery applications. The HA/PLL films can host biomacromolecules such as proteins and thus mimic real ECM, which contains soluble signaling molecules of protein nature (e.g. growth factors, hormones, etc.).

5.4 Caged ATP

5.4.1 Stability and light activation

Bioactive compounds inactivated by binding to a caging group through a photolabile bond are commonly used for stimulation of cells.[16–19] Solutions of cATP are shown to be rather stable and do not generate uncaged ATP in normally illuminated ambient conditions during a period of six days. Their UV light-sensitive photolabile bond is cleaved and ATP is released instantaneously upon exposure to UV light, showing the sensitivity of the caging covalent bond to UV light (Fig. 4.23). NPE-ATP and DMNPE-ATP are uncaged completely within tens of seconds of irradiation, though the efficiency of DMNPE-ATP uncaging is a bit higher. Unfortunately, DMB-ATP demonstrated a low uncaging yield and was thus omitted from further experiments, although one study[249] claimed it to be quite effective. Observed uncaging efficiency for NPE-ATP and DMNPE-ATP is much higher than 63 % achieved by Kageyama and coworkers.[250]

Although cATP contain ATP as a major constituent, uncaged cATP were not able to trigger luciferase reactions (Fig. 4.24), most probably due to the fact that the caging group is bound to the tertiary phosphate group. Being blocked, tertiary phosphate group cannot act as a substrate for the luciferase. As concentrations of both ATP and cATP are determined using the luciferase assay cATP has to be uncaged prior to the measurement), it is important that cATP do not interfere with the measurement.

5.4.2 Loading into and release from the films

As described in Section 5.2, $(HA/PLL)_{24}$ films have high reservoir capacity for SCM. The same applies for cATP. Since the loading efficiency (Section 4.2.1) of cATP is shown to be roughly 2-3 times lower than the one of ATP, it is to speculate that caging groups screen the negative charge of ATP, thus decreasing the binding capacity of cATP. Results of both incubation- and QCM-loading (Section 4.5.2) show that ATP and cATP are homogenously loaded/distributed throughout the film, regardless of the film's thickness and number of bilayers. Another observation is that the saturation of the film is achieved with either of these methods.

Interestingly, when the dissociated DMNPE-ATP (which contains an equimolar amount of ATP and its cage DMNPE) is loaded into the film the increase in the mass is ~2 %, which by far surpasses the loading maximum of either ATP or cATP. Since ATP can be loaded only up to ~0.14 %, it is obvious that the rest of the mass comes from DMNPE. Free DMNPE obviously has a significant affinity to the film, much higher than that of cATP. Its affinity is severely decreased as long as it is bound to ATP, hence 30 times lower binding of cATP is observed. Free DMNPE is deposited into/onto the film (Section 4.5.2), probably because the π-electrons of the aromatic ring (Fig. 3.2) let it interact with amino groups of PLL, similarly to the way CF interacts with PLL (Section 5.2.3). Another possibility could be that the formation of intermolecular DMNPE π-stacking interactions is additionally emphasized by high number of free charge in the film. Whichever mechanism is correct, the most important consequence is that upon uncaging in the film, the caging compound will remain bound in the film and ATP can diffuse out.

5.4.3. UV-triggered release of ATP from cATP stored in the film

The property of HA/PLL films to withhold cATP, as well as a number of other SCM is rather promising. However, the ability to deliver these SCM on demand from a film as a reservoir is even more attractive. The $(HA/PLL)_{24}$ films loaded with DMNPE-ATP released 0.88 ± 0.37 pmol of ATP from the irradiated zone after a single irradiation period (Fig. 4.26). Since 320 pmol of DMNPE-ATP can be stored into one $(HA/PLL)_{24}$ film (Section 4.5.2), with 0.88 ± 0.37 pmol being released after each irradiation, theoretical ~360 deliveries of ATP from one loaded film can be done. On the other hand, the surface of a film deposited on a 12 mm glass slide is ~1000x larger than the 40 x 30 μm^2 of one irradiation zone. The explanation for the fact that 1/1000 of the surface releases 1/360 parts of stored ATP could be found in the fact that during the irradiation, which is a 45 s long process, the irradiation

zone is locally being depleted of cATP, and cATP is constantly being replenished by diffusion from the surrounding film into depleted area. Thus, the constant release of ATP is ensured, although the irradiated zone itself could not provide a sufficient amount of cATP. This is as well in line with the homogeneity of the cATP distribution in the film (previous section).

5.5 Light triggered cell activation

5.5.1 Real-time monitoring of cellular response

In addition to their use for storage and release of SCM, $(HA/PLL)_{24}$ films were employed as platforms for stimulation of cells. For that, the detection of the response of HeLa cells had to be optimized. ATP was used as an extracellular cell-stimulation biomolecule delivered from the film. ATP induces the increase in [iCa^{2+}] in HeLa cells which was monitored. The sensitivity of Ca^{2+}-sensitive fluorophores in the applied system was tested (Fig. 4.27) and it was shown that the optimal results are obtained when 10 µM OG was used (Table 4.6). Although 20 µM OG and Fluo-3 provides a more pronounced fluorescence increase, the application of 20 µM and higher concentrations of fluorophores was shown to affect cell viability, probably due to the fact that increased concentration of DMSO used for the preparation of dye stock solutions can harm cells. Another important observation is that the fluorescence intensity measured on individual cells reaches its maximum 6-10 s after the addition of ATP to the system, which is the same as the lag period reported[251] for human pulmonary fibroblasts. The lag period depends heavily on the intracellular signal transduction, as the extracellular interaction of ATP and P2 receptor family is established in less than 1 s.[150]

Results in Fig. 4.28 show for the first time that the stimulation of cells by ATP released from cATP stored in the $(HA/PLL)_{24}$ film using the light-triggered uncaging is possible. The irradiation of a well-defined area of the cATP-loaded film with 355 UV laser was able to uncage and deliver enough ATP to activate HeLa cells growing in the scratched area of the film. Furthermore, another irradiation of the same area had the same effect on cells. The difference in the fluorescence before and after the second irradiation is 25 %, compared to 40 % for the first irradiation. The effect is repetitive, though with decreased intensity, which could be a consequence of depletion of locally stored cATP in the irradiated zone of the film. Another reason might as well be that OG is bleached due to the constant exposure to 492 nm excitation light (Fig. 4.28D). It is also noteworthy that the third irradiation of the same area did not stimulate cells, which, apart from two potential causes discussed above, might as well be explained by depletion of intracellular calcium storage and by binding of iCa^{2+} to all OG molecules. Control experiments with non-loaded films did not elicit intracellular Ca^{2+}(Fig. 4.28D). The viability of cells outside the irradiation zone is not decreased (Fig. 4.31)

Fig. 4.28D shows that cells growing on the film loaded with ATP are not stimulated when the film is irradiated. This means that the irradiation does not release ATP bound in the film. On the other hand, irradiation of cATP-loaded films yields ATP that readily stimulates cells (Fig. 4.28-4.29). The question remains why irradiation of cATP-loaded films activates the cells, whereas irradiation of ATP-loaded films does not. If two to three times higher binding affinity of ATP to the film then that of the cATP is considered (Section 4.5.2), it is reasonable to assume that the UV irradiation energy can weaken cATP-film interaction, but not ATP-film interaction. A certain portion of cATP can be released from the film and simultaneously converted to ATP by UV light – ATP generated in this manner is already located outside the film and can affect cells. ATP loaded in the film is firmly bound in the film and cannot be released by applied UV irradiation.

On the other hand, when a single HeLa cell was observed after irradiation at two different areas of the film, the increase after both irradiations was almost 100 % compared to the resting levels before the irradiation (Fig. 4.29). This supports the assumption that the second irradiation of the same area depletes the cATP stored locally, since the second response is lower than the original one. Depletion in only local, since the subsequent irradiations of areas only 150 µM away from each other stimulate the cells with the same intensity. Released ATP diffuses away uniformly in all directions from the irradiation zone, and cells at the same distances but on opposite sides of the irradiation zone increase their [iCa^{2+}] by the same value (Fig. 4.30).

The discussed experiment points out the possibilities of this method for triggered and highly localized drug delivery. Furthermore, the utilization of cATP ensures that no spontaneous stimulation of cells takes place as all supplies of bioactive molecules are kept non-active - the caged compound can be locally activated only by light.

5.5.2 Spatio-temporal characteristics of activation and further application

Different mammalian cell lines have been shown to respond to ATP concentrations as low as 10 nM.[139,251–253] One irradiation releases ~17 nM into 50 µL sample, which is a volume much larger compared to the one that surrounds a single observed cell. This indicates that the concentration of locally released ATP surpasses a range of a few of tens of nM, which is more than enough to activate cells.

Interestingly, activation of cells at different distances from the film occurs simultaneously (Fig. 4.32A-B). This should not be surprising as the diffusion of released ATP might be rather fast due to the necessary movement of the stage with the sample during irradiation and/or slight heating by UV light during the experiment. Supportive is the report from Iwabuchi[223] who shows concentric spreading of uncaged glutamate which is so rapid that all cells are simultaneously affected, regardless of the distance. Apart from demonstrating the analogues effect for ATP and mammary epithelial cells, Furuya[253] also visualizes the formation of a concentration gradient through concentric spreading of ATP added into the solution or released by mechanical stimulation of films. Furuya's work could

also explain the lower levels of iCa^{2+} elicitation in cells at increasing distances from the irradiation point (Fig. 4.32B-C). The level of the increase of iCa^{2+} is related to the distance of cells from the irradiation zone, and it decreases with the square distance. The concentration of released ATP decreases with distance and beyond 120 µm it is most probably too low to induce cellular stimulation. Even the increased irradiation time above 45 s did not produce a response of cells at distance beyond 120 µm, which suggests that a stable concentration profile of released ATP is formed during 45 s and that further irradiation cannot yield higher ATP concentration. Thus, for the first time the localized release of bioactive molecules from the film was demonstrated.

It is possible that 30 s is the minimum time necessary to release enough ATP to establish a concentration which is sufficient to evoke a measurable increase in iCa^{2+} levels in cells (Fig. 4.32D). However, irradiations longer than 30 s do not result in the additional iCa^{2+} increase. This might indicate that a stable ATP concentration profile around the irradiation zone is formed after 30 s of irradiation. In other words, during the irradiation, ATP is being released and at the same time it diffuses away from area of irradiation. When the balance between ATP generation and its dilution through diffusion is achieved (~30 s, Fig. 4.32D), a change in concentration profile is not possible anymore. Therefore, gradual increase of cell stimulation due to prolonged irradiation periods is not possible.

A major goal of using localized release of drugs is to affect cells and tissues. However, very few systems have been described to be non-harmful. This study for the first time reports the controlled release of a non-covalently bound drug from the polymer films that is both highly localized and non-harmful. A key aspect is that it could help to establish a cell and tissue assay based on controlled delivery of bioactive molecules.

6 CONCLUSIONS

In the current study, a new approach for the non-invasive and highly precise presentation of biomolecules to cells by irradiation with light has been developed. The main principle exploits i) competitive intermolecular interactions between bioactive molecules and the LbL films which act as their hosts and ii) the ability of these films to support cell growth. Light-triggered uncaging of caged ATP (model biomolecule) results in release of bioactive ATP from the LbL films. Consequentially, the cells grown on the film are stimulated by the released ATP. For the proof of the concept, the following aspects of the proposed approach have been developed, tested, and optimized as discussed below.

HA/PLL LbL films are shown to be effective reservoirs for storage of SCM including the model molecule ATP. Concentration of the SCM in the LbL films can be up to three orders of magnitude higher than in solution, due to electrostatic binding of SCM to free charges of the polymer network in the film. Release of the loaded molecules is proposed to be driven by polymer dynamics in the LbL films and is considerably limited by mass transport and charge on film-solution interface. Full understanding of the loading and release mechanisms would be of interest and would provide broader possibilities for the embedding of biomolecules which would be delivered on demand in order to control the cell fate.

The LbL films can be both cell-adhesive and cell-repellent depending on their thickness (higher thickness results in cell-repellent properties). AuNPs coatings of the LbL films surface can be used to enhance cellular adhesion. The multifunctional nature of the coatings has been additionally proven by showing the semipermeable characteristics of the coatings with cut-off in the range of molecular weights of biomacromolecules such as proteins. The cut-off can easily be adjusted by altering the thickness of the AuNPs coatings. Furthermore, the coatings preserves LbL films against biodegradation likely due to the reduction of enzyme diffusion into the film. Thus, the AuNPs coatings is demonstrated to be an effective and simple way to control the cell-film interaction as well as to control molecular transport into/from the film. The perspectives of this transport phenomenon could be considered in order to expand its application and fabricate a series of various LbL films resistant to enzymatic degradation since the protection from enzymatic degradation of the films is of the indispensable importance and would contribute to the stability of the films in the cellular environment.

Light has been shown to be very perspective stimulus for localized release according to the developed approach. Micrometer-sized area can be irradiated by focused laser light which allows application of light in areas comparable to or below cellular size, without distortion of cell functions and viability. The competition to interact with charged polymer constituents of the film, between initially loaded cATP and uncaged (free) ATP formed after light irradiation, regulates the release of free active ATP as well as the binding of the caging groups to the film. Most probably, electrostatic and hydrophobic interactions play the main

role in the binding competition, which could be exploited to achieve the control of the release rate or to diminish the potential toxic effect of certain caging groups.

The exposure of cells to ATP elicits intracellular calcium which can be monitored using fluorescent calcium probes. This has been shown to be an effective method for real time monitoring of fast cellular response to the chosen bioactive molecule ATP.

The first attempts to understand temporal and spatial limitations for the developed approach have shown that cellular response can be observed on the scale of cellular dimensions. The spatio-temporal analysis of the stimulation has revealed that the effectivity of ATP is rather localized to nearby cells and the level of cell stimulation depends on both the cell distance from the irradiation zone and on the duration of irradiation. This shows that the level of stimulation can be finely tuned by duration of irradiation and chosen distance between a cell and irradiation zone, which provides a powerful tool for controlled targeted stimulation of selected cells.

To sum up, the work presented here gives a considerable description of a system designed for stimulation of cells. It provides the foundation for the development of a cell assay that enables non-harmful and controlled delivery of bioactive molecules for highly localized extracellular stimulation of cells up to a level of a single cell. Thus, it will help to understand fundamental biological pathways in greater depth, and at the same time it can be applied as a method for directing cellular growth and tissue engineering.

References

[1] R. R. Costa, J. F. Mano, *Chemical Society reviews* **2014**, *43*, 3453.
[2] R. K. Iler, *Journal of Colloid and Interface Science* **1966**, *21*, 569.
[3] G. Decher, J. D. Hong, J. Schmitt, *Thin Solid Films* **1992**, *210-211*, 831.
[4] Y. Lvov, G. Decher, G. Sukhorukov, *Macromolecules* **1993**, *26*, 5396.
[5] Y. Lvov, G. Decher, H. Haas, H. Möhwald, A. Kalachev, *Physica B: Condensed Matter* **1994**, *198*, 89.
[6] G. Decher, *Science* **1997**, *277*, 1232.
[7] B. M. Wohl, J. F. J. Engbersen, *Journal of controlled release official journal of the Controlled Release Society* **2012**, *158*, 2.
[8] T. Boudou, T. Crouzier, K. Ren, G. Blin, C. Picart, *Advanced materials (Deerfield Beach, Fla.)* **2010**, *22*, 441.
[9] S. A. Sukhishvili, S. Granick, *Macromolecules* **2002**, *35*, 301.
[10] A. Guyomard, G. Muller, K. Glinel, *Macromolecules* **2005**, *38*, 5737.
[11] C. R. Kinnane, K. Wark, G. K. Such, A. P. R. Johnston, F. Caruso, *Small (Weinheim an der Bergstrasse, Germany)* **2009**, *5*, 444.
[12] G. Francius, J. Hemmerlé, J.-C. Voegel, P. Schaaf, B. Senger, V. Ball, *Langmuir* **2007**, *23*, 2602.
[13] R. A. Ghostine, M. Z. Markarian, J. B. Schlenoff, *Journal of the American Chemical Society* **2013**, *135*, 7636.
[14] J. J. Richardson, M. Björnmalm, F. Caruso, *Science (New York, N.Y.)* **2015**, *348*, aaa2491.
[15] C. Picart, A. Schneider, O. Etienne, J. Mutterer, P. Schaaf, C. Egles, N. Jessel, J.-C. Voegel, *Adv. Funct. Mater.* **2005**, *15*, 1771.
[16] A. L. Larkin, R. M. Davis, P. Rajagopalan, *Biomacromolecules* **2010**, *11*, 2788.
[17] K. Manabe, K.-H. Kyung, S. Shiratori, *ACS applied materials & interfaces* **2015**, *7*, 4763.
[18] K. Ren, T. Crouzier, C. Roy, C. Picart, *Adv. Funct. Mater* **2008**, *18*, 1378.
[19] L. Richert, F. Boulmedais, P. Lavalle, J. Mutterer, E. Ferreux, G. Decher, P. Schaaf, J.-C. Voegel, C. Picart, *Biomacromolecules* **2004**, *5*, 284.
[20] T. Crouzier, K. Ren, C. Nicolas, C. Roy, C. Picart, *Small (Weinheim an der Bergstrasse, Germany)* **2009**, *5*, 598.
[21] J. Blacklock, A. Vetter, A. Lankenau, D. Oupický, H. Möhwald, *Biomaterials* **2010**, *31*, 7167.
[22] D. V. Volodkin, N. Madaboosi, J. Blacklock, A. G. Skirtach, H. Möhwald, *Langmuir the ACS journal of surfaces and colloids* **2009**, *25*, 14037.
[23] R. v. Klitzing, *Phys. Chem. Chem. Phys* **2006**, *8*, 5012.
[24] M. Schönhoff, V. Ball, A. R. Bausch, C. Dejugnat, N. Delorme, K. Glinel, R. v. Klitzing, R. Steitz, *Colloids and Surfaces A: Physicochemical and Engineering Aspects* **2007**, *303*, 14.
[25] T. Crouzier, T. Boudou, C. Picart, *Current Opinion in Colloid & Interface Science* **2010**, *15*, 417.
[26] S. S. Shiratori, M. F. Rubner, *Macromolecules* **2000**, *33*, 4213.
[27] S. E. Burke, C. J. Barrett, *Macromolecules* **2004**, *37*, 5375.
[28] L. Shen, P. Chaudouet, J. Ji, C. Picart, *Biomacromolecules* **2011**, *12*, 1322.
[29] K. Glinel, C. Déjugnat, M. Prevot, B. Schöler, M. Schönhoff, R. v. Klitzing, *Colloids and Surfaces A: Physicochemical and Engineering Aspects* **2007**, *303*, 3.
[30] L. Richert, Y. Arntz, P. Schaaf, J.-C. Voegel, C. Picart, *Surface Science* **2004**, *570*, 13.
[31] E. Blomberg, E. Poptoshev, F. Caruso, *Langmuir the ACS journal of surfaces and colloids* **2006**, *22*, 4153.
[32] K. Ren, Y. Wang, J. Ji, Q. Lin, J. Shen, *Colloids and surfaces. B, Biointerfaces* **2005**, *46*, 63.
[33] T. Crouzier, C. Picart, *Biomacromolecules* **2009**, *10*, 433.
[34] C. Porcel, P. Lavalle, G. Decher, B. Senger, J.-C. Voegel, P. Schaaf, *Langmuir the ACS journal of surfaces and colloids* **2007**, *23*, 1898.
[35] C. Picart, P. Lavalle, P. Hubert, F. J. G. Cuisinier, G. Decher, P. Schaaf, J.-C. Voegel, *Langmuir* **2001**, *17*, 7414.
[36] C. Picart, J. Mutterer, L. Richert, Y. Luo, G. D. Prestwich, P. Schaaf, J.-C. Voegel, P. Lavalle, *Proceedings of the National Academy of Sciences* **2002**, *99*, 12531.
[37] J. J. Ramsden, Y. Lvov, G. Decher, *Thin Solid Films* **1995**, *254*, 246.
[38] C. Porcel, P. Lavalle, V. Ball, G. Decher, B. Senger, J.-C. Voegel, P. Schaaf, *Langmuir* **2006**, *22*, 4376.
[39] G. Ladam, P. Schaad, J. C. Voegel, P. Schaaf, G. Decher, F. Cuisinier, *Langmuir* **2000**, *16*, 1249.
[40] K. Ariga, Y. Yamauchi, G. Rydzek, Q. Ji, Y. Yonamine, K. C.-W. Wu, J. P. Hill, *Chem. Lett* **2014**, *43*, 36.
[41] T. Boudou, T. Crouzier, K. Ren, G. Blin, C. Picart, *Adv. Mater.* **2010**, *22*, 441.
[42] D. Volodkin, A. Skirtach, H. Mohwald, in *Bioactive Surfaces*, Vol. 240 (Eds.: H. G. Borner, J. F. Lutz), Springer-Verlag Berlin. Berlin **2011**, p. 135.
[43] D. Volodkin, R. von Klitzing, *Current Opinion in Colloid & Interface Science* **2014**, *19*, 25.

[44] S. T. Dubas, J. B. Schlenoff, *Langmuir* **2001**, *17*, 7725.
[45] P. Podsiadlo, Z. Tang, B. S. Shim, N. A. Kotov, *Nano Lett* **2007**, *7*, 1224.
[46] S. Schmidt, N. Madaboosi, K. Uhlig, D. Köhler, A. Skirtach, C. Duschl, H. Möhwald, D. V. Volodkin, *Langmuir* **2012**, *28*, 7249.
[47] G. Decher, J.-D. Hong, *Makromolekulare Chemie. Macromolecular Symposia* **1991**, *46*, 321.
[48] C. Picart, *CMC* **2008**, *15*, 685.
[49] O. Guillame-Gentil, O. Semenov, A. S. Roca, T. Groth, R. Zahn, J. Vörös, M. Zenobi-Wong, *Adv. Mater.* **2010**, *22*, 5443.
[50] D. V. Volodkin, N. G. Balabushevitch, G. B. Sukhorukov, N. I. Larionova, *Biochem.-Moscow* **2003**, *68*, 236.
[51] K. Uhlig, N. Madaboosi, S. Schmidt, M. S. Jager, J. Rose, C. Duschl, D. V. Volodkin, *Soft Matter* **2012**, *8*, 11786.
[52] N. G. Balabushevich, M. A. Pechenkin, E. D. Shibanova, D. V. Volodkin, E. V. Mikhalchik, *Macromol. Biosci* **2013**, *13*, 1379.
[53] C. M. Jewell, D. M. Lynn, *Adv. Drug Deliv. Rev.* **2008**, *60*, 979.
[54] H. F. Chuang, R. C. Smith, P. T. Hammond, *Biomacromolecules* **2008**, *9*, 1660.
[55] A. Schneider, C. Vodouhê, L. Richert, G. Francius, E. Le Guen, P. Schaaf, J.-C. Voegel, B. Frisch, C. Picart, *Biomacromolecules* **2007**, *8*, 139.
[56] C. Vodouhê, E. Le Guen, J. Mendez Garza, G. Francius, C. Déjugnat, J. Ogier, P. Schaaf, J.-C. Voegel, P. Lavalle, *Biomaterials* **2006**, *27*, 4149.
[57] F. Boulmedais, P. Schwinté, C. Gergely, J.-C. Voegel, P. Schaaf, *Langmuir* **2002**, *18*, 4523.
[58] D. T. Haynie, S. Balkundi, N. Palath, K. Chakravarthula, K. Dave, *Langmuir* **2004**, *20*, 4540.
[59] P. Schwinté, J.-C. Voegel, C. Picart, Y. Haikel, P. Schaaf, B. Szalontai, *J. Phys. Chem. B* **2001**, *105*, 11906.
[60] R. Pei, X. Cui, X. Yang, E. Wang, *Biomacromolecules* **2001**, *2*, 463.
[61] C. M. Jewell, J. Zhang, N. J. Fredin, D. M. Lynn, *Journal of controlled release official journal of the Controlled Release Society* **2005**, *106*, 214.
[62] J. Zhang, L. S. Chua, D. M. Lynn, *Langmuir the ACS journal of surfaces and colloids* **2004**, *20*, 8015.
[63] D. Volodkin, R. von Klitzing, H. Moehwald, *Polymers* **2014**, *6*, 1502.
[64] A. Schneider, C. Picart, B. Senger, P. Schaaf, J.-C. Voegel, B. Frisch, *Langmuir the ACS journal of surfaces and colloids* **2007**, *23*, 2655.
[65] B. G. de Geest, N. N. Sanders, G. B. Sukhorukov, J. Demeester, S. C. de Smedt, *Chemical Society reviews* **2007**, *36*, 636.
[66] Z. Tang, Y. Wang, P. Podsiadlo, N. A. Kotov, *Adv. Mater* **2006**, *18*, 3203.
[67] D. Volodkin, A. Skirtach, N. Madaboosi, J. Blacklock, R. von Klitzing, A. Lankenau, C. Duschl, H. Mohwald, *J. Controlled release* **2010**, *148*, e70-1.
[68] B. B. Hsu, M.-H. Park, S. R. Hagerman, P. T. Hammond, *Proceedings of the National Academy of Sciences of the United States of America* **2014**, *111*, 12175.
[69] C. Vodouhê, E. Le Guen, J. M. Garza, G. Francius, C. Déjugnat, J. Ogier, P. Schaaf, J.-C. Voegel, P. Lavalle, *Biomaterials* **2006**, *27*, 4149.
[70] X. Wang, J. Ji, *Langmuir* **2009**, *25*, 11664.
[71] M. C. Berg, L. Zhai, R. E. Cohen, M. F. Rubner, *Biomacromolecules* **2006**, *7*, 357.
[72] E. Kharlampieva, S. A. Sukhishvili, *Langmuir the ACS journal of surfaces and colloids* **2004**, *20*, 9677.
[73] M. J. Serpe, K. A. Yarmey, C. M. Nolan, L. A. Lyon, *Biomacromolecules* **2005**, *6*, 408.
[74] A. J. Chung, M. F. Rubner, *Langmuir* **2002**, *18*, 1176.
[75] K. Ariga, J. P. Hill, Q. Ji, *Phys. Chem. Chem. Phys* **2007**, *9*, 2319.
[76] L. Xu, H. Zhang, E. Wang, D. G. Kurth, Z. Li, *J. Mater. Chem.* **2002**, *12*, 654.
[77] S. Liu, D. G. Kurth, H. Möhwald, D. Volkmer, *Adv. Mater.* **2002**, *14*, 225.
[78] A. G. Agrios, I. Cesar, P. Comte, M. K. Nazeeruddin, M. Grätzel, *Chem. Mater.* **2006**, *18*, 5395.
[79] T. Cui, F. Hua, Y. Lvov, *IEEE Trans. Electron Devices* **2004**, *51*, 503.
[80] A. J. Nolte, M. F. Rubner, R. E. Cohen, *Langmuir* **2004**, *20*, 3304.
[81] J. T. Han, Y. Zheng, J. H. Cho, X. Xu, K. Cho, *The journal of physical chemistry. B* **2005**, *109*, 20773.
[82] V. Gribova, R. Auzely-Velty, C. Picart, *Chem. Mater* **2012**, *24*, 854.
[83] M. P. Lutolf, J. A. Hubbell, *Nature biotechnology* **2005**, *23*, 47.
[84] H. Ai, S. A. Jones, Y. M. Lvov, *CBB* **2003**, *39*, 23.
[85] P. Lavalle, J.-C. Voegel, D. Vautier, B. Senger, P. Schaaf, V. Ball, *Adv. Mater* **2011**, *23*, 1191.
[86] M. Matsusaki, H. Ajiro, T. Kida, T. Serizawa, M. Akashi, *Advanced materials (Deerfield Beach, Fla.)* **2012**, *24*, 454.
[87] C. Picart, F. Caruso, J.-C. Voegel, *Layer-by-layer films for biomedical applications*, Wiley-VCH, Weinheim **2015**.

[88] C. Boura, P. Menu, E. Payan, C. Picart, J. C. Voegel, S. Muller, J. F. Stoltz, *Biomaterials* **2003**, *24*, 3521.
[89] C. Brunot, B. Grosgogeat, C. Picart, C. Lagneau, N. Jaffrezic-Renault, L. Ponsonnet, *Dental materials official publication of the Academy of Dental Materials* **2008**, *24*, 1025.
[90] L. Mhamdi, C. Picart, C. Lagneau, A. Othmane, B. Grosgogeat, N. Jaffrezic-Renault, L. Ponsonnet, *Materials Science and Engineering: C* **2006**, *26*, 273.
[91] P. Tryoen-Tóth, D. Vautier, Y. Haikel, J.-C. Voegel, P. Schaaf, J. Chluba, J. Ogier, *Journal of biomedical materials research* **2002**, *60*, 657.
[92] C. R. Wittmer, J. A. Phelps, C. M. Lepus, W. M. Saltzman, M. J. Harding, P. R. van Tassel, *Biomaterials* **2008**, *29*, 4082.
[93] J. D. Mendelsohn, S. Y. Yang, J. Hiller, A. I. Hochbaum, M. F. Rubner, *Biomacromolecules* **2003**, *4*, 96.
[94] Q. Tan, J. Ji, F. Zhao, D.-Z. Fan, F.-Y. Sun, J.-C. Shen, *Journal of materials science. Materials in medicine* **2005**, *16*, 687.
[95] S. Grohmann, H. Rothe, M. Frant, K. Liefeith, *Biomacromolecules* **2011**, *12*, 1987.
[96] A. Khademhosseini, K. Y. Suh, J. M. Yang, G. Eng, J. Yeh, S. Levenberg, R. Langer, *Biomaterials* **2004**, *25*, 3583.
[97] N. Berthelemy, H. Kerdjoudj, C. Gaucher, P. Schaaf, J.-F. Stoltz, P. Lacolley, J.-C. Voegel, P. Menu, *Advanced materials (Deerfield Beach, Fla.)* **2008**, *20*, 2674.
[98] T. Groth, A. Lendlein, *Angewandte Chemie (International ed. in English)* **2004**, *43*, 926.
[99] C. S. Hajicharalambous, J. Lichter, W. T. Hix, M. Swierczewska, M. F. Rubner, P. Rajagopalan, *Biomaterials* **2009**, *30*, 4029.
[100] N. Madaboosi, K. Uhlig, S. Schmidt, M. S. Jager, H. Mohwald, C. Duschl, D. V. Volodkin, *Lab on a Chip* **2012**, *12*, 1434.
[101] J. Fukuda, A. Khademhosseini, J. Yeh, G. Eng, J. J. Cheng, O. C. Farokhzad, R. Langer, *Biomaterials* **2006**, *27*, 1479.
[102] L. Richert, P. Lavalle, E. Payan, X. Z. Shu, G. D. Prestwich, J.-F. Stoltz, P. Schaaf, J.-C. Voegel, C. Picart, *Langmuir* **2004**, *20*, 448.
[103] T. C. Laurent, *The chemistry, biology, and medical applications of hyaluronan and its derivatives*, Portland Press, London, Miami **1998**.
[104] L. Lapčík, S. de Smedt, J. Demeester, P. Chabreček, *Chem. Rev* **1998**, *98*, 2663.
[105] S. Shima, S. Heiichi, *Agricultural and Biological Chemistry* **1977**, *41*, 1807.
[106] R. Muzzarelli, C. Jeuniaux, G. W. Gooday (Eds.), *Chitin in Nature and Technology*, Springer US, Boston, MA **1986**.
[107] S. T. Dubas, J. B. Schlenoff, *Macromolecules* **1999**, *32*, 8153.
[108] M. Salomäki, I. A. Vinokurov, J. Kankare, *Langmuir the ACS journal of surfaces and colloids* **2005**, *21*, 11232.
[109] H. L. Tan, M. J. McMurdo, G. Pan, Van Patten, P. Gregory, *Langmuir* **2003**, *19*, 9311.
[110] C. Üzüm, J. Hellweg, N. Madaboosi, D. Volodkin, R. von Klitzing, *Beilstein J. Nanotechnol.* **2012**, *3*, 778.
[111] N. Madaboosi Srinivasan, *Engineering hyaluronic acid / poly-L-lysine films as a platform for controlling cell behaviour* **2012**.
[112] N. Jouon, M. Rinaudo, M. Milas, J. Desbrières, *Carbohydrate Polymers* **1995**, *26*, 69.
[113] J. Necas, L. Bartosikova, P. Brauner, J. Kolar, *Veterinarni Medicina* **2008**, *53*, 397.
[114] C. Pozos Vázquez, T. Boudou, V. Dulong, C. Nicolas, C. Picart, K. Glinel, *Langmuir* **2009**, *25*, 3556.
[115] A. Schneider, G. Francius, R. Obeid, P. Schwinté, J. Hemmerlé, B. Frisch, P. Schaaf, J.-C. Voegel, B. Senger, C. Picart, *Langmuir* **2006**, *22*, 1193.
[116] K. Ren, L. Fourel, C. G. Rouvière, C. Albiges-Rizo, C. Picart, *Acta Biomaterialia* **2010**, *6*, 4238.
[117] G. Francius, J. Hemmerlé, J. Ohayon, P. Schaaf, J.-C. Voegel, C. Picart, B. Senger, *Microscopy research and technique* **2006**, *69*, 84.
[118] O. Etienne, A. Schneider, C. Taddei, L. Richert, P. Schaaf, J.-C. Voegel, C. Egles, C. Picart, *Biomacromolecules* **2005**, *6*, 726.
[119] P. Podsiadlo, A. K. Kaushik, E. M. Arruda, A. M. Waas, B. S. Shim, J. Xu, H. Nandivada, B. G. Pumplin, J. Lahann, A. Ramamoorthy, N. A. Kotov, *Science (New York, N.Y.)* **2007**, *318*, 80.
[120] B. Fiedler, F. H. Gojny, M. H. Wichmann, M. C. Nolte, K. Schulte, *Composites Science and Technology* **2006**, *66*, 3115.
[121] L. Richert, A. J. Engler, D. E. Discher, C. Picart, *Biomacromolecules* **2004**, *5*, 1908.
[122] A. J. Engler, L. Richert, J. Y. Wong, C. Picart, D. E. Discher, *Surface Science* **2004**, *570*, 142.
[123] O. V. Semenov, A. Malek, A. G. Bittermann, J. Vörös, A. H. Zisch, *Tissue Engineering Part A* **2009**, *15*, 2977.
[124] H. Niwa, *Development (Cambridge, England)* **2007**, *134*, 635.

[125] A. Tezcaner, D. Hicks, F. Boulmedais, J. Sahel, P. Schaaf, J.-C. Voegel, P. Lavalle, *Biomacromolecules* **2006**, *7*, 86.
[126] S. Yamanlar, S. Sant, T. Boudou, C. Picart, A. Khademhosseini, *Biomaterials* **2011**, *32*, 5590.
[127] S. K. Hahn, A. S. Hoffman, *Biotechnol. Bioprocess Eng.* **2004**, *9*, 179.
[128] J. J. Hwang, S. Jelacic, N. T. Samuel, R. V. Maier, C. T. Campbell, D. G. Castner, A. S. Hoffman, P. S. Stayton, *Journal of Biomaterials Science, Polymer Edition* **2005**, *16*, 237.
[129] J. Y. Park, S. J. Yoo, E.-J. Lee, D. H. Lee, J. Y. Kim, S.-H. Lee, *BioChip J* **2010**, *4*, 230.
[130] K. Ren, J. Ji, J. Shen, *Biomaterials* **2006**, *27*, 1152.
[131] M. Westwood, D. Roberts, R. Parker, *Carbohydrate Polymers* **2011**, *84*, 960.
[132] J. A. Burdick, C. Chung, X. Jia, M. A. Randolph, R. Langer, *Biomacromolecules* **2005**, *6*, 386.
[133] J. M. Garza, N. Jessel, G. Ladam, V. Dupray, S. Muller, J.-F. Stoltz, P. Schaaf, J.-C. Voegel, P. Lavalle, *Langmuir* **2005**, *21*, 12372.
[134] J. R. Knowles, *Annual review of biochemistry* **1980**, *49*, 877.
[135] M. Yoshida, E. Muneyuki, T. Hisabori, *Nature reviews. Molecular cell biology* **2001**, *2*, 669.
[136] J. Hanoune, N. Defer, *Annual review of pharmacology and toxicology* **2001**, *41*, 145.
[137] P. V. Minorsky, *PLANT PHYSIOLOGY* **2010**, *154*, 602.
[138] K. Tanaka, S. J. Swanson, S. Gilroy, G. Stacey, *PLANT PHYSIOLOGY* **2010**, *154*, 705.
[139] M. J. Jaffe, *PLANT PHYSIOLOGY* **1973**, *51*, 17.
[140] S.-J. Wu, Y.-S. Liu, J.-Y. Wu, *Plant & cell physiology* **2008**, *49*, 617.
[141] S. Chivasa, A. M. Murphy, J. M. Hamilton, K. Lindsey, J. P. Carr, A. R. Slabas, *The Plant journal for cell and molecular biology* **2009**, *60*, 436.
[142] J. C. Brasen, L. F. Olsen, M. B. Hallett, *Biochimica et biophysica acta* **2011**, *1813*, 1446.
[143] P. J. Hanley, B. Musset, V. Renigunta, S. H. Limberg, A. H. Dalpke, R. Sus, K. M. Heeg, R. Preisig-Müller, J. Daut, *Proceedings of the National Academy of Sciences of the United States of America* **2004**, *101*, 9479.
[144] M. G. Mahoney, C. J. Randall, J. J. Linderman, D. J. Gross, L. L. Slakey, *Molecular Biology of the Cell* **1992**, *3*, 493.
[145] B. S. Khakh, G. Burnstock, *Scientific American* **2009**, *301*, 84-90, 92.
[146] G. Burnstock, A. Verkhratsky, *Acta physiologica (Oxford, England)* **2009**, *195*, 415.
[147] G. Burnstock, *Cellular and molecular life sciences CMLS* **2007**, *64*, 1471.
[148] M. P. Abbracchio, G. Burnstock, J.-M. Boeynaems, E. A. Barnard, J. L. Boyer, C. Kennedy, G. E. Knight, M. Fumagalli, C. Gachet, K. A. Jacobson, G. A. Weisman, *Pharmacological reviews* **2006**, *58*, 281.
[149] B. S. Khakh, R. A. North, *Nature* **2006**, *442*, 527.
[150] M. W. Grol, A. Pereverzev, S. M. Sims, S. J. Dixon, *Journal of cell science* **2013**, *126*, 3615.
[151] S.-Y. Ryu, P. M. Peixoto, J. H. Won, D. I. Yule, K. W. Kinnally, *Cell calcium* **2010**, *47*, 65.
[152] D. Cao, G. Lin, E. M. Westphale, E. C. Beyer, T. H. Steinberg, *Journal of cell science* **1997**, *110 (Pt 4)*, 497.
[153] A. H. Cornell-Bell, S. M. Finkbeiner, M. S. Cooper, S. J. Smith, *Science (New York, N.Y.)* **1990**, *247*, 470.
[154] K. Enomoto, K. Furuya, S. Yamagishi, T. Maeno, *Cell calcium* **1992**, *13*, 501.
[155] N. R. Jorgensen, S. T. Geist, R. Civitelli, T. H. Steinberg, *The Journal of Cell Biology* **1997**, *139*, 497.
[156] S. O. Song, J. Varner, *PloS one* **2009**, *4*, e6758.
[157] M. D. Bootman, K. Rietdorf, T. Collins, S. Walker, M. Sanderson, *Cold Spring Harbor protocols* **2013**, *2013*, 122.
[158] G. C. R. Ellis-Davies, *Nature methods* **2007**, *4*, 619.
[159] D. M. Rothman, E. J. Petersson, M. E. Vázquez, G. S. Brandt, D. A. Dougherty, B. Imperiali, *Journal of the American Chemical Society* **2005**, *127*, 846.
[160] J. W. Walker, S. H. Gilbert, R. M. Drummond, M. Yamada, R. Sreekumar, R. E. Carraway, M. Ikebe, F. S. Fay, *Proceedings of the National Academy of Sciences of the United States of America* **1998**, *95*, 1568.
[161] M. Ghosh, X. Song, G. Mouneimne, M. Sidani, D. S. Lawrence, J. S. Condeelis, *Science (New York, N.Y.)* **2004**, *304*, 743.
[162] G. Marriott, *Biochemistry* **1994**, *33*, 9092.
[163] D. Mendel, J. A. Ellman, P. G. Schultz, *J. Am. Chem. Soc.* **1991**, *113*, 2758.
[164] H. Ando, T. Furuta, R. Y. Tsien, H. Okamoto, *Nature genetics* **2001**, *28*, 317.
[165] W. T. Monroe, M. M. McQuain, M. S. Chang, J. S. Alexander, F. R. Haselton, *Journal of Biological Chemistry* **1999**, *274*, 20895.
[166] J. W. Walker, A. V. Somlyo, Y. E. Goldman, A. P. Somlyo, D. R. Trentham, *Nature* **1987**, *327*, 249.
[167] J. H. Kaplan, B. Forbush, J. F. Hoffman, *Biochemistry* **1978**, *17*, 1929.
[168] J. W. Walker, G. P. Reid, J. A. McCray, D. R. Trentham, *J. Am. Chem. Soc.* **1988**, *110*, 7170.
[169] G. C. R. Ellis-Davies, J. H. Kaplan, *J. Org. Chem.* **1988**, *53*, 1966.

[170] G. C. Ellis-Davies, J. H. Kaplan, *Proceedings of the National Academy of Sciences of the United States of America* **1994**, *91*, 187.
[171] S. Geibel, A. Barth, S. Amslinger, A. H. Jung, C. Burzik, R. J. Clarke, R. S. Givens, K. Fendler, *Biophysical Journal* **2000**, *79*, 1346.
[172] K. Hartung, E. Grell, W. Hasselbach, E. Bamberg, *Biochimica et Biophysica Acta (BBA) - Biomembranes* **1987**, *900*, 209.
[173] F. von Germar, A. Galan, O. Llorca, J. L. Carrascosa, J. M. Valpuesta, W. Mantele, A. Muga, *Journal of Biological Chemistry* **1999**, *274*, 5508.
[174] T. Fischer, N. Rotermund, C. Lohr, D. Hirnet, *Purinergic signalling* **2012**, *8*, 191.
[175] G. I. Hatton, *Advan in Physiol Edu* **2002**, *26*, 225.
[176] H. Thirlwell, J. E. Corrie, G. P. Reid, D. R. Trentham, M. A. Ferenczi, *Biophysical Journal* **1994**, *67*, 2436.
[177] H. Thirlwell, J. A. Sleep, M. A. Ferenczi, *J Muscle Res Cell Motil* **1995**, *16*, 131.
[178] D. Geissler, W. Kresse, B. Wiesner, J. Bendig, H. Kettenmann, V. Hagen, *Chembiochem a European journal of chemical biology* **2003**, *4*, 162.
[179] T. Fischer, A. Agarwal, H. Hess, *Nature nanotechnology* **2009**, *4*, 162.
[180] J. Xue, M. A. Cooney, V. J. Hall, N. A. Korfiatis, R. T. Tecirlioglu, A. J. French, N. T. Ruddock, *Reprod. Fertil. Dev.* **2004**, *16*, 781.
[181] Y. V. Il'ichev, M. A. Schwörer, J. Wirz, *Journal of the American Chemical Society* **2004**, *126*, 4581.
[182] R. C. Huxford, J. Della Rocca, W. Lin, *Current opinion in chemical biology* **2010**, *14*, 262.
[183] K. C. Wood, J. Q. Boedicker, D. M. Lynn, P. T. Hammond, *Langmuir the ACS journal of surfaces and colloids* **2005**, *21*, 1603.
[184] C. Wang, S. Ye, L. Dai, X. Liu, Z. Tong, *Biomacromolecules* **2007**, *8*, 1739.
[185] A. Szarpak, Di Cui, F. Dubreuil, B. G. de Geest, L. J. de Cock, C. Picart, R. Auzély-Velty, *Biomacromolecules* **2010**, *11*, 713.
[186] A. A. Antipov, G. B. Sukhorukov, H. Möhwald, *Langmuir* **2003**, *19*, 2444.
[187] J.-Z. Du, X.-J. Du, C.-Q. Mao, J. Wang, *Journal of the American Chemical Society* **2011**, *133*, 17560.
[188] L. Wang, K.-f. Ren, H.-b. Wang, Y. Wang, J. Ji, *Colloids and surfaces. B, Biointerfaces* **2015**, *125*, 127.
[189] F. Boulmedais, C. S. Tang, B. Keller, J. Vörös, *Adv. Funct. Mater.* **2006**, *16*, 63.
[190] N. Fomina, J. Sankaranarayanan, A. Almutairi, *Advanced Drug Delivery Reviews* **2012**, *64*, 1005.
[191] G. Liu, W. Liu, C.-M. Dong, *Polym. Chem.* **2013**, *4*, 3431.
[192] R. Tong, D. S. Kohane, *Wiley interdisciplinary reviews. Nanomedicine and nanobiotechnology* **2012**, *4*, 638.
[193] Y. Zhao, *Macromolecules* **2012**, *45*, 3647.
[194] J. Jiang, X. Tong, D. Morris, Y. Zhao, *Macromolecules* **2006**, *39*, 4633.
[195] K. C. Hribar, M. H. Lee, D. Lee, J. A. Burdick, *ACS nano* **2011**, *5*, 2948.
[196] R. Weissleder, *Nature biotechnology* **2001**, *19*, 316.
[197] D. V. Volodkin, A. G. Skirtach, H. Möhwald, *Angewandte Chemie (International ed. in English)* **2009**, *48*, 1807.
[198] D. V. Volodkin, M. Delcea, H. Möhwald, A. G. Skirtach, *ACS applied materials & interfaces* **2009**, *1*, 1705.
[199] A. G. Skirtach, C. Déjugnat, D. Braun, A. S. Susha, A. L. Rogach, G. B. Sukhorukov, *J. Phys. Chem. C* **2007**, *111*, 555.
[200] B. Radt, T. A. Smith, F. Caruso, *Adv. Mater.* **2004**, *16*, 2184.
[201] G. Wu, A. Mikhailovsky, H. A. Khant, J. A. Zasadzinski, in *Chapter 14 - Synthesis, characterization, and optical response of gold nanoshells used to trigger release from liposomes.*, Vol. 464 (Ed.: Wu G, Mikhailovsky A, Khant HA, Zasadzinski JA.), Elsevier, Academic Press. Amsterdam [u.a.] **2009**, p. 279.
[202] X.-D. Zhang, Di Wu, X. Shen, P.-X. Liu, F.-Y. Fan, S.-J. Fan, *Biomaterials* **2012**, *33*, 4628.
[203] J. Olejniczak, J. Sankaranarayanan, M. L. Viger, A. Almutairi, *ACS macro letters* **2013**, *2*, 683.
[204] H. J. Koester, D. Baur, R. Uhl, S. W. Hell, *Biophysical Journal* **1999**, *77*, 2226.
[205] K. König, T. W. Becker, P. Fischer, I. Riemann, K.-J. Halbhuber, *Opt. Lett.* **1999**, *24*, 113.
[206] M. L. Viger, W. Sheng, K. Doré, A. H. Alhasan, C.-J. Carling, J. Lux, C. de Gracia Lux, M. Grossman, R. Malinow, A. Almutairi, *ACS nano* **2014**, *8*, 4815.
[207] C.-J. Carling, F. Nourmohammadian, J.-C. Boyer, N. R. Branda, *Angewandte Chemie (International ed. in English)* **2010**, *49*, 3782.
[208] H. S. Choi, W. Liu, P. Misra, E. Tanaka, J. P. Zimmer, B. Itty Ipe, M. G. Bawendi, J. V. Frangioni, *Nature biotechnology* **2007**, *25*, 1165.
[209] M. F. Bédard, B. G. de Geest, A. G. Skirtach, H. Möhwald, G. B. Sukhorukov, *Advances in Colloid and Interface Science* **2010**, *158*, 2.
[210] N. Fomina, C. McFearin, M. Sermsakdi, O. Edigin, A. Almutairi, *Journal of the American Chemical Society* **2010**, *132*, 9540.

[211] E. Cabane, V. Malinova, W. Meier, *Macromol. Chem. Phys.* **2010**, *211*, 1847.
[212] E. Cabane, V. Malinova, S. Menon, C. G. Palivan, W. Meier, *Soft Matter* **2011**, *7*, 9167.
[213] B. Wang, K. Chen, R. Yang, F. Yang, J. Liu, *Carbohydrate Polymers* **2014**, *103*, 510.
[214] I. Tomatsu, K. Peng, A. Kros, *Advanced Drug Delivery Reviews* **2011**, *63*, 1257.
[215] Q. Yi, G. B. Sukhorukov, *Soft Matter* **2014**, *10*, 1384.
[216] C.-J. Carling, M. L. Viger, V. A. N. Huu, A. V. Garcia, A. Almutairi, *Chemical science (Royal Society of Chemistry 2010)* **2015**, *6*, 335.
[217] A. Muñoz Javier, P. del Pino, M. F. Bedard, D. Ho, A. G. Skirtach, G. B. Sukhorukov, C. Plank, W. J. Parak, *Langmuir the ACS journal of surfaces and colloids* **2008**, *24*, 12517.
[218] S. Carregal-Romero, M. Ochs, P. Rivera-Gil, C. Ganas, A. M. Pavlov, G. B. Sukhorukov, W. J. Parak, *Journal of controlled release official journal of the Controlled Release Society* **2012**, *159*, 120.
[219] R. H. Kramer, D. L. Fortin, D. Trauner, *Current opinion in neurobiology* **2009**, *19*, 544.
[220] T. Milburn, N. Matsubara, A. P. Billington, J. B. Udgaonkar, J. W. Walker, B. K. Carpenter, W. W. Webb, J. Marque, W. Denk, *Biochemistry* **1989**, *28*, 49.
[221] F. Palma-Cerda, C. Auger, D. J. Crawford, A. C. C. Hodgson, S. J. Reynolds, J. K. Cowell, K. A. D. Swift, O. Cais, L. Vyklicky, J. E. T. Corrie, D. Ogden, *Neuropharmacology* **2012**, *63*, 624.
[222] M. Canepari, L. Nelson, G. Papageorgiou, J. Corrie, D. Ogden, *Journal of Neuroscience Methods* **2001**, *112*, 29.
[223] S. Iwabuchi, T. Watanabe, K. Kawahara, *Neurochemistry international* **2013**, *62*, 1020.
[224] P. Shum, J.-M. Kim, D. H. Thompson, *Advanced Drug Delivery Reviews* **2001**, *53*, 273.
[225] S. SEIFFERT, W. OPPERMANN, *J Microsc* **2005**, *220*, 20.
[226] F. Boulmedais, M. Bozonnet, P. Schwinté, J.-C. Voegel, P. Schaaf, *Langmuir* **2003**, *19*, 9873.
[227] M. L. Graber, D. C. DiLillo, B. L. Friedman, E. Pastoriza-Munoz, *Analytical Biochemistry* **1986**, *156*, 202.
[228] F. Foret, J. Kutter, D. Milanova, R. D. Chambers, S. S. Bahga, J. G. Santiago, *ELECTROPHORESIS* **2011**, *32*, 3286.
[229] Y. Umezawa, M. Kataoka, W. Takami, E. Kimura, T. Koike, H. Nada, *Anal. Chem* **1988**, *60*, 2392.
[230] V. Ball, *Materials* **2012**, *5*, 2681.
[231] I. Langmuir, *J. Am. Chem. Soc.* **1916**, *38*, 2221.
[232] K. Vijayaraghavan, T. V. N. Padmesh, K. Palanivelu, M. Velan, *Journal of hazardous materials* **2006**, *133*, 304.
[233] S. Kundu, A. K. Gupta, *Chemical Engineering Journal* **2006**, *122*, 93.
[234] E. Demirbas, M. Kobya, A. E. S. Konukman, *Journal of hazardous materials* **2008**, *154*, 787.
[235] S. Brunauer, P. H. Emmett, E. Teller, *J. Am. Chem. Soc.* **1938**, *60*, 309.
[236] H. Freundlich, *J. Phys. Chem* **1906**, *57*, 385.
[237] F. Haghseresht, G. Q. Lu, *Energy Fuels* **1998**, *12*, 1100.
[238] J. Zeldowitsch, *Acta Phys. Chim. URSS* **1934**, *1*.
[239] K. Y. Foo, B. H. Hameed, *Chemical Engineering Journal* **2010**, *156*, 2.
[240] P. Costa, Sousa Lobo, José Manuel, *European Journal of Pharmaceutical Sciences* **2001**, *13*, 123.
[241] W. I. Higuchi, *J. Pharm. Sci.* **1967**, *56*, 315.
[242] J. Siepmann, N. A. Peppas, *International journal of pharmaceutics* **2011**, *418*, 6.
[243] A. W. Hixson, J. H. Crowell, *Ind. Eng. Chem.* **1931**, *23*, 923.
[244] S. Dash, P. N. Murthy, L. Nath, P. Chowdhury, *Acta poloniae pharmaceutica* **2010**, *67*, 217.
[245] N. V. Mulye, S. J. Turco, *Drug Development and Industrial Pharmacy* **1995**, *21*, 943.
[246] L. Jourdainne, S. Lecuyer, Y. Arntz, C. Picart, P. Schaaf, B. Senger, J.-C. Voegel, P. Lavalle, T. Charitat, *Langmuir* **2008**, *24*, 7842.
[247] M. Bonizzoni, S. R. Long, C. Rainwater, E. V. Anslyn, *The Journal of organic chemistry* **2012**, *77*, 1258.
[248] J. Siepmann, *Advanced Drug Delivery Reviews* **2001**, *48*, 139.
[249] H. Thirlwell, J. A. Sleep, M. A. Ferenczi, *Journal of muscle research and cell motility* **1995**, *16*, 131.
[250] T. Kageyama, M. Tanaka, T. Sekiya, S.-Y. Ohno, N. Wada, *Photochemistry and photobiology* **2011**, *87*, 653.
[251] L. J. Janssen, L. Farkas, T. Rahman, M. R. J. Kolb, *The international journal of biochemistry & cell biology* **2009**, *41*, 2477.
[252] S. Bruzzone, S. Kunerth, E. Zocchi, A. de Flora, A. H. Guse, *The Journal of Cell Biology* **2003**, *163*, 837.
[253] K. Furuya, M. Sokabe, R. Grygorczyk, *Methods (San Diego, Calif.)* **2014**, *66*, 330.

Appendix

List of Abbreviations

AFM	atomic force microscopy
ATP	adenosine triphosphate
AuNPs	gold nanoparticles
BET	Brunauer–Emmett–Teller adsorption model
bL	bilayer
cAMP	cyclic adenosine monophosphate
cATP	caged ATP
CF	carboxyfluorescein
CLSM	confocal laser scanning microscope
DLS	dynamic light scattering
DMB-ATP	adenosine-triphosphate-P^3-(1-(3',5'-dimethoxyphenyl)-2-oxo-2-phenyl-ethyl)-ester
DMEM	Dulbecco's modified eagles' medium (HEPES modification)
DMNPE-ATP	adenosine-triphosphate-P^3-(1-(4,5-dimethoxy-2-nitrophenyl)ethyl)-ester
DNA	deoxyribonucleic acid
ECM	extracellular matrix
EDTA	ethylene diamine tetra-acetate
FBS	foetal bovine serum
FITC	fluoresceinisothiocyanate
HA	hyaluronic acid
iCa^{2+}	intracellular Ca^{2+}
LbL	layer-by-layer
MSC	mesenchymal stem cells
NPE-ATP	adenosine-triphosphate-P^3-(1-(2-nitrophenyl)ethyl)-ester
PAH	poly(allylamine hydrochloride)
PALM	photoactivated localization microscopy
PBS	phosphate-buffered saline
PDADMAC	poly(diallyldimethyl ammonium chloride)
PEI	polyethyleneimine
PEM	polyelectrolyte multilayers
PI	propidium iodide
PLL	poly-L-lysine
PSS	polystyrene sulphonate
QCM	quartz crystal microbalance
Rho	rhodamine
SCM	small charged molecules
γ	number of theoretical monolayers on AuNPs on the film surface

List of Publications

1. Vladimir Prokopovic, Claus Duschl, Dmitry Volodkin. Hyaluronic Acid/Poly-l-Lysine Multilayers as Reservoirs for Storage and Release of Small Charged Molecules, *Macromol Biosci.*, 2015, 15 (10) : 1357-63

2. Alena Sergeeva, Natalia Feoktistova, Vladimir Prokopovic, Dmitry Gorin, Dmitry Volodkin. Design of Porous Alginate Hydrogels by Sacrificial $CaCO_3$ Templates: Pore Formation Mechanism, *Adv. Mater. Interfaces*., 2015, *in press*

3. Vladimir Prokopovic, Claus Duschl, Dmitry Volodkin. Hyaluronic acid/poly-L-lysine multilayers coated with gold nanoparticles: cellular response and permeability study, *Polym. Adv. Technol.*, 2014, 25 (11) : 1342-8

4. Vladimir Prokopovic, Milica Popovic, Uros Andjelkovic, Aleksandra Marsavelski, Brankica Raskovic, Marija Gavrovic-Jankulovic, Natalija Polovic. Isolation, biochemical characterization and anti-bacterial activity of BPIFA2 protein. *Arch Oral Biol.*, 2014, 59 (3) : 302-9

5. Milos R Filipovic, Mirjam Eberhardt, Vladimir Prokopovic, Ana Mijuskovic, Zorana Orescanin-Dusic, Peter Reeh, Ivana Ivanovic-Burmazovic. Beyond H2S and NO Interplay: Hydrogen Sulfide and Nitroprusside React Directly to Give Nitroxyl (HNO). A New Pharmacological Source of HNO, *J. Med. Chem.*, 2013, 56 (4) : 1499–508

Conferences

1. 2nd International conference on Bio-based Polymers and Composites, 2014, Visegrad, Hungary; oral presentation

2. 12th International conference on Polymers for Advanced Technologies, 2014, Berlin, Germany; oral presentation